Non-selective Late-stage Functionalisation for the Diversification of Drug-like Molecules;

Or, Making the Best of a Bad Reaction.

A thesis submitted in partial fulfilment of the requirements for the degree of Bachelor of Science (Advanced) (Honours) in the School of Chemistry at The University of Sydney

Conor Patrick Sheedy Graham

January 2018

Abstract

Functionalisation of carbon–hydrogen bonds (found ubiquitously throughout organic molecules) may be used to improve a drug's potency, reduce its clearance rate, or change the its distribution in an organism. Functionalisations at these bonds at the end of a drug's synthesis (or, late-stage functionalisation, LSF) is a powerful new strategy for the production of a diverse library of derivatives from a complex biologically active substrate. There has been little research aimed at optimising a LSF methodology to form as many derivatives as possible, which would aid in the synthesis of a drug library and require fewer steps compared to traditional methodology.

We present a new metric to quantify non-selective product formation in a reaction (Reaction Non-selectivity Score, RNS) and investigate methods towards optimising an aliphatic azidation reaction towards non-selective product formation from the non-steroidal anti-inflammatory drug (NSAID), ibuprofen. Using design of experiments (DOE) and the RNS metric, we identified that each condition tested (reaction concentration, sodium azide aqueous solution concentration, equivalents of catalyst, azide and oxidant, temperature and time) had a significant effect on the reaction's non-selective formation of both the benzylic azide and ketone product. We also trialled a range of different late-stage hydroxylation and fluorination reactions on active compounds from Open Source Malaria's (OSM) Series 4 antimalarial compounds, leading to the preparation of two novel derivatives that were evaluated for biological potency.

Statement of Student Contribution

The initial concept of a non-selective methodology for drug-lead diversification was provided by A/Prof. Matthew Todd. The reaction methodologies we explored for C–H azidation, hydroxylation and fluorination were chosen by myself after consultation with A/Prof. Todd. The construction of a reaction non-selectivity score (RNS) to quantify a reaction's non-selective formation of products relative to ideal was performed by myself. The decision to use a design of experiments methodology to investigate non-selective aliphatic azidation was made by myself. The experiment design was made by myself with guidance from E/Prof. Brynn Hibbert and A/Prof. Todd. Modifications to solvent and reagent systems were made by myself with consultation from A/Prof. Todd.

Nuclear magnetic resonance (NMR) spectroscopy data was obtained by either myself, staff from the NMR facility under Dr. Ian Turner, or Mr. Edwin Tse. Low resolution mass spectrometry was performed by staff from the Mass Spectrometry Facility under Dr. Nick Proschogo. Liquid-chromatography mass spectrometry was run with guidance from Dr. Cody Szczepina and performed by myself thereafter.

The elucidation of the solid-state structures of several compounds using X-ray crystallography was performed by Dr Peter Turner.

Biological evaluation of compounds against the malaria parasite *Plasmodium falciparum* was performed by Dr Irene Hallyburton, The University of Dundee.

This thesis was written by myself and proofread by A/Prof. Todd and Mr. Edwin Tse.

I certify that this thesis contains work by myself except otherwise acknowledged.

Conor P. S. Graham

Acknowledgements

My deepest thanks to my supervisor, A/Prof. Matthew Todd, for suggesting to me an idea for a unique project that left me engaged from day 1 to today. This project forced me to think creatively and approach the literature from a very different perspective, which I found to be deeply engaging. I always felt more confident and capable walking out after a meeting with you, than walking in.

To A/Prof. Peter Rutledge, for always keeping me on my toes when I had to present at group meetings. Your questions would often challenge me to think in a different way about the subject matter I was talking about. Thank you for your suggestion of using Fe(II)TPA as a catalyst for non-selective hydroxylation.

To Dr. Malcolm Spain, for showing me how approach new reaction methodologies and for sharing your wisdom on chemistry, life, and everything in between. I recall many weekends made more enjoyable for your company.

To Mr. Edwin Tse, for all your help in answering my continuous and unrelenting questions, as well as for proofreading this thesis.

To my fellow honours students, thank you for the fantastic banter and craic. Monitoring a reaction was always more fun when there was at least one of you.

To my fellow members of the Todd and Rutledge groups, thank you for creating such a friendly and optimistic atmosphere. In particular to Mr. Jamie Batten, for playing some of the best tunes of the past fifty years.

Thank you to the staff of the level four service room, Mr. Carlo Piscicelli and Dr. Shane Wilkinson for your support for the lab and your assistance with finding unique glassware.

List of Abbreviations

Ac	acetyl
AKA	also known as
Anal.	elemental analysis
APCI	atmospheric pressure chemical ionisation
AUC	area under curve
BDE	bond dissociation energy
Bu	butyl
Calcd	calculated
CCD	central composite design
CTCL	cutaneous T-cell lymphoma
d	doublet
DCM	dichloromethane
dd	doublet of doublets
df	degrees of freedom
DFT	density functional theory
DIPEA	*N*,*N*-diisopropylethylamine
DMDO	dimethyldioxirane
DMF	dimethylformamide
DMSO	dimethylsulfoxide
DNA	deoxyribonucleic acid
DOE	design of experiments
ESI	electrospray ionisation
Et	ethyl
FGI	functional group interconversion
GSK	GlaxoSmithKline
h	hour or hours
HAT	hydrogen atom transfer
HRMS	high-resolution mass spectrometry
IC_{50}	half-maximal inhibitory concentration
LCMS	liquid-chromatography mass spectrometry
LRMS	low-resolution mass spectrometry

LSF	late-stage functionalisation
M	molar
m	multiplet
m	metre
m.p.	melting point
Me	methyl
MMV	Medicines for Malaria Venture
MOF	molecular organic framework
n	nano
NCE	new chemical entity
NFSI	*N*-fluorobenzenesulfonimide
NK_1	neurokinin 1
NMO	*N*-methylmorpholine *N*-oxide
NMR	nuclear magnetic resonance
o/n	overnight
OFAT	one factor at a time
OSM	Open Source Malaria
PCET	proton-coupled electron transfer, *see hydrogen atom transfer*
PDP	(-)-2-(((*R*)-2-((*R*)-1-(pyridin-2-ylmethyl)pyrrolidin-2-yl)pyrrolidin-1-yl)methyl)pyridine
Pfal	*Plasmodium falciparum*
Ph	phenyl
PPAR	peroxisome proliferator activated receptor
ppm	parts per million
pyr	pyridine
pyrz	pyrazine
q	quarter
RAR	retinoic acid receptor
RNS	reaction non-selectivity score
rt	room temperature
RXR	retinoid X receptors
s	singlet

salen	2,2'-((1*E*,1'*E*)-(ethane-1,2-diylbis(azaneylylidene))bis(methaneylylidene))diphenol
SAR	structure-activity relationship
SD	standard deviation
SOMO	singularly occupied molecular orbital
$ß_0$	reaction constant term
$ß_1$ and $ß_2$	coefficients of linear terms
$ß_{11}$ and $ß_{22}$	quadratic terms
$ß_{12}$	interaction term
T	temperature
t	time
t-BuOOH, *tert*-BuOOH	*tert*-butylhydroperoxide
T3P	propylphosphonic anhydride
TBADT	tetrabutylammonium decatungstate
tert	tertiary
TFDO	methyl(trifluoromethyl)dioxirane
THF	tetrahydrofuran
TLC	thin-layer chromatography
TMP	trimethylphenylporphyrin
TMS	tetramethylsilane
TPA	tris(pyridin-2-ylmethyl)amine
TPP	tetraphenylporphyrin
μ	micro

Table of Contents

Abstract i

Statement of Student Contribution ii

Acknowledgements iii

List of Abbreviations iv

Table of Contents vii

1 Introduction and Background 1

1.1 Developing New Chemical Entities (NCEs) 1

1.2 Late-stage Functionalisation (LSF) 3

1.3 LSF and the Functionalisation of C–H Bonds 5

1.4 Knowledge Gap and Aims 11

2 Project Design and Preparation 12

2.1 Model Substrates 12

2.1.1 Ibuprofen Methyl Ester 12

2.1.2 OSM Series 4 Compounds 13

2.1.3 Bexarotene 17

2.2 Design of Experiments 19

2.2.1 Why Design of Experiments? 19

2.2.2 Reaction Non-Selectivity Score (RNS) 22

3 Results and Discussion for LSF Reactions 23

3.1 Progress Towards Non-Selective C–H Azidation 23

3.2 C–H Hydroxylation 29

3.3 C–H Fluorination 34

4 Conclusions and Future Work 40

5 Experimental Details 42

5.1 General Experimental Details 42

5.2 General Analytical Details 42

5.3 Experimental Procedures 43

5.3.1 LSF Substrates and their Derivatives 43

5.3.2 Preparation of Reagents 55
5.3.3 Synthesis of Catalysts 56

References 61

Appendix 68

A.1 Example ^{1}H and ^{13}C NMR spectrum of a Series 4 compound, 5-Phenethoxy-3-(pyridin-4-yl)-[1,2,4]triazolo[4,3-*a*]pyrazine, 19. 68

A.2 Example LCMS chromatogram from aliphatic azidation using Fe(salen)Cl 70

A.3 LCMS data of trifluoromethylation reaction on 20. 71

A.4 Crystals of 19 grown in diethyl ether and methanol. 72

A.5 Multiple linear regression statistics for DOE example. 73

A.6 Correction to levels chosen for aliphatic azidation experiment on 11. 74

A.7 Cooling apparatus used for DOE 75

A.8 Further experiments needed to optimise non-selective yield of aliphatic azidation. 76

A.8 Experimental setup for the synthesis of DMDO and TFDO. 77

A.9 Colour change when using TBADT catalyst in acetonitrile 78

A.10 Reaction mechanism for TBADT-catalysed fluorination of aliphatic bonds using NFSI as fluorine source. 79

1 Introduction and Background

In this thesis I describe progress towards developing reactions for non-selective product formation, specifically through C–H azidation, hydroxylation and fluorination. This work was performed because new methods of forming derivatives of drug leads are needed to reduce the high cost and time involved in producing drugs. We begin this section with a survey of how drugs are typically produced, followed by a brief review of new methodologies that have emerged to produce drug leads, known as late-stage functionalisation (LSF).

1.1 Developing New Chemical Entities (NCEs)

The cost of developing a new drug to be approved for human use ranges from 0.8 to 2 billion dollars.[1] Much of this cost is accounted for by the lengthy process of synthesising hundreds, if not thousands of novel molecules, requiring multi-step synthetic routes that begin from simple organic materials. The development of new synthetic methods that reduce the time and capital needed to produce the large numbers of realistic drug-like molecules required for testing will ultimately reduce the cost and time involved in providing patients with effective new medicines.

Drug discovery relies on the initial identification of a new chemical entity (NCE) that is efficacious, as judged by some biological assay. In so-called "rational" drug discovery, activity is assessed against a specific target so that the NCE can be intentionally designed for better activity. An alternative approach is a phenotypic drug discovery programme, which evaluates the ability of an NCE to affect a phenotype, such as reducing formation of ß-amyloid plaque or killing an infectious organism like the malaria parasite. In the rational approach the mechanism of action of an NCE is known (or thought to be known), whereas phenotypic drug discovery operates (sometimes to completion) without knowledge of the details of how the NCE achieves its effect.

Most of the first pharmacological NCEs are (sometimes semisynthetic) natural products or their derivatives, with much of the biological activity already provided through the molecule's core scaffold. Small changes to these core scaffolds *via* a functional group interconversion (FGI) would often produce NCEs with an improved drug profile (with respect to e.g. potency or selectivity) *vs*. the original. A classic example is morphine (Fig. 1), a naturally occurring anaesthetic found in the flowering plant, *Papaver somniferum*. Changes to its core structure have allowed for the semisynthetic manufacture of more than a dozen NCEs with

varying properties, such as diacetylmorphine (AKA heroin), dihydrocodeine, buprenorphine, hydrocodone and many others,[2, 3] and is still an important area of research today.[4]

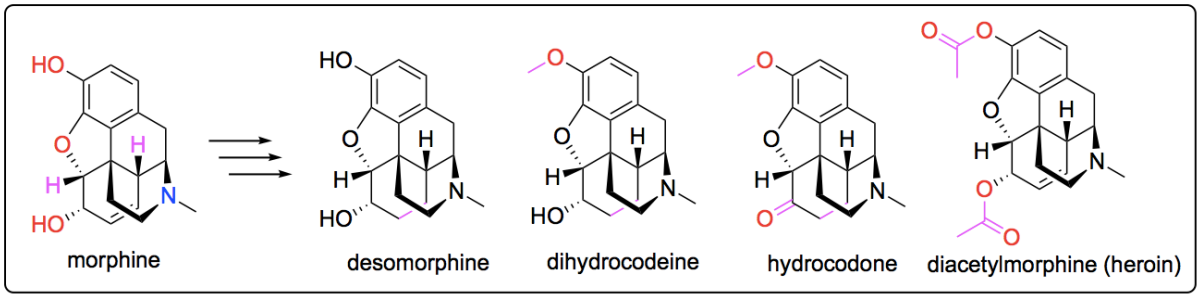

Figure 1. Semisynthetic derivatives of morphine formed through FGIs. There are however, 11 C–H "functional groups," within the morphine core structure that might be targeted through new methodologies.

FGIs traditionally occur on pre-functionalised positions across the molecule, such as an easily accessible hydroxyl group, or a ketone. The ability to modify instead more typically inert positions in a core structure (e.g., C–H bonds) might allow for the synthesis of an even wider range of NCEs that are more challenging to produce through traditional FGIs.

The screening process during the drug discovery phase often occurs quickly compared to the slow and laborious work involved during the following drug development stage. Drug discovery aims at identifying compounds known as "hits", which are lead compounds with good biological activity sourced from known compounds stored in chemical libraries of synthetic and natural products. Drug development aims to improve the pharmacological properties of these hits by synthesising a diverse range of "bespoke" NCEs that share similar motifs. Compared to the drug discovery phase, there is considerably less automation involved in the synthesis of NCEs during the drug development phase. This is particularly relevant in academic laboratories, where the high cost of automated systems is a barrier to entry.[5] Drug development requires complex multi-step syntheses performed by experienced chemists, with purifications and characterisations necessary at each step. Drug development's intensive use of resources contributes significantly to the final cost of a drug that makes it to market, and the time needed to reach it.

Traditionally this drug development process has relied on *de novo* synthetic techniques, where complex molecules are made from cheap readily available starting materials, often over many steps. Such an approach is the primary method for obtaining synthetic samples of natural products where the structure is already known. *However, in situations where it is unknown which molecule will produce the desired effect, the limitations of* de novo *synthesis become more apparent*. Step-wise synthesis is not an optimised process for producing a *diverse* library

of NCEs, especially when those NCEs contain similar features. Usually where two drug leads are similar (but not related by an FGI), the structural alteration takes place in the early stages of synthesis due to the difficulty of effecting more complicated changes on a fully elaborated molecule. Traditional synthetic strategies, as outlined in, *The Logic of Chemical Synthesis*,[6] would perform any C–H modifications at unactivated carbons in the early stages, saving milder transformations for later synthetic steps.

Therefore, the basic logic of a *de novo* synthetic strategy requires prefunctionalisation of the substrate at positions to be later functionalised. Recent methodologies show increased promise as they have succeeded in performing transformations at unactivated C–H bonds in complex molecules in the late-stage of their synthesis. Late-stage functionalisation (LSF) has become an increasingly useful drug development strategy over the past two decades for its ability to directly produce new derivatives from biologically active compounds. Historically C–H bonds have not been considered a functional group. More recent methodologies have challenged this assumption by performing modifications at these bonds under mild conditions, making them amendable to a LSF strategy.

1.2 Late-stage Functionalisation (LSF)

Sometimes all it takes to advance a drug lead with poor pharmacokinetic or pharmacodynamic properties into a potent drug is the substitution of a single C–H bond. For example, aprepitant (**3**, Fig. 2) is a neurokinin 1 (NK_1) receptor antagonist, used to treat side-effects of chemotherapy, and was approved by the FDA in 2003.[7] It took more than a decade to reach market after the lead compound, CP-96,345 (**1**), was discovered in 1991 as the first non-peptidic NK_1 receptor antagonist. Its potency of 3.4 ± 0.8 nM is expressed as its IC_{50}, which is the molar concentration of the drug required to decrease activity by 50%.[8] Structure-activity relationships (SARs) were determined by synthesising thousands of derivatives over seven years, resulting in the synthesis of the advanced lead, **2**, which was more than thirty times as potent as **1**. Still, further improvements were required after *in vitro* studies showed poor metabolic stability of **2** at the two highlighted C–H bonds (purple), preventing its progression through to clinical trials.[9] Small changes were methodically and laboriously introduced to these sites to reduce their metabolic degradation, resulting in the substitution of a benzylic hydrogen with a methyl group, and an aromatic hydrogen atom with a fluorine atom. The small changes between **2** and **3** occurred at metabolically susceptible C–H bonds. A LSF reaction (perhaps one able to mimic the reactivity pattern of drug-metabolising enzymes) may have identified **3** earlier. Strategies that mimic enzymatic C–H reactivity patterns can be used to directly improve the metabolic

stability of a drug lead by substitution with a metabolically resistant functional group like fluorine or the trifluoromethyl (CF_3) group.[10] Further, a non-regioselective installation of the fluorine atom in **3** over a single step would have generated a large number of derivatives over fewer steps and reduced cost. Unfortunately, a LSF strategy was not used to produce this drug because at that time such approaches were not being pursued.

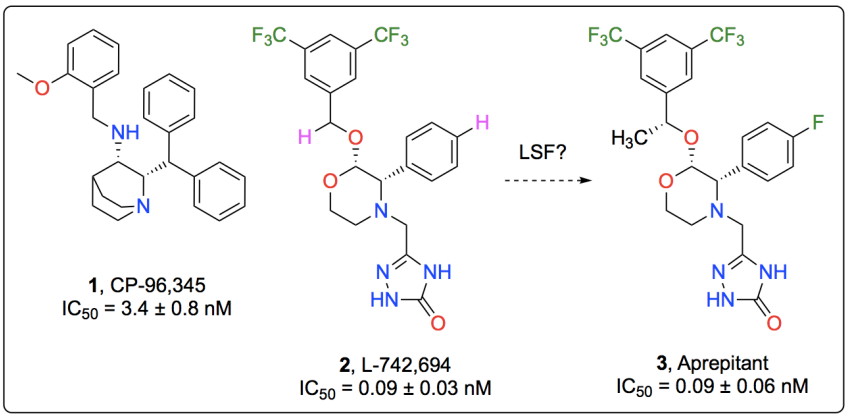

Figure 2. Lead compound **1** was improved to **2** after lengthy SAR studies. *In vitro* metabolic studies on **2** identified two C–H positions prone to metabolic degradation (shown in purple). These positions were blocked with a methyl group and a fluorine atom to produce the clinical drug aprepitant **3**. A LSF strategy could have accelerated the development of **3** directly from **2**.

LSF that introduces a functional group such as an azide, fluorine or hydroxyl group can offer several other advantages to drug development compared to *de novo* synthesis. Substitution with fluorine can be used for the rapid synthesis of radiopharmaceuticals containing fluorine-18.[11] The high electronegativity and lone pairs of fluorine allow it to act as a bioisostere for the hydroxyl group,[12] while the CF_3 group can act as a bioisostere for methyl groups in a molecule.[13] For example, the antidepressant fluoxetine (Prozac, *Eli Lilly*) contains an aryl CF_3 group. Substitution of the lead compound's aryl methyl group with a CF_3 group increased the drug's potency by six-fold.[14] Reduced conformational flexibility in the trifluoromethylated-derivative – due to the larger steric bulk of the group compared to a methyl – was determined to be the cause.[15] LSF also allows for the installation of an innately reactive functional group, such as an azide (N_3), or an alcohol (OH), which may otherwise require the use of protecting groups or pre-functionalisation of the substrate if installed in earlier stages.[16] Azides are particularly useful for their potential to be reacted with an alkyne *via* a 1,3-dipolar cycloaddition ("click reaction") to form a large number of derivatives.[17] Still, the main advantage of LSF methodologies to drug development is in the construction of a diverse library of derivatives from a single compound to aid SAR studies.

When using LSF strategies to produce drug derivatives, C–H bonds make good targets for functionalisation due to their ubiquity throughout organic molecules. Fortunately, there has been recent progress towards developing increasingly mild reactions that can target C–H bonds for substitution with another functional group.

1.3 LSF and the Functionalisation of C–H Bonds

The development of new techniques for C–H bond activation are found in many areas of chemistry. For example, C–H bond activation can be used to convert simple chemicals such as methane into more useful substrates like methanol.[18] In these cases, the C–H bond activation method need not be mild due to the simplicity of the starting material. In other cases, milder C–H bond activation methods may be required for LSF methodologies to prevent decomposition or unwanted side-reactions from destroying the (often highly functionalised) substrate. Mild C–H substitution reactions have been recently used in the post-synthetic modification of molecular organic frameworks (MOFs), catalysts, or photoactive organic polymers.[19]

LSF methodologies are most successfully implemented in medicinal chemistry for the synthesis of derivatives for SAR studies. A recent review on the literature of late-stage C–H substitution methodologies used in drug-lead development groups reactions into two classes as dependent on their mechanism: guided or innate.[16] Guided methodologies rely on directing groups already installed within the substrate, or direction by catalyst sterics.[20] For example, Dai *et al*. (2011) demonstrated use of sulfonamides as intramolecular directing groups to guide the installation of olefins, carboxyls, carbonyls, iodine, and aryl/alkyl groups at aromatic C–H positions using palladium(II) acetate as a catalyst.[21] The scope of this work is limited to the requirement of an intramolecular aryl sulfonamide on substrates. Still, derivatives of sulfonamide-containing active compounds, such as celecoxib, sumatriptan or azosemide, have been produced using this LSF method, circumventing what otherwise would have required many more steps *via* a *de novo* methodology.

In contrast to a guided methodology, C–H substitution methodologies reliant on innate bond reactivities are more appropriate for a LSF drug diversification strategy. While innate C–H substitution reactions occur at the most innately reactive hydrogen atom, several C–H bonds in a complex molecule may have similar enough reactivity such that regio-nonselective functionalisation occurs. LSF *via* innate mechanisms can occur through four different pathways: hydrogen atom transfer (HAT or proton-coupled electron transfer, PCET), substitution at acidic C–H bonds, and addition-elimination reactions at either electrophilic or

nucleophilic sp^2 carbons.[16] It is possible for a reaction to rely on both guided and innate mechanisms for functionalisation, as in the case of bio-enzymatic functionalisation.

Many of the reactions we investigated in this thesis proceed through HAT and involve the transfer of a proton and electron from the substrate to a reagent or catalyst, forming a radical intermediate which can be attacked to form a desirable derivative. Carbon-based free radical intermediates follow a reactivity pattern of $sp^3 > sp^2 > sp$, with the homolytic bond-dissociation energies (BDE) of sp^3 carbons increasing as benzylic > tertiary > secondary > primary.[22] HAT reactions are therefore now commonly used for functionalising sp^3 benzylic and tertiary carbons.[16] Carbon-centred radicals can be generated either catalytically or through a stoichiometric amount of a radical initiator. Catalytic methods often use a high-spin first-row transition metal ion, such as iron(III) or manganese(III), which may be oxidised to form a metal-oxo intermediate ("oxo" referring to the M=O bond), which can abstract a proton to form a radical on the substrate.[23, 24] This process is not dissimilar to the hydrogen abstraction mechanism used by some cytochrome P450 enzymes to metabolise drugs.[25] For this reason, synthetic methods that proceed through HAT can be thought of as a form of "bio-mimicry". The pattern of reactivity can also be affected by stabilising effects like hyperconjugation, resonance, lone pairs on adjacent atoms, bond strain of the radical intermediate, and solvent effects.[26] Electron-richness of the hydrogen-abstraction source and its accessibility to different C–H bonds across the substrate can also play a role in reaction selectivity.[16] Stability of the carbon-centred radical intermediate is affected by many factors, holding promise for functionalising several C–H bonds in a single substrate.

Early C–H activation methods through HAT were limited to simple substrates and lacked tolerance towards of more complex molecules. The subject of late-stage C–H activation is large and several reviews may be consulted,[16, 20, 27] but it is instructive to consider several reports that together address a useful LSF reaction, azidation. An early example is a manganese-catalysed C–H azidation (Scheme 1a) that demonstrated functionalisations of alkyl hydrogens at secondary and tertiary positions in simple alkyl substrates through a HAT mechanism.[28] The methodology allowed for the installation of the azide functional group at unactivated C–H bonds in cyclohexane using a manganese(III)-porphyrin catalyst. However, the reaction was not chemoselective, with oxygen-containing side products also formed.

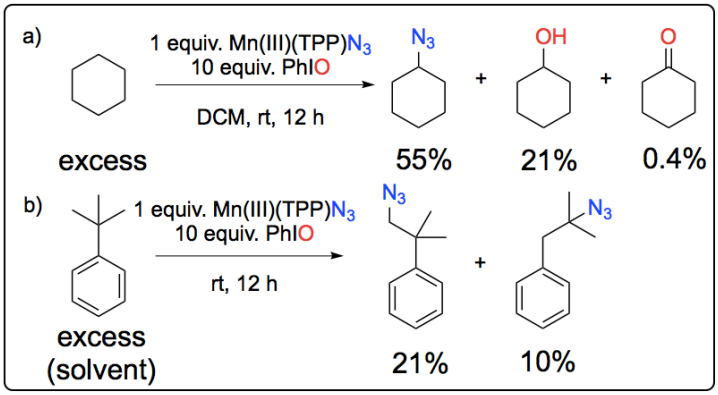

Scheme 1. a) Azidation of the simple aliphatic molecule cyclohexane using manganese(III)(tetraphenylporphyrin)azide and iodosylbenzene as oxidant. The reaction also formed a modest yield of the alcohol, and trace yields of the ketone. Reaction has an RNS(3) of 1.3% (See section 2.2.2, Reaction Non-Selectivity Score). Yields are proportional to added Mn(III)TPPN$_3$. b) Azidation of *tert*-butylbenzene forming two products. Reaction has an RNS(2) of 8.4%. Yields are proportional to added Mn(III)TPPN$_3$.

Attempts at extending this methodology to the slightly more complex substrate of *tert*-butylbenzene resulted in both low yield of the desired product, and formation of a rearrangement product (Scheme 1, b). New developments in C–H azidation strategies have since improved on this work, extending functionalisation at C–H bonds to more complex substrates. An example is the azidation of a range of complex substrates, such as a tetrahydrogibberellic acid derivative (Scheme 2), using an iron-oxazoline catalyst and a hypervalent iodine reagent as azide source.[29] Notably, no protection of the carboxylic acid was needed for this reaction to proceed in good yield.

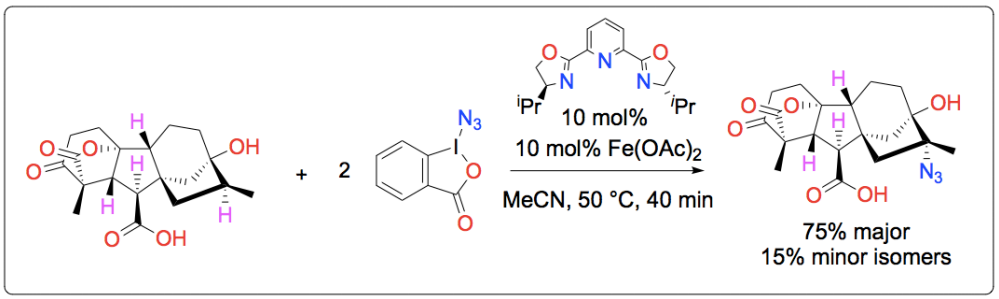

Scheme 2. Azidation of tertiary C–H bonds in a tetrahydrogibberellic acid derivative using an iron-oxazoline catalyst and a hypervalent iodine reagent as azide source.

The above methods were still limited to functionalisations at tertiary or benzylic positions. It was known that manganese-porphyrin (Fig. 3a, Mn(III)(TMP)Cl) and manganese-salen catalysts (Jacobsen's (*R*,*R*) catalyst) could halogenate unactivated C–H bonds.[30] It was theorised that an azide anion may act in a similar fashion as a

"pseudohalogen", allowing for access to substitutions at secondary, tertiary and benzylic positions with an azide group.[31] For example, using Jacobsen's catalyst azidation could be effected at a secondary position, such as for N_3-ibuprofen methyl ester (Fig. 3b, **4**). A ketone was also observed as a side-product. The suggested mechanism for this reaction proceeds through radical C–H abstraction with the activated manganese(V)-oxo catalyst intermediate (Scheme 3c, iii) acting as the hydrogen abstractor.[31] Initially, a pseudohalogen exchange (i to ii) prepares the catalyst for azidation. The active manganese(V)-oxo catalyst intermediate is formed through oxidation of the metal centre with iodosylbenzene (PhIO) (Fig. 3c). Innately reactive C–H hydrogens on the substrate can be abstracted by this active intermediate to form a radical intermediate on the substrate. This radical may then be attacked by the terminal nitrogen in the axial azide group.[31]

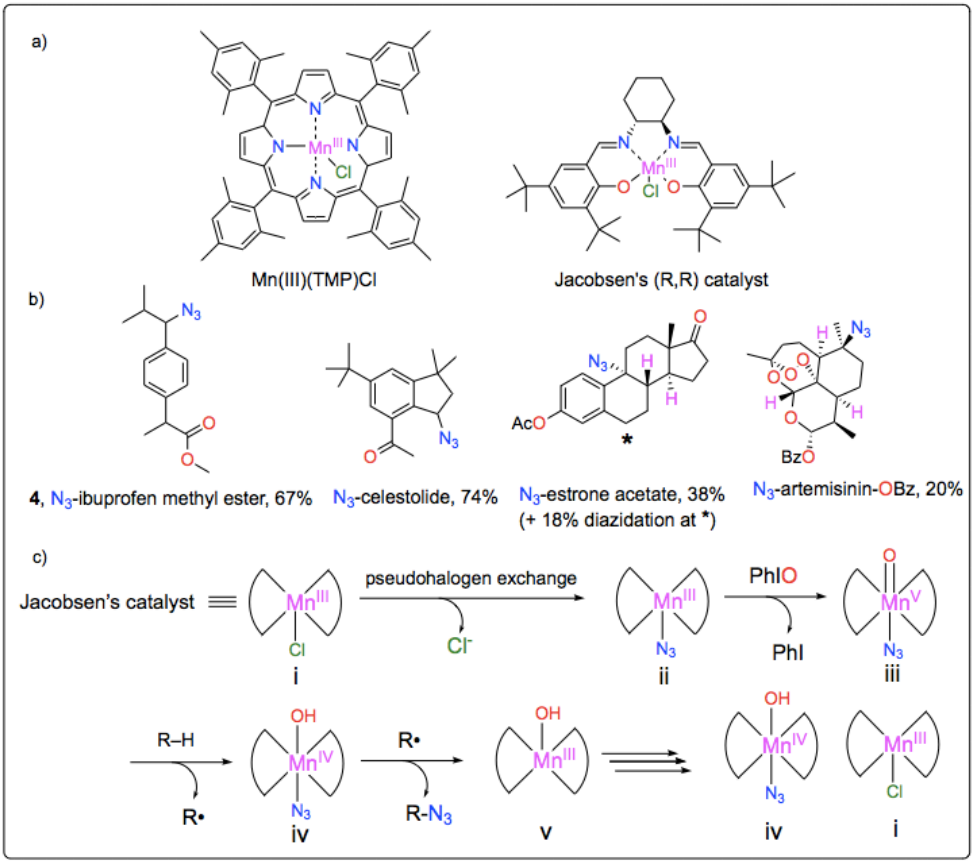

Figure 3. a) Manganese(III)(trimethylphenylporphyrin)chloride (Mn(III)(TMP)Cl) (*left*) and Jacobsen's (*R,R*) catalyst (*right*). b) Conditions applied to precursor substrate (where N_3 is H): 3–5 mol% Jacobsen's catalyst, 3–6 equivalents of 1.5 M $NaN_{3(aq)}$, 3–6 equivalents PhIO, EtOAc, rt, under N_2 or air, 3–12 h. RNS(2) for N_3-estrone acetate formation is 27%. c) Pseudohalogen exchange (i to ii) allows displacement of the chloride for the azide anion. Iodosylbenzene then activates the complex (ii to iii) for hydrogen abstraction (iii to iv) to form a radical on the substrate. Rebound of the azide forms the desired azidation product (iv to v).

Other C–H functionalisations have been shown with HAT-based mechanisms, for example hydroxylation using iron(II)-containing catalysts: Fe(II)PDP (Fig. 4a, **5**) can selectively functionalise aliphatic C–H bonds to form complex molecule derivatives, such as from artemisinin (Fig. 4b) or a tetrahydrogibberellic acid analogue under oxidising conditions.[32] Fe(II)TPA (**6**) has been shown to perform similar oxidations on less complex substrates with low selectivity. This includes forming hydroxylated products at C–H centres in simple alkanes like *trans*-1,2-dimethylcyclohexane, affording secondary and tertiary alcohols in a 1:1 ratio with >99% retention of stereochemistry for tertiary functionalisation (Fig. 4c).[33, 34, 35] The iron(II) centre of each catalyst is bound to a tetradentate nitrogen donor ligand, with two *cis*-sites occupied by labile acetonitrile groups. Their iron(II) centres and HAT mechanism of C–H functionalisation make them biomimetic in their substitution pattern, reacting similarly to cytochrome P450 enzymes.[36] As catalysts of non-biological origin, they can tolerate a greater range of reaction conditions than enzymes.

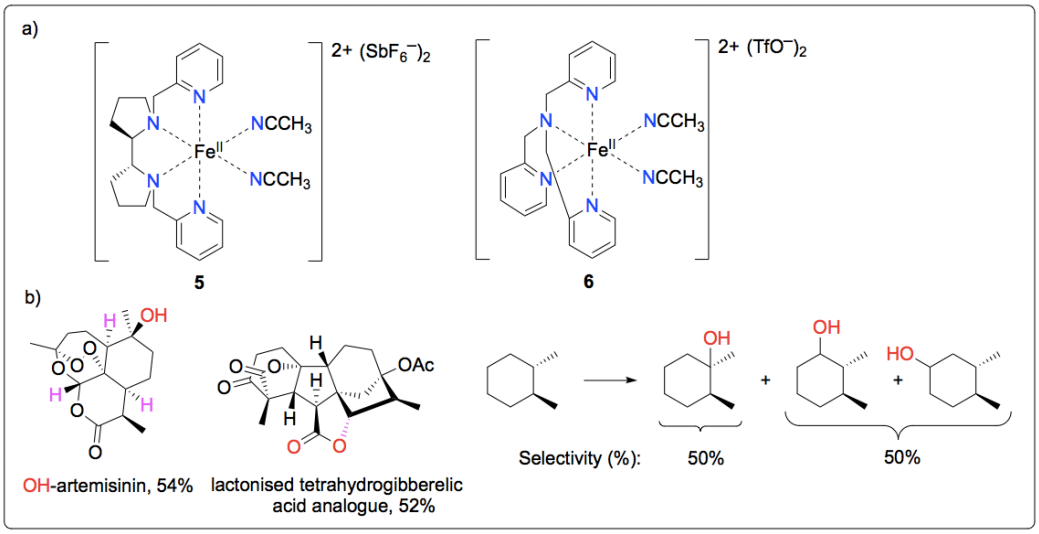

Figure 4. a) Two iron(II) C–H hydroxylation catalysts, Fe(II)PDP (**5**) and Fe(II)TPA (**6**). b) Two complex products derived using **5** as catalyst under oxidising conditions. The artemisin-derived product was formed by hydroxylation at the most electron-rich and least sterically hindered C–H bond in 54% yield after recycling the substrate twice. C–H hydroxylation, followed by carboxylate-directed lactonisation allows for the diastereoselective lactonisation of a tetrahydrogibberellic acid analogue in 52% yield `after recycling the substrate once. c) Hydroxylation of tertiary and secondary positions in *trans*-1,2-dimethylcyclohexane occurs with equal ratio when using **6** as catalyst under oxidising conditions.

Electrophilic fluorinating reagents are commonly used for C–H fluorination, with reactions proceeding through several different pathways. Silver(II) fluoride (Fig. 5a, **7**) can fluorinate C–H bonds in nitrogen-containing heterocycles.[37] The proposed mechanism proceeds

by coordination of silver(II) to a basic ring-nitrogen followed by addition of fluoride to the heteroaromatic π-system, which would favour addition to electron-deficient rings. Oxidation of the heterocycle through HAT affords the fluorinated product. This method has been used to form fluorinated derivatives of biologically active substrates, such as from the methyl ester-protected anticancer drug, vismodegib (Fig. 5b).[37] Following, nucleophilic aromatic substitution of the C–F bond can then be used to afford an even greater range of derivatives, such as those formed from the COX-2 inhibitor, etoricoxib (Fig. 5b).[37] *N*-Fluorobenzenesulfonimide (NFSI) (Fig. 5c, **8**) can be used as an electrophilic fluorine source, fluorinating simple aromatic molecules at C–H bonds under refluxing conditions with a high loading of reagent (range of 1–50 equivalents) (Fig. 5d).[38] The reagent also been used with the photocatalyst tetrabutylammonium decatungstate to fluorinate sp^3 C–H positions, for example to form two fluorinated derivatives of sclareolide (Fig. 5e).[39] Sodium trifluoromethylsulfinate (Fig. 5f, **9**) has been used to trifluoromethylate C–H bonds in biologically active compounds such as caffeine, nicotine, melatonin and allopurinol under oxidising conditions through an electrophilic radical substitution mechanism (Fig. 5g).[40]

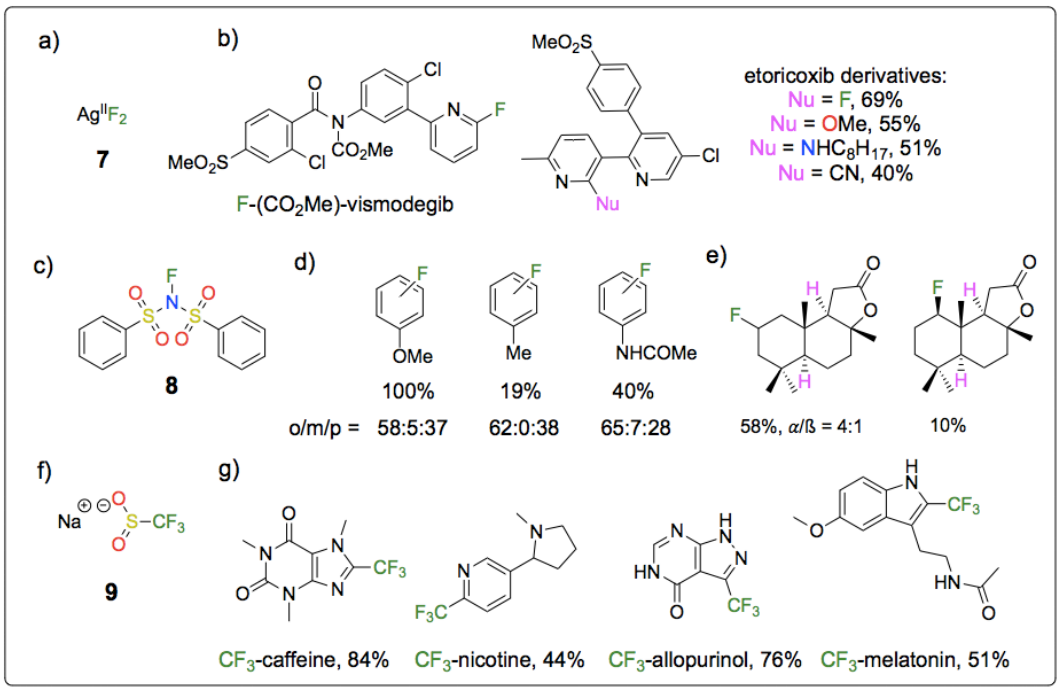

Figure 5. a) Silver(II) difluoride **7**. b) **7** has been used to form fluorinated derivatives of vismodegib and etoricoxib at heterocyclic C–H bonds *alpha* to a basic aromatic nitrogen. Subsequent nucleophilic substitution at the C–F bond can be used to form a diverse range of derivatives. c) *N*-fluorobenzenesulfonimide (NFSI) **8**. Figure 5d. **8** has been used to form fluorinated derivatives of simple aromatic molecules under reflux conditions through an electrophilic aromatic substitution mechanism. d). Two fluorinated derivatives of sclareolide formed in a single step using tetrabutylammonium decatungstate as catalyst and **8** as fluorine-source. Reaction has an

RNS(3) of 15%. f) Sodium trifluoromethylsulfinate **9**. g) **9** has been used to form trifluoromethylated derivatives of caffeine, nicotine, melatonin and allopurinol under oxidising conditions through an electrophilic radical substitution mechanism.

1.4 Knowledge Gap and Aims

The importance and relevance of LSF to forming derivatives of biologically active molecules is well established.[16, 20] Despite the benefits of forming multiple derivatives in a single reaction, there is still a collective focus in LSF on *increasing* reaction selectivity. In the process of searching the relevant literature, we found only one paper that deemed a reaction's ability to form multiple derivatives in a single step as worthwhile.[41] There were no papers that optimised a reaction for the formation of multiple products. We explored a wide range of aliphatic and aromatic late-stage C–H substitution reactions for their potential to form derivatives of biologically active and inactive compounds *non-selectively*, i.e. where several variants of a complex molecule, desirably functionalised, are made in a single step in a way that provides useful quantities of each for further evaluation. To achieve this, we proposed to:

1) Synthesise a set of substrate molecules with relevance to medicinal chemistry to evaluate LSF methodologies for exploration
2) Develop a method to quantify a reaction's non-selective formation of products, and deploy statistical approaches towards an experimental design to improve non-selectivity
3) Empirically judge the success of several possible LSF methods, and modify these methods in response to the data obtained.

These aims were intended to provide ways towards quickly optimising C–H substitution reactions for non-selective LSF methodologies. These methodologies can be employed to better diversify candidate medicines in the future.

2 Project Design and Preparation

In this section, we explain the rationale in our choice of substrates on which to explore new LSF methodologies, as well as their preparation from *de novo* methodologies. We also briefly describe the fundamental usefulness of a design of experiments (DOE) approach, and a new method of quantifying and comparing reaction non-selectivity. The use of these substrates in new LSF methodologies is described in Section 3, Results and Discussion.

2.1 Model Substrates

As we would be trialling a diverse range of LSF methodologies, we required several model substrates on which to assess the regio- and chemo-nonselectivity of different LSF reactions.

2.1.1 Ibuprofen Methyl Ester

We found ibuprofen (Scheme 4, **10**) to be near ideal as a model substrate for assessing C–H functionalisation at sp^2 and sp^3 positions for three key reasons. Firstly, it is inexpensive ($3.9/g, *Alfa Aesar*),[42] as it is a commonly used drug and therefore produced on a large scale industrially. Secondly, this molecule has been used previously by many groups focussed on developing LSF reactions, allowing us to directly use/compare their methodologies. Most importantly, the molecule contains many types of sp^3 C–H bonds, specifically at primary, secondary, tertiary, benzylic and aromatic carbons, making it ideal for assessing the regio- and chemo-selectivity of a reaction. For most of the LSF reactions trialled, ibuprofen required protection by forming the methyl ester, **11**, which was simple to perform in good yield (95%) *via* esterification using thionyl chloride and methanol (Scheme 3).

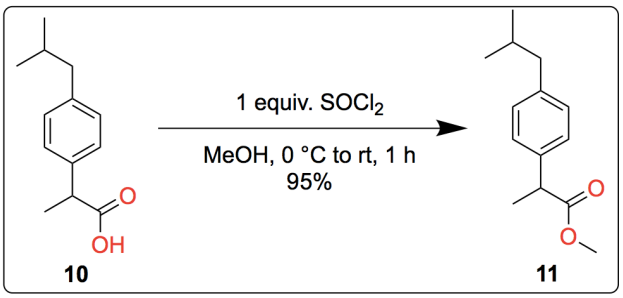

Scheme 3. Ibuprofen (**10**) was used as a model substrate. However, for many reactions the substrate required esterification to **11** to protect its carboxylic functionality.

2.1.2 OSM Series 4 Compounds

Open Source Malaria (OSM) is a drug discovery programme that uses the public to aid research into a new line of antimalarial drugs, accelerated by its open access platform.[43] Malaria's increasing resistance to the most commonly used antimalarial drugs necessitates the constant production of new classes of antimalarial compounds.[44] Through both SAR studies funded by the Medicines for Malaria Venture (MMV), and previous work performed by Pfizer and GlaxoSmithKline (GSK), a new series of antimalarial drugs is being developed by OSM known as Series 4. The compounds in this series are designed around a triazolopyrazine core (Fig. 6, *left*), but have been refined (based on extensive optimisation) into two basic structures, containing either an amide or an ether linkage attached to the core's north-west region (Fig. 6, *middle* and *right* respectively). These compounds are highly toxic to *Plasmodium falciparum* (*Pfal*), the deadliest species of the protozoan mosquito parasite that causes malaria,[45] but non-toxic to mammalian cells, making them highly promising drug leads. Compounds are tested against a strain of *Pfal*, NF54, which has no resistance to any known antimalarials. Inhibition of uptake of a radiolabelled nucleic acid precursor is used as a measure of activity and expressed as the IC_{50}.[46]

The shared triazolopyrazine motif of this series idealises it for a LSF diversification strategy. Through SAR studies it has become clear that modifications to the core such as N to C or C to N, or substitution of the C8 hydrogen atom, can have a profound impact on activity and metabolic clearance parameters. The installation of functionality across the series' aromatic, heteroaromatic and benzylic C–H positions to address key challenges faced by the OSM community with this series relating to *in vitro* metabolic clearance, solubility and potency.

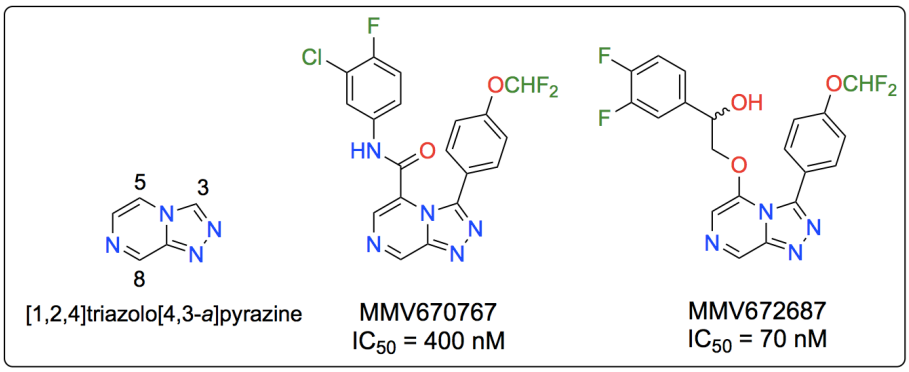

Figure 6. The triazolopyrazine core (left) and active representative compounds from the amide (middle) and ether (right) subseries of OSM Series 4.

For the evaluation of model LSF reactions, two novel OSM Series 4 substrates, **15** (MMV1557948) and **19** (MMV1557947) were synthesised over four steps (Schemes 4 and 5), alongside one known-active compound, **20** (Scheme 6). The two new compounds were of the ether and amide series and were designed to be free of any highly reactive functionality, while maintaining the triazolopyrazine core motif and realistic pendants. Both had a heteroaromatic pyridine side-group, so that differences in selectivity between this moiety and the heteroaromatic core could be determined.

To synthesise the amide substrate, commercially available 6-chloropyrazine-2-carboxylic acid is coupled with 4-aminopyridine using the peptide coupling reagent propylphosphonic acid anhydride (T3P) under basic conditions to form the product **12** in 53% yield. Nucleophilic aromatic substitution of **12** by hydrazine monohydrate under reflux conditions forms the product **13** in 55% yield. Imine formation to give **14** is achieved by condensation of **13** with benzaldehyde in 41% yield and finally oxidative cyclisation of **14** using (diacetoxy)iodobenzene affords the final product **15** in 51% yield (6% overall).

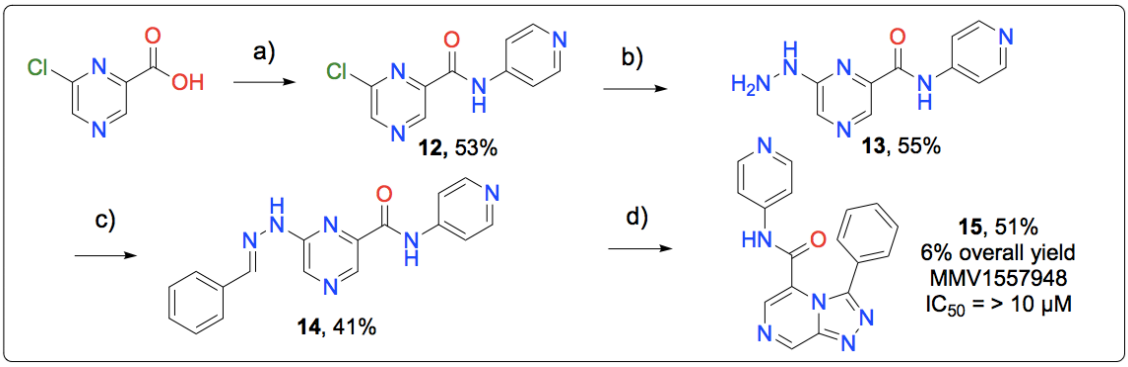

Scheme 4. Synthesis of **15**. a) pyridin-4-amine, T3P, DIPEA, EtOAc/DMF, 24 h, rt, 53%; b) hydrazine monohydrate, EtOH, reflux, 24h, 55%; c) benzaldehyde, EtOH, 4 h, rt, 41%; d) (diacetoxy)iodobenzene, anhydrous DCM, rt, 2.5 h, 51%. Overall yield 6%.

The ether series could be accessed using a similar synthetic sequence (Scheme 5) that gave the penultimate compound **18**. Nucleophilic aromatic substitution of the chlorine atom in this compound under basic conditions using 18-crown-6 ether as catalyst gave the final product **19** in 49% yield. Solvents were screened for recrystallisation and it was found that **19** was slightly soluble in diethyl ether at elevated temperatures. Recrystallisation of **19** from diethyl ether/methanol yielded several large yellow-orange crystals (See Appendix A.4). X-ray crystallography was used to elucidate the first crystal structure of a compound from this series, valuable data that confirms the compound's identity and solid-state conformation (Scheme 6, inset). When tested at The University of Dundee, compounds **15** and **19** were found to be

ineffective against *Pfal* inhibition (IC_{50} = >10 μM). Despite the inactivity of **19**, its solid-state structure still provides important information on intramolecular interactions and may be useful in the future following identification and structural characterisation of the biological target.

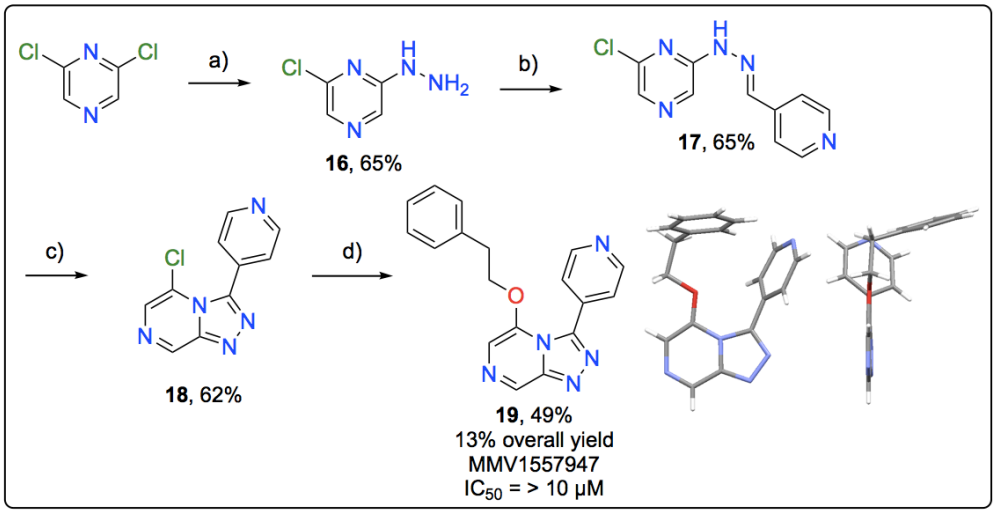

Scheme 5. Synthesis of **19**. a) hydrazine monohydrate, EtOH, reflux, 2h, 65%; b) isonicotinaldehyde, ethanol, rt, o/n, 65%; c) (diacetoxy)iodobenzene, anhydrous DCM, rt, 18 h, 62%; d) 2-phenylethan-1-ol, KOH, cat. 18-crown-6, toluene, rt, 3.5 h, 49%. Overall yield 13%. Shown next to the final product is its crystal structure from front and side angle, with pyridine group facing the viewer.

It became clear that the synthesised amide (**15**) was a poor model substrate for LSF reactions due to its low solubility in conventional reaction, purification and spectroscopic solvents, only dissolving fully in dimethylsulfoxide. This clearly limits its usefulness also as a drug candidate, and while the identification of a suitable hydroxylation reaction could offset this challenge, it was decided to focus attentions on the ether compound (**19**). The amide series had also displayed interaction with hERG,[47] a biological target associated with potential negative cardiovascular side-effects,[48] leading to the current prioritisation of the ether series in OSM.

We also synthesised a previously made active compound from the series, **20** (Scheme 7) when it was clear that multiple successive LSF reactions would likely be unsuccessful at forming a biologically active derivative from **19**. Starting material for this compound was produced by Mr. Edwin Tse through a similar route as **18**. We also obtained structural confirmation of this product by X-ray crystallography.

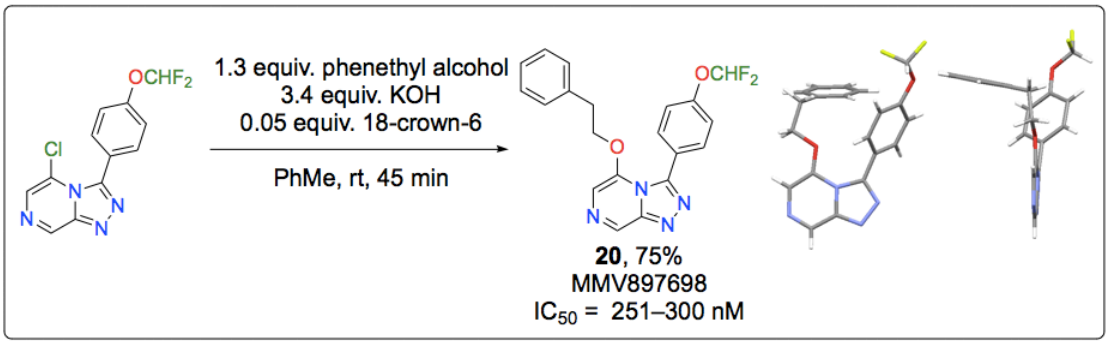

Scheme 6. Synthesis of **20**. Shown next to the chemical structure of the product is its crystal structure from front and side angles, with difluoromethoxyphenyl side-group facing the viewer.

A comparison was made between the structures of **19** and **20** to better understand the structural differences between active and inactive compounds in the series. We overlaid the X-ray structures of **19** and **20**, connecting them at their triazolopyrazine cores (Fig. 7). X-ray data was in agreement with density functional theory (DFT) calculations performed by an OSM contributor on a similar substrate, showing rotation of the difluoromethoxyphenyl side-group relative to the core.[49] Both **19** and **20** contain a phenethyl ether side group, shown in their crystal structures to be perpendicular to the core, but in opposing directions. This perpendicularity may be an important feature for binding. Further studies will be needed to examine the size of the local energy minimum to determine whether this structure might persist in solution. The angle between the planes of the pyridine and difluoromethoxyphenyl aromatic rings relative to the triazolopyrazine core suggests π-electrons are not significantly delocalised between the two aromatic systems. Further work is needed to determine conformation in aqueous solution, while SAR studies affecting changes to the carbon chain length of the ether attachment might provide evidence for the importance of the phenethyl ether's perpendicularity to the heteroaromatic core.

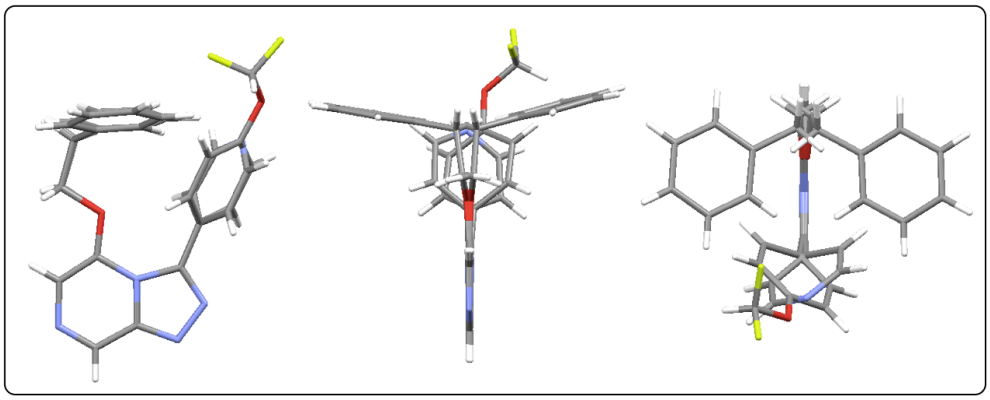

Figure 7. Crystal structure of the inactive compound, **19**, overlaid at the core with active compound **20**. Overlays shown from front (*left*), side (*middle*) and top (*right*) views.

2.1.3 Bexarotene

For the evaluation of new LSF methods, we sought to use another active compound, one rich with a diverse range of C–H bond types. Bexarotene (brand name Targretin, *Ligand Pharmaceuticals*) (Fig. 8, **21**), is a synthetic third-generation retinoidal drug sold as an anticancer agent for its ability to induce apoptosis in cutaneous T-cell lymphoma (CTCL).[50, 51] Bexarotene mimics the structure of an endogenous retinoid, 9-*cis* retinoic acid (Fig. 8), and has a higher selectivity for retinoid X receptors (RXR) over retinoic acid receptors (RAR) than 9-*cis* retinoic acid.[52] RXRs and RARs act as gene transcription factors,[52] the effect of which is highly dependent on the nature of the drug-bound RXR complex.[53] Recent studies have also reported the neuroprotective benefits of bexarotene and its derivatives in rodent models of Alzheimer's[54] and Parkinson's disease.[55, 56] A simple substitution of a single C–H bond in bexarotene could improve its ability to treat these diseases. For example, replacement of an aromatic hydrogen with a fluorine, as in **22** (Fig. 8), resulted in an improvement in the drug's selectivity for the RXR protein.[57] Compound **22** was synthesised *via de novo* techniques, but may have been identified faster by directly functionalising bexarotene with a late-stage non-selective fluorination.

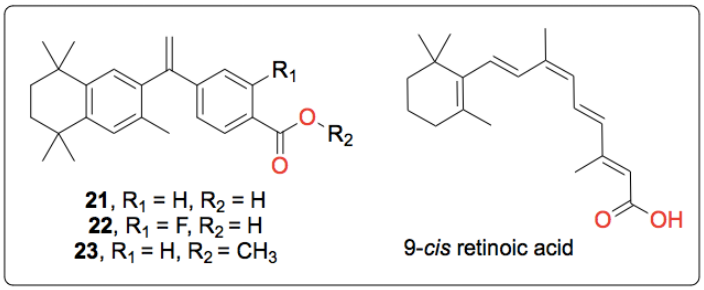

Figure 8. Chemical structures of bexarotene, **21**, a known fluorinated derivative of bexarotene, **22**, and as the methyl-protected form, **23**, to be used for LSF.

Unlike ibuprofen, which is inexpensive and readily available, bexarotene is a very expensive drug produced by a small number of manufacturers. It can be synthesised from three readily available starting materials; 2,5-dimethylhexane-2,5-diol **25** ($41/100 g, Sigma-Aldrich),[58] toluene ($57/L, Sigma-Aldrich)[59] and terephthalic acid **27**. ($42/500 g, Sigma-Aldrich)[60] through a convergent synthesis (Scheme 7).

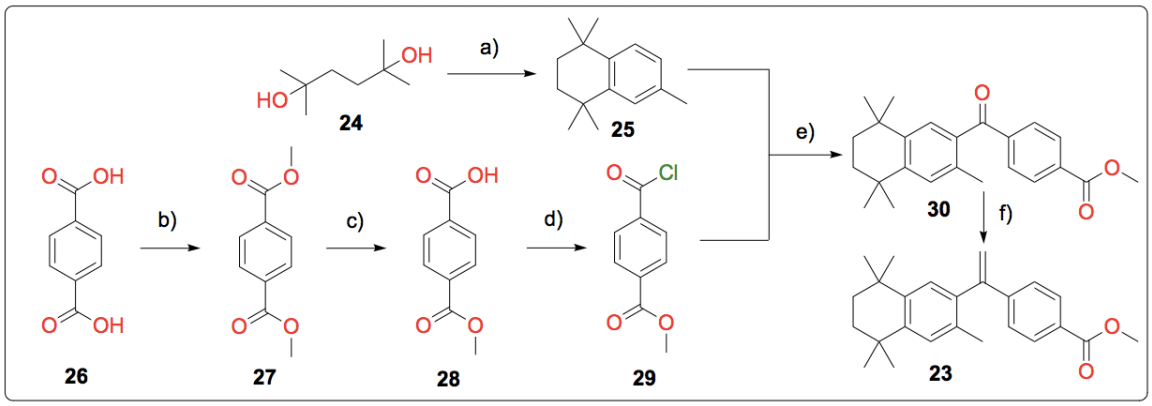

Scheme 7. Adapted literature synthesis of **23**. a) conc. $HCl_{(aq)}$, rt, 3 h, then, anhydrous PhMe, cat. $AlCl_3$, 0 °C to rt, o/n, 43%; b) $SOCl_2$ (excess), MeOH, 0 °C to reflux, o/n, 87%; c) KOH, MeOH, rt, o/n, 77%; d) $SOCl_2$, 0 °C to reflux, 3 h, isolated as crude, 105%; e) $AlCl_3$, anhydrous DCM, 0 °C to rt, 30 min, rt to reflux, 15 min, 22%; f) $CH_3P(Ph)_3Br$, sodium amide, anhydrous THF, 48 h, then, **30**, rt, 45 min, 13%. Overall yield 1.2%.

The final step, ester cleavage under basic conditions (not shown), can be saved for after LSF for reactions that require methyl ester protection. Friedel-Crafts alkylation using a catalytic amount of aluminium trichloride formed **25** in moderate yield (43%), while Friedel-Crafts acylation (with **29**, derived from **26**) using a stoichiometric amount of aluminium trichloride formed **30** in low yield (22%). Improving the yield of these reactions was complicated by the range of temperature and time conditions reported in the literature for both, which are often performed on a large scale (*ca.* 500 g) to form bexarotene.[57, 61] The modifications to the procedure we made included increased reaction time, adding the catalyst in smaller portions over a longer period, varying the reaction temperature from 0 °C to reflux, and using solvents dried over 3Å molecular sieves. Reasons for the low yield of **23** following Wittig alkenation of the ketone **30** are unknown. Preparation of the phosphonium ylide using sodium hydride was faster (1–3 *vs* 48 h) but led to more side-products in the reaction mixture than sodium amide. We found improvements in yield by azeotropically drying the methyltriphenylphosphonium bromide reagent with toluene. Use of a different base, such as *n*-butyllithium, to activate the ylide may be an avenue for improving yield. Unfortunately, the low overall yield of **23** ultimately obtained prevented our use of it as a substrate for LSF. Still, having solved several synthetic hurdles in this synthesis, it will be easier to synthesise **23** in a larger scale for evaluation in future LSF trials.

2.2 Design of Experiments

The term design of experiments (DOE) refers to the logical, systematic design of an experiment so that data can be best used to model the effect of different variables on a response.[62] Performing a series of experiments under different conditions, with each variable changed independently of the other, allows for more reliable, accurate inferences to be made.[62]

2.2.1 Why Design of Experiments?

A key use of DOE in chemistry is the optimisation of reaction yield. For example, a chemist may be performing a series of small-scale reactions to determine optimal conditions so that yield can be maximised (and costs reduced) for an industrial scale reaction process. For this reaction, the chemist has identified two factors, temperature (T) and time (*t*), as having a significant effect on reaction yield, and seeks to investigate their effect within the ranges of 0–40 °C and 0–60 minutes. The chemist may start from what they feel is an obvious starting point, identifying the optimal temperature for the reaction. It makes *intuitive* sense that the best way to assess the impact of some variable on a reaction is to hold all others steady, while seeing how the response changes across the variable's range. They begin by first varying temperature at a constant time of 60 minutes (Table 1), over five experiments. After finding their two highest yields 53.5% and 52.3% at 10 °C and 20 °C respectively, they then test four temperatures between this range (11, 12, 13 and 14 °C), and find they can produce a yield of 53.6% at 12 °C (Table 1, *left*, shown in green).

Table 1. Effects of temperature on yield at constant time (1 hour) (*left*). Effects of time on yield at constant temperature (12 °C) (*right*). Optimised conditions for each trial are shown in green. A total of at least 15 experiments were used to "optimise" the reaction to 55.6% yield.

First Round Run #	Temp (°C)	Yield (%)	Second Round Run #	Time (minutes)	Yield (%)
1	0	50.4	1	10	18.6
2	10	53.5	2	20	34.6
3	20	52.3	3	30	46.1
4	30	46.9	4	40	53.1
5	40	37.3	5	50	56.1
n	12	53.9	6	60	53.9

They move onto the next factor, time, and proceed in a similar fashion, holding temperature constant at 12 °C. They find their highest yield, 55.6%, at 50 minutes (Table 1, *right*, shown in green), and find no conditions on either side of this time that can produce a higher yield. The chemist believes they have *finally* optimised the reaction and can proceed with these conditions to an industrial scale.

However, by changing the two variables one factor at a time (OFAT), interactions between these variables cannot be accounted for. The yield for which they have optimised is heavily dependent on the conditions of the first experiments. They have optimised the reaction at 12 °C for 50 minutes. That is, they have only optimised towards a *local* maximum, not the *global* maximum. A better way to view their data would be using a graph (Fig. 9). It is clear that they have not succeeded in best charting the total reaction space, with significant areas lacking data. It is not valid for them to claim to have found the global maximum.

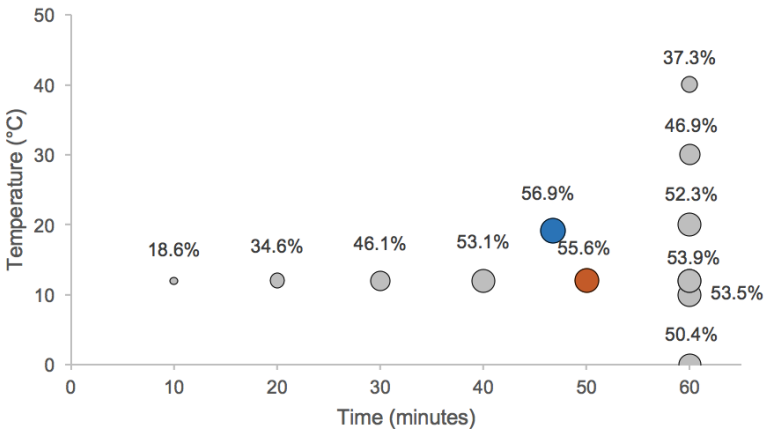

Figure 9. OFAT conditions surveyed (grey), with the local maximum (red) identified. The use of OFAT optimisation has meant that the chemist has missed a series of important data points, and so has not found the global maximum (blue) of the reaction.

A better way to optimise the reaction would be to change the two variables independently of one another, allowing for a full charting of the whole reaction space. Below (Fig. 10) is an example of such a series of experiments. As little as nine experiments (grey circles) are sufficient to map the total reaction space over the range of temperature and time given.

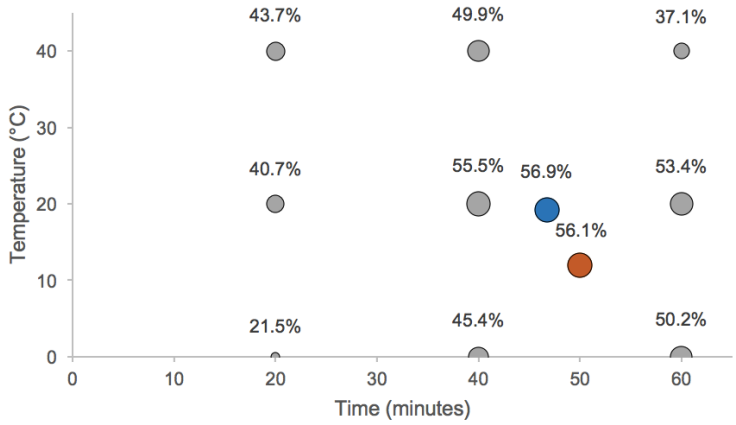

Figure 10. Grey circles are the nine experiments recommended by a DOE approach and allow for a more total coverage of the reaction space. Red circle is the local optimum achieved by the chemist using a OFAT approach. Blue circle is the global optimum as found by modelling the reaction space using regression analysis. Circle diameter is proportional to yield obtained.

One of the points assessed (20 °C, 40 minutes) has already succeeded in beating the previous "maximum" yield of 53.9%. Already, the chemist should be pleased that their work has been improved upon with fewer experiments: but we can go further still. With the nine experiments already performed, multiple linear regression software (*e.g.*, *Microsoft Excel*, see Ref. 64) can be used to find values for the reaction constant term ($ß_0$), coefficients of the linear terms for each variable ($ß_1$ and $ß_2$ for temperature and time respectively), the interaction term ($ß_{12}$) and the quadratic terms ($ß_{11}$ and $ß_{22}$ for temperature and time respectively), from which it can be shown (Appendix A.5) that a maximum yield of 56.9% may be obtained when temperature is 19.2 °C and reaction time is 46.7 minutes (Fig. 10 and 11, blue circle). The yield obtained through this method is not only higher than that of the OFAT approach (56.9% *vs*. 53.9%), but occurs at a temperature closer to room temperature, and with a shorter reaction time, allowing for cooling and labour costs to be reduced as well. This summarises the basics of a DOE approach and is not an exhaustive explanation of the complex field, for which in-depth texts are available.[63]

A DOE approach aids the chemist by not only optimising reaction yield, but also allowing for quantification of the significance of different variables involved in a reaction, as well as the degree to which these variables interact. It also reduces the total number of experiments required, allowing fewer resources to go further.

Most reactions have more than just two variables that affect yield. In this case, we can imagine an *n*-dimensional reaction space in which to chart their effect. The first step towards optimisation in the case where many variables exist is to identify those that most significantly

affect yield, allowing for some to be discarded in the following experiments to reduce the total number to be performed.

2.2.2 Reaction Non-Selectivity Score (RNS)

Whilst DOE is a useful tool for optimising a reaction for the maximum yield of a product it falters where multiple products are desired in equal yield. Our objective was to define a metric that could represent the success of a multiproduct forming reaction relative to ideal. This response variable can then be used to compare different reactions for their ability to form multiple products, or be used as the response variable to optimise a reaction using DOE.

In a reaction where starting material is converted into N products, it is evident that an ideal multiple-product reaction (from the point of view of an LSF protocol) should generate each product in equal yield, or $\frac{1}{N}$ x 100% yield for each product. An ideal success score, S_N, is calculated as the total product of each yield (expressed as a coefficient). Where $N = 4$, it is clear that S_4 is $(\frac{1}{4})^4$. In the below example, a reaction has formed three products, n_1, n_2, n_3 and n_4 with yields of 8%, 18%, 22% and 33% respectively. A comparison to ideal product formation can be made in three steps as follows:

1) Ideal Success Score (S_N)	2) Reaction Score (R)	3) Express as a ratio
$S_N = n_1 \times n_2 \times \ldots \times n_N$ $= (\frac{1}{N})^N$ $S_4 = (\frac{1}{4})^4$ $= 3.9 \times 10^{-3}$	$R = n_1 \times n_2 \times n_3 \times n_4$ $= 0.08 \times 0.18 \times 0.22 \times 0.33$ $= 1.0 \times 10^{-3}$	$\mathrm{RNS}(N) = \frac{R}{S_N} \times 100\%$ $\mathrm{RNS}(N) = 26\%$

The RNS metric is effectively a ratio of the experimental success of a multiple-product forming reaction (R), compared to success under ideal conditions (S). An ideal reaction will have an RNS(N) of 100%. This number can then be used to easily compare different or similar reactions for their ability to best form multiple products, or be used as the response variable for a DOE protocol focussed on optimising for multiple product formation.

3 Results and Discussion for LSF Reactions

With starting materials in hand, and a new protocol defined that could quantitatively express the effectiveness of an LSF reaction, we began to search for appropriate derivatisation methods. This section describes attempts towards the identification of methods for non-selective late-stage i) C–H azidation, ii) C–H hydroxylation, and iii) C–H fluorination and trifluoromethylation.

3.1 Progress Towards Non-Selective C–H Azidation

We focused on developing the previously mentioned aliphatic azidation reaction (Fig. 3) for non-selectivity for several reasons. First, the azide source (sodium azide, NaN_3) is inexpensive. Second, this methodology showed functionalisation at secondary as well as tertiary positions, allowing us to possibly expand its scope of regio-nonselectivity to primary positions as well. Third, selectivity when using the salen-type catalyst, rather than the porphyrin-type catalyst, was lower. Fourth, salen-type catalysts are less expensive and easier to synthesise than porphyrin catalysts. Fifth, the opportunity of isolating oxidative side-products as well as azidation products would allow us to extend our research from regio-nonselectivity to chemo-nonselectivity. This reaction presented an exciting opportunity to investigate how a reaction may be optimised towards non-selectivity using DOE.

It is important to note however, that the reaction is not an "ideal" LSF reaction, in that it still requires the use of protecting groups for some functional groups. The reaction would oxidise secondary alcohols to ketones, for example, so benzyl-group protection was required, while amines required protection (*e.g.,* with the Boc group), likely (though this was not explored) due to catalyst poisoning. Carboxylic acids were protected as their methyl ester, and phenolic groups were acetylated. Still, the reaction tolerated a wide range of functionalities found in drug-like compounds, such as amides, esters, ketones, carbamates, tertiary alcohols, terminal alkynes, and heteroaromatics like pyridine, thiophene and pyrimidine. The reaction even tolerated the sensitive peroxide group, as found in artemisinin.

After synthesising the oxidant iodosylbenzene (**32**) by base hydrolysis of (diacetoxy)iodobenzene (**31**) in good yield (88%, Scheme 6, a), we attempted to replicate the high yields of N_3–ibuprofen methyl ester (67%, Scheme 8a, **4)** described in the paper. These attempts were complicated by a lack of any *specific* protocol for the published work, with only a range of conditions for reagent addition, catalyst addition and timing provided. Our first

attempt (2 equivalents iodosylbenzene, 5 mol% Jacobsen's (*R*,*R*) catalyst, 2.4 equivalents sodium azide, room temperature, four hours) resulted in 13% yield of the azide and 58% yield of the ketone product with an RNS(2) of 30%. OFAT trials improved the yield of azide product to 24% but reduced ketone product to 41% with an RNS(2) of 39%, but further OFAT trials would be a tedious and time-consuming way to a higher RNS. We hypothesised that it should be possible to optimise this azidation reaction for a high yield of multiple products by first determining the factors which most affect the reaction's non-selectivity.

Before turning to a DOE approach, we thought it important to further investigate one of the discontinuous variables: type of catalyst. The salen-type (Jacobsen's) catalyst used by the original authors to perform aliphatic azidation is chiral, and contains several large, bulky groups. These groups were originally used to promote dissymmetry in the catalyst-substrate transition structure in the epoxidation of olefins.[70] We hypothesised that by removing these groups, we may be able to access a greater range of positions (regio-nonselectivity) across our model substrate, by reducing steric hindrance involved in the hydrogen-abstraction transition state. We conducted a study to determine: 1) whether an achiral non-bulky salen catalyst could produce the desired azide product; 2) whether this catalyst had reduced selectivity compared to the more sterically hindered Jacobsen's catalyst, and 3) whether catalysts made using the same achiral non-bulky salen-ligand, but with different first-row transition elements of the same valency, would be able to affect the reaction's non-selectivity.

There is an extensive body of work that demonstrates the ability of porphyrin and salen-ligand catalysts containing first-row transition elements to catalyse oxidations at C–H bonds. Most of this work has focussed on improving their selectivity. Porphyrin catalysts containing iron, manganese, cobalt and chromium centres have demonstrated ability to catalyse the hydroxylation of cyclohexane, with the iron catalyst showing the highest activity.[64] Oxochromium(V) and oxomanganese(V) bound to salen ligands can catalyse the formation of epoxides, with their activity enhanced by the addition of pyridine *N*-oxide.[65, 66] Iron-containing porphyrins have also been shown to catalyse the formation of epoxides and alcohols from allylic substrates,[67, 68] and regiospecifically hydroxylate simple hydrocarbons at C–H bonds.[69]

We synthesised four non-bulky catalysts containing manganese(III), cobalt(III), iron(III) and chromium(III) centres. The Mn(III)(salen)Cl (**33**) and Co(III)(salen)Cl (**34**) catalysts were synthesised from the original literature procedure[70] in low yields (7 and 30% respectively) possibly because of extensive washing and recrystallisation steps that were carried out to ensure purity (Scheme 8b). The other two catalysts, Fe(III)(salen)Cl (**35**) and Cr(III)(salen)Cl (**36**), were synthesised according to a more recent procedure.[71]

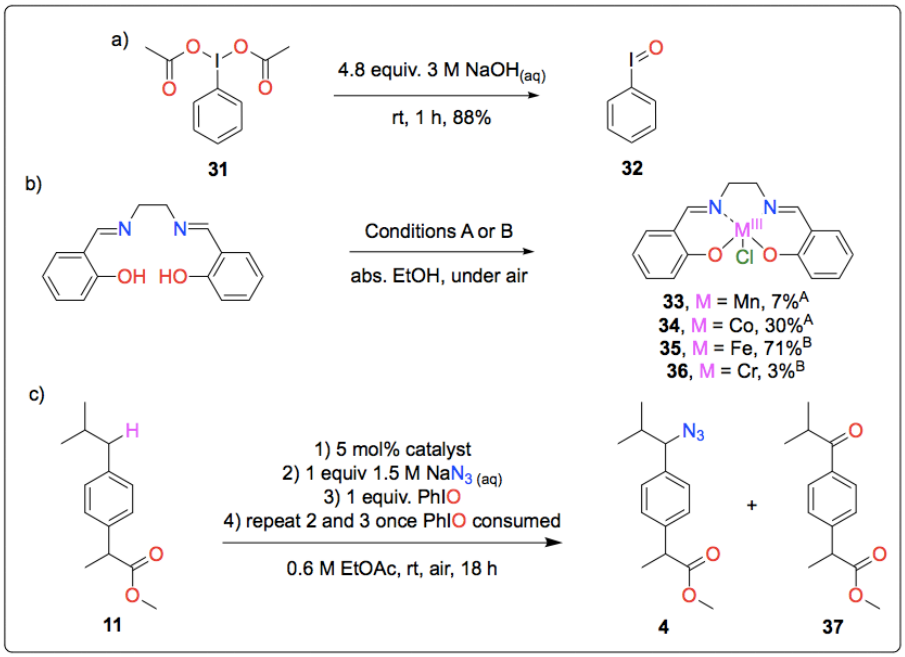

Scheme 8. Progress towards non-selective aliphatic azidation of ibuprofen methyl ester, including the synthesis of reagents and catalysts used. a) Base hydrolysis of (diacetoxy)iodobenzene, **31**, to form iodosylbenzene, **32**, in 88% yield. b) Synthesis of salen-type catalysts **33**–**36** using one-pot protocols. Conditions A: 2 equivalents metal(II) acetate, reflux, 1 h; then, 3 equivalents lithium chloride, reflux, 30 min. Conditions B: 1.1 equivalents metal(III) chloride, reflux, 1h; then 2 equivalents triethylamine, reflux, 30 min; then rt o/n. All yields are for recrystallised samples. c) Conditions used to determine which catalyst could least-selectively form **4** and **37** least selectively.

We trialled each catalyst's ability to perform aliphatic azidation on **11** to form **4** and **37** (Scheme 8c). A small amount of these mixtures was prepared for liquid-chromatography mass-spectrometry (LCMS) analysis. LCMS was used as we had hoped to discover the formation of regioisomers of azide and oxidation products, which would appear as ions of the same mass, but with (hopefully) different retention times on the column. Electrospray ionisation (ESI), and a mobile phase of acetonitrile/water with 0.1% formic acid were used as defaults. Conversion was determined by integrating the area under curve (AUC) at 254 nm at retention times determined by running standards of starting material, azide and ketone products, and then subjected to the RNS protocol to determine the least selective catalyst (Table 2). Areas were not calibrated to a standard curve in this initial screen.

Changing the catalyst ligand significantly affected conversion, with both the manganese(III) (Entry 3) and iron(III) (Entry 4) salen-type catalysts providing conversion to azide product. Under these conditions Jacobsen's catalyst (Entry 1) did not significantly form azide product (< 1%) from starting material. However, conversion of starting material to the ketone product when using Jacobsen's catalyst was still higher than when no catalyst was used

(92% *vs*. 57%), suggesting that the catalyst was active, just less selective towards azidation under these conditions. The RNS when using the iron(III) catalyst was more than twice that of the manganese(III) catalyst, reflecting its lower selectivity. The chromium(III) (Entry 2) and cobalt(III) (Entry 5) catalysts both effected higher conversions to the ketone product than control (78% and 72% respectively *vs*. 57%), but less than the manganese(III) and iron(III) catalysts.

Table 2. Results from metal ion assay. Remaining starting material (blue) and conversions to benzylic azide and benzylic ketones products are shown. Conversions and RNSs greater than 5% are shown in green, while those lower than 5% are shown in red.

Entry	Catalyst	Remaining starting material (%)	Benzylic azide product (%)	Benzylic ketone product (%)	RNS (%)
1	Jacobsen's (*R,R*) catalyst	7.8	< 1	92	< 1
2	Cr(III)(salen)Cl	22	< 1	78	< 1
3	Mn(III)(salen)Cl	6.4	2.4	91	8.9
4	Fe(III)(salen)Cl	12	5.4	83	19
5	Co(III)(salen)Cl	28	< 1	72	< 1
6	No catalyst (control)	43	< 1	57	< 1

We did not observe regioisomers in this assay (as products of different retention time but the same mass), either due to co-elution or very low conversion. It may also be evidence that functionalisation was not taking place on the molecule elsewhere besides the isobutyl benzylic position. The electron-deficiency of the active metal(V)-oxo catalyst intermediate favours hydrogen abstraction at electron-rich positions.[31] Functionalisation at only the isobutyl benzylic position may have been due to its electron richness, compared to the benzylic hydrogen near the electron-withdrawing ester, highlighted by its appearance further downfield in the ^{1}H NMR spectrum of the substrate (3.69 *vs*. 2.44 ppm). The presence of regioisomers was checked by examining the crude reaction product with ^{1}H NMR spectroscopy. The results indicated that we have in this case *not* overcome the inherent reactivity of the substrate for isobutyl benzylic functionalisation.

These results were still promising, as they showed that not only could a less bulky salen-ligand catalyst catalyse the formation of azide and ketone products, but that a change of the

metal-centre from manganese(III) to iron(III) performed this with lower selectivity. We carried through the iron(III) catalyst to the next part of our optimisation procedure, using DOE to determine the most significant variables involved in reaction non-selectivity.

The first step was to define which factors we would vary, and the range within which we wanted to test. Since the range of conditions given by the original paper's general procedure included the amount of catalyst, equivalents of azide and oxidant, and the length of the reaction, we included these in our design, as well as temperature, reaction concentration and sodium azide solution concentration. We did not explore pH as a variable due to the potential of forming the highly toxic and explosive gas, hydrazoic acid (HN_3), under acidic conditions. As the experiment performed iterative additions of the oxidant and azide source (this would have been difficult to control across the range of variables), we decided to perform a total of three additions of these reagents, evenly spaced. We used a balanced central composite design (CCD) with $k = 3$ and $\alpha = 1.41$ with three centre runs (Table 3 and 4).[i] Runs were randomised to reduce experimental error. Appropriate ranges were chosen for upper and lower limits, but some were narrowed for safety and practical reasons, *e.g.*, limiting temperature to between 0 and 60 °C due to the risk of explosive decomposition, or reducing time from 24 to 9 hours to avoid overnight aliquot removal.

Table 3. Conditions, ranges and levels used to identify significant variables by DOE.

Conditions	**Levels**				
	Lower limit (–α, –1.41)	–1	0 (Control)	+1	Upper limit (+α, 1.41)
Solution molarity (M)	0.10	0.24	0.30	0.51	0.60
Catalyst (mol%)	2.5	4.3	5.0	8.5	10
Equivalents of azide	1.1	2.4	3.0	5.1	6.0
Sodium azide solution molarity (M)	1.0	2.4	3.0	4.4	5.0
Equivalents of iodosylbenzene	1.1	2.4	3.0	5.1	6.0
Temperature (°C)	0	17	24	49	60
Time (h)	1.0	3.8	5.0	7.8	9.0

[i] Immediately before submission of this thesis it was noticed that the value for α used in these calculations should have been 1.68 rather than 1.41. Use of the correct value leads to only minor changes in levels used (e.g. solution molarity of 0.22 *vs* 0.24 M) and does not qualitatively change the conclusions in this section of the thesis. See Appendix A.6 for corrected table.

We conducted these runs using a similar methodology as the metal-ion assay, but on a smaller scale (20 mg). Temperature control for the 49 °C condition was maintained by stirring the reaction vials (2 mL) on a heated aluminium block, while the 17 °C condition was controlled by placing the reaction vials in sand cooled by a condenser hose containing water at 10 °C. A thermometer linked to a heating element was then inserted into the sand to maintain the temperature at 17–18 °C (Appendix A.7).

Table 4. Experimental design matrix showing conditions used across eight runs, with positive deviations (+1) in red, and negative deviations (–1) in blue. Main effects of each variable are shown with their significance as determined by two-tailed Student's *t*-distribution ($df = 2$).

Run #	Conditions						
	Solution molarity	Equivalents of catalyst	Equivalents of azide	Azide molarity	Amount of oxidant	Temperature	Time
1	–	–	–	–	+	+	+
2	–	–	+	+	–	–	+
3	–	+	–	+	–	+	–
4	–	+	+	–	+	–	–
5	+	–	–	+	+	–	–
6	+	–	+	–	–	+	–
7	+	+	–	–	–	–	+
8	+	+	+	+	+	+	+
Main Effect	0.99	2.7	3.1	0.77	4.5	– 0.93	–1.0
Significance	0.006	0.001	0.001	0.009	0.000	0.006	0.005

Runs 4 and 8 (Table 5) both had the two highest RNSs (7.8 and 7.6% respectively), representing conditions most favourable to non-selectivity. Most interestingly, these two runs had near perfectly inverse azide to ketone product ratios of 0.49 and 2.1 respectively, showing that selective formation of either product is possible by tuning reaction conditions. Similar RNS for these runs reinforces that it is not important what the product actually *is* for a high RNS score, simply that yields are distributed in preparatively useful amounts.

Table 5. Conversion (%) of products from starting material across runs, and their RNS. Conversions and RNSs less than 5% are shown in red, while those more than 5% are shown in green.

Run #	Benzylic azide (%)	Benzylic ketone (%)	RNS (%)
Control (n = 3) (SD)	2.4 (0.40)	3.1 (0.74)	< 1
1	< 1	1.5	< 1
2	4.9	1.6	< 1
3	1.9	< 1	< 1
4	9.8	20	7.8
5	15	6.4	3.8
6	15	1.1	< 1
7	8.3	< 1	< 1
8	20	9.6	7.6

Each variable significantly affected the reaction's non-selectivity. Of these, the most significant was the amount of oxidant, followed by amount of azide, and then the amount of catalyst (main effects 4.5, 3.1 and 2.7 respectively). Each was positive: therefore values higher than control improve reaction non-selectivity. Interestingly, both temperature and time had *negative* main effects, suggesting that temperatures and times less than control improve reaction non-selectivity. This may reflect instability of the azide product to decomposition with higher temperatures and reaction times, or decomposition of the catalyst.

These results were encouraging as they demonstrated that each variable had significant effects on the response as measured by their RNS. Use of DOE coupled with our RNS protocol allowed for the identification of un-intuitive trends, such as lower temperature improving reaction non-selectivity. More experiments are required however, to determine the interactions between these variables. Since each variable was found to be significant, 14 more experiments (not including controls) are required to obtain the necessary data to fully optimise this reaction for non-selectivity (Appendix A.8). These experiments were not performed due to time constraints. Having demonstrated it is possible to determine reaction non-selectivity in this way, it was thought more useful to apply this strategy to a more realistic substrate for LSF.

3.2 C–H Hydroxylation

The late-stage installation of a hydroxyl group (-OH) into a drug-like molecule is a major area of research within the field of LSF. Hydroxylation can improve a lead compound's drug-like

properties by increasing hydrophilicity, or by providing hydrogen bond donor and acceptor motifs to the molecule to better affect target-binding. As a reactive polar protic group, hydroxyl typically requires protection when installed in earlier stages. Despite the obvious advantages of a late-stage method of C–H hydroxylation, there are still only a few methods able to perform such a transformation under mild conditions.

We sought to employ hydroxylation strategies against compounds from OSM Series 4, rather than ibuprofen methyl ester (**11**), with the hopes of producing a more 'realistic' drug-like derivative. A current key issue with the OSM Series 4 compounds is their poor hydrophiliciity, which may be improved by hydroxylation. To produce a hydroxylated derivative we used two catalyst-based strategies, and two reagent based strategies. The first catalyst, Fe(II)PDP (AKA Chen-White catalyst, **5**) was chosen for its ability to hydroxylate unactivated sp^3 C–H positions on complex molecules with *high* regioselectivity.[72] Prior to the synthesis of this catalyst, late-stage hydroxylation at sp^3 C–H bonds in complex substrates had only been demonstrated on activated positions either next to heteroatoms or π-systems,[41] or by using directing groups.[73, 74, 75] The ligand (**38**) for **5** was synthesised according to reported procedure *via* the alkylation of (2*R*,2'*R*)-2,2'-bipyrrolidine with 2-picoyl chloride under basic conditions in 65% yield (Scheme 9).[72] Metal complexation of the ligand using iron(II) chloride proceeded in 67% yield, while counterion metathesis of the precatalyst **39** using silver(I) hexafluoroantimonate to form the final product occurred in 96% yield. This final step is required to activate the catalyst to the catalytically active electrophilic cation.

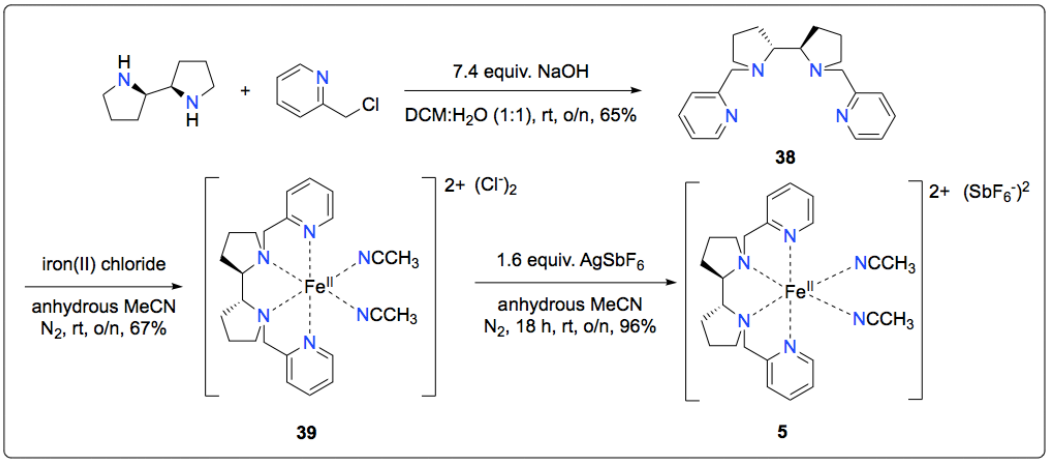

Scheme 9. Synthesis of the Chen-White catalyst, Fe(II)PDP (**5**), to be used as an aliphatic hydroxylation catalyst. Yield given for **5** is following recrystallisation.

The TPA (**40**) ligand for **6** was synthesised in a one-pot procedure.[76] First, 2-(aminomethyl)pyridine reacts with pyridine-2-carboxaldehyde to form an imine, which is

reduced by sodium triacetoxyborohydride to form a secondary amine. The secondary amine reacts with another pyridine-2-carboxaldehyde to form an imine, which is then reduced by sodium triacetoxyborohydride to form **40** in 61% yield. Metal complexation using iron(II) triflate gives **6** in 40% yield after recrystallisation.

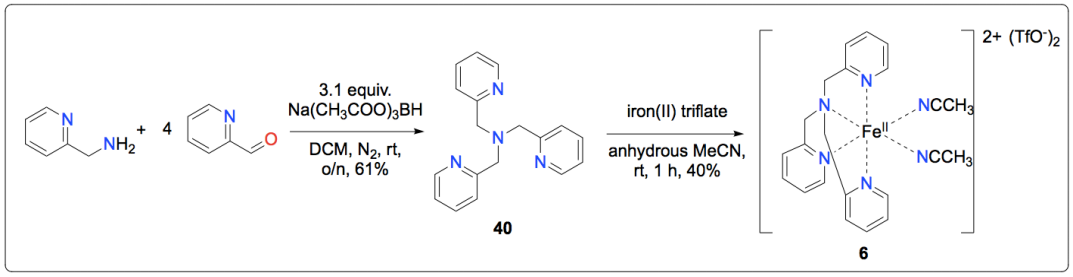

Scheme 10. Synthesis of Fe(II)TPA (**6**), to be employed as a comparison hydroxylation catalyst system with Fe(II)PDP, to determine whether it can afford lower selectivity than Fe(II)PDP (**5**).

The two catalysts were tested under the same conditions using an iterative addition protocol, with oxidation predicted at the benzylic position (Scheme 11).[72] Unfortunately, under these conditions neither of these catalysts were successful in producing a derivative of an OSM Series 4 compound. Examination of their crude ^{1}H NMR spectra showed broad and poorly defined peaks, suggesting decomposition of the substrate. Formation of the pyridine-*N*-oxide was not observed either by NMR spectroscopy. Starting material (58%) was reclaimed from the reaction using Fe(II)TPA as catalyst, with none reclaimed using Fe(II)PDP. Longer reaction times and slower oxidant addition did not affect the outcome.

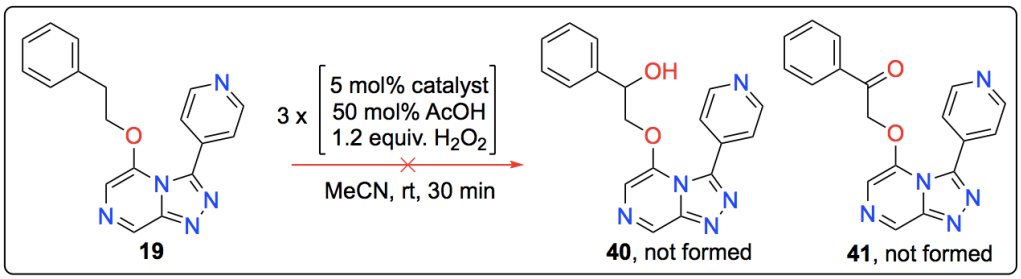

Scheme 11. Attempted hydroxylation of **19** using Fe(II)PDP (**5**) and Fe(II)TPA (**6**) as catalysts. Expected oxidative products **40** and **41** were not identified.

With the failure of using catalytic methods to functionalise the substrate, we turned to a reagent-based method. Dimethyldioxirane (DMDO) (**42**) and methyl(trifluoromethyl)dioxirane (TFDO) (**43**) are three-membered ring peroxides, used as effective mild oxidising reagents with a wide variety of applications. Due to their sensitivity to heat and light, they are usually synthesised in low yield in a dilute solution with

acetone/trifluoroacetone, by oxidation of acetone/trifluoroacetone with oxone (AKA potassium peroxymonosulfate) (Scheme 12). The volatile product is collected at –78 °C as a distillate *via* a cold finger (Appendix A.8). Care must be taken to ensure glassware is free of any trace metal contaminants.

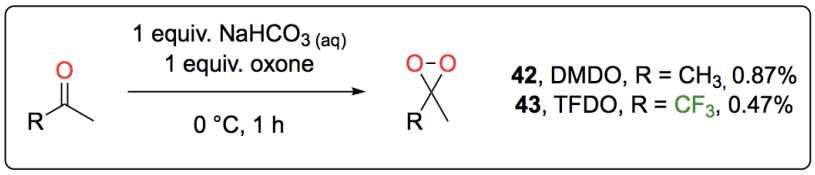

Scheme 12. Synthesis of DMDO (**42**) and TFDO (**43**) from acetone and trifluoroacetone using oxone.

DMDO has previously demonstrated direct mono- and polyhydroxylation of activated and unactivated C–H bonds under mild conditions through electrophilic oxygen atom transfer.[41, 77, 78] Aromatic ring hydroxylation and polyhydroxylation of electron-rich flavanones has also been demonstrated in neutral and acidic media using an excess of DMDO.[79] The reagent can perform other oxidations, such as, but not limited to, oxidising secondary alcohols to the corresponding ketone, *N*-oxide formation, and epoxide formation from alkenes and polycyclic aromatics.[77] TFDO is a similar oxidant to DMDO, but is more electrophilic due to the highly electron-withdrawing CF_3 group, making it a useful alternative where DMDO fails. TFDO can also form dialdehydes from benzene or oxidise primary alkylamines to cyclic products.[78] DMDO and TFDO perform these oxidations with high retention of stereochemistry (>99%) when the substrate is chiral.[80]

Attempts at using DMDO to afford a hydroxylated product of an OSM Series 4 compound were unsuccessful, with no conversion of starting material taking place. However, TFDO produced an oxidised derivative of **20** in low yield (23%) (Scheme 13). The ESI mass spectrum of the isolated product showed a parent peak ion at *m/z* 399, which is a mass increase of 16 and consistent with the addition of a single oxygen atom to the molecule. Analysis by ^{1}H NMR spectroscopy showed loss of the most downfield proton, previously shown to correspond with the C8 position,[81] however assignment of the spectrum was difficult due to the presence of broad peaks, and peaks with integrals less than unity. The ^{13}C NMR spectrum of the product contained more peaks than expected. We hypothesised that this may be due to the presence of both tautomers **46a** and **46b** in solution.

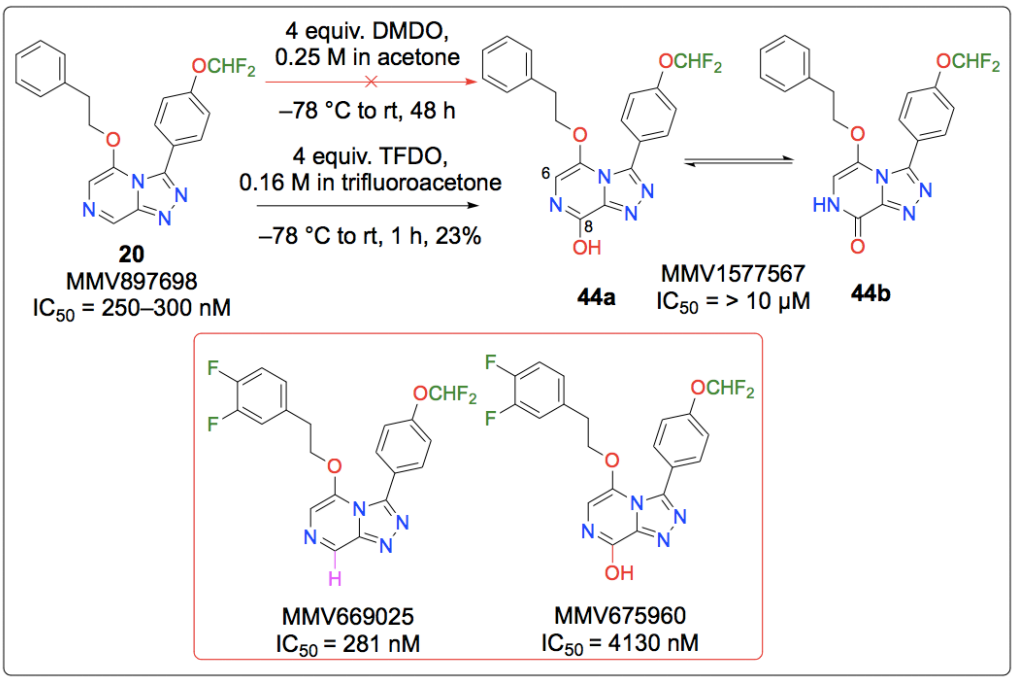

Scheme 13. Attempts to form an oxidised derivative of **20** using DMDO (**42**) and TFDO (**43**), the latter of which successfully formed derivative **44**. Starting material (60%) was recovered from the reaction. Below is shown a similar substrate to the starting material, MMV669025, and its hydroxylated derivative, MMV675960. Similar to hydroxylation of the C8-position as in **44**, activity of the derivative was reduced compared to the parent compound.

When **44** was evaluated for biological activity, it was found that activity was completely lost (> 10 μM), compared to the starting material (250–300 nM).[82] Functionalisation at this position in a similar substrate has also been shown to reduce activity, as compared to the unfunctionalised derivative (Scheme 13, red border).[83, 84] However, the data for these compounds was inherited by OSM from a private company and for which no spectroscopic data were available to validate the structure tested. The data obtained here therefore strengthen the series' SAR showing functionalisation at the C8 position is expected to reduce activity, compared to the parent compound.

Given that an excess of oxidant was used, the reason for the low yield of product was unknown. We hypothesised that an *N*-oxide catalysed decomposition of the reagent may be occurring, forming molecular oxygen and acetone/trifluoroacetone as products (Scheme 14), following previous research that shows that DMDO can deoxygenate tertiary amine-oxides.[85]

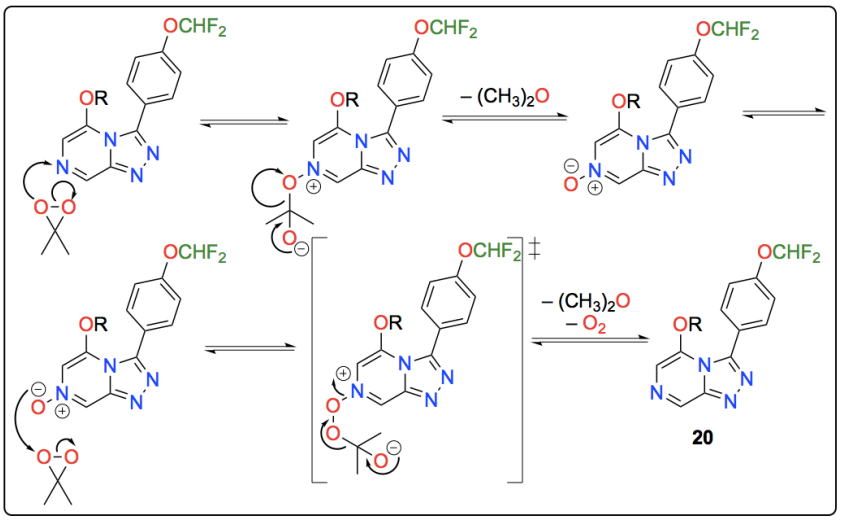

Scheme 14. Potential catalytic decomposition of DMDO (or TFDO) through *N*-oxidation of **20**.

3.3 C–H Fluorination

As we have shown that derivatives of an OSM Series 4 compound may be produced by LSF, we turned our sights to a new transformation, the introduction of fluorine into a molecule. We first examined the use of the organic N–F bond-containing fluorinating agent, NFSI (Fig. 5c, **8**) using ibuprofen-methyl ester as a model compound, to see if any multiple-fluorinated products could be derived in a simple case. We succeeded in replicating a LSF methodology that uses the photocatalyst tetrabutylammonium decatungstate ($(NBu)_4W_{10}O_{32}$, TBADT) to monofunctionalise selectively the benzylic-isobutyl position with a fluorine atom with 60% conversion according to an analysis of the crude reaction mixture by ^{1}H NMR spectroscopy (Scheme 15).[86] The active catalytic species is the polyoxometallate decatungstate anion, synthesised from tetrabutylammonium bromide and sodium tungstate under basic conditions in good yield (68%). Excitation of the decatungstate anion with UV-light ($\lambda \sim 350$–400 nm) causes a ligand-to-metal charge-transfer to form a locally excited state, which quickly decays to a relaxed excited state that has oxyradical-like character, due to electron-deficient oxygen-centres.[87, 88] The excited state of the catalyst in acetonitrile can be observed as a colour change from clear or cloudy white to a deep blue hue that stays for several minutes following removal of UV light (Appendix A.9). This oxyradical-like decatungstate species has high reactivity towards organic substrates, capable of forming carbon-centred radicals *via* HAT at aliphatic positions (Appendix A.10). Homolytic cleavage of the weak N–F bond in NFSI allows for electrophilic attack of the substrate radical intermediate by the fluorine atom, while HAT from the catalyst to the fluorine donor completes the catalytic cycle.

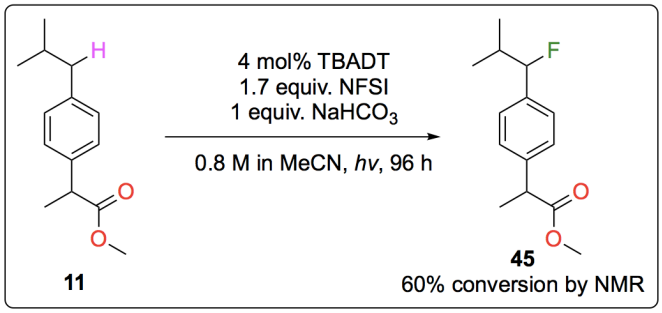

Scheme 15. TBADT-catalysed fluorination of ibuprofen methyl-ester using NFSI as fluorine source.

Attempts to extend the selectivity from the benzylic position to other carbons in the substrate by OFAT alteration of variables such as reaction time, concentration, catalyst loading and fluorine equivalents did not result in improved non-selectivity. Further, substituting NFSI with the reagent Selectfluor resulted in no conversion. Conditions resulting in highest conversion are reported. Rigorous degassing of the solvent by several freeze-pump-thaw cycles and a long reaction time (4 days) were required to afford good conversion.

Extending this reaction to the OSM Series 4 compounds **19** and **20** was not successful. Reaction under the same conditions did not progress, with no new peaks observed in the ^{19}F NMR spectrum of the crude reaction mixture. A small amount of an uncharacterised, intractable mixture of non-fluorine containing products eluted in hexanes. Electrophilic heteroaromatic fluorination using silver(II) fluoride in acetonitrile did not generate a fluorinated derivative of **19** or **20** either,[37] however the scope of substrates used in the original procedure did not include electron-rich heterocycles.

As an alternative to reactions which form C–F bonds, we investigated strategies for the formation of the C-CF_3 group instead. Since a major concern of the OSM Series 4 compounds is their high lipophilicity, trifluoromethylation may still provide important new SAR data and permit the probing of positions on the molecule that are important for metabolic clearance.

Radical trifluoromethylation methodologies have been known for some time. The $^{\bullet}CF_3$ radical can be generated thermally from trifluoroiodomethane (CF_3I) and can then be used to functionalise aromatic rings.[89] This methodology *might* be amenable to a LSF strategy, but sadly the reagent is harsh to both the substrate and the chemist: CF_3I is a highly toxic gas and one that it is preferable to avoid if possible. Instead, we followed a recent modification[90] of an older radical trifluoromethylation reaction,[91] which uses sodium trifluoromethanesulfinate (Fig. 5f, **9**) as the reagent. The report describes the trifluoromethylation of 2-methylquinoxaline (Scheme 16) in which reasonable yields of up to four different products were obtained, providing an excellent starting point for a diversification strategy. The suggested mechanism

was through an electrophilic radical substitution. The cause of the radical initiation step to form the *t*-BuO• radical was unclear, but trace metals were suggested as a source. With the *t*-BuO• radical generated, the trifluoromethanesulfinate anion is attacked to form a radical, which decomposes to sulfur dioxide and the required •CF_3 radical. The •CF_3 radical can then attack the heteroaromatic system. The •CF_3 radical is strongly electrophilic, and unlike the planar •CH_3 radical, is pyramidal.[92] The strong electrophilicity of the •CF_3 radical, due to the high electronegativity of the fluorine and its low-lying singularly occupied molecular orbital (SOMO) as a result, means it reacts faster with electron-rich positions.[62] However, the reaction is less selective than zinc-based radical fluoroalkylation reagents.[93]

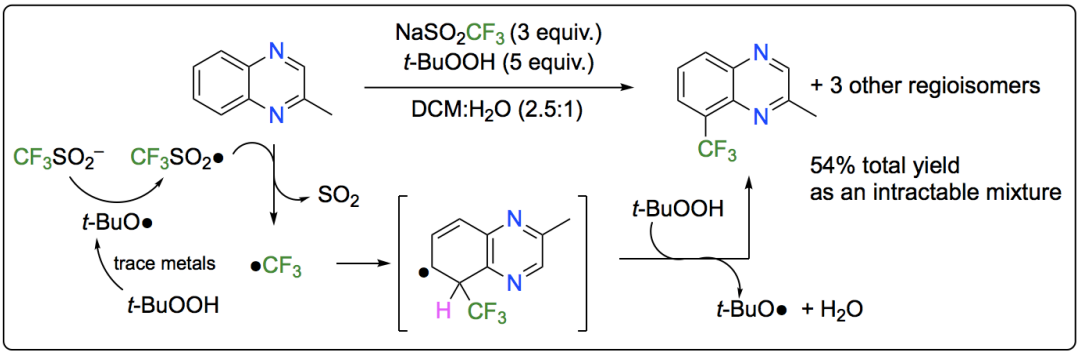

Scheme 16. Literature trifluoromethylation of 2-methylquinoxaline using sodium trifluoromethanesulfinate (**9**) under oxidative conditions, resulting in an intractable mixture of regioisomers.[40]

We applied this reaction to our model compound **19**, to assess the regioselectivity of the reaction on a compound with more than one heterocycle. Two additions of sodium trifluoromethanesulfinate (7 equivalents) and two additions dropwise of *tert*-butylhydroperoxide (12 equivalents) yielded a single major product in 29% yield after 48 hours' reaction time (Scheme 17).[90] The second addition was performed due to the presence of remaining starting material after 24 hours (as judged by TLC analysis of the reaction mixture). Our low yield of product (29%) and the recovery of a small amount of starting material (16%), despite addition of excess reagent, suggested there were other decomposition pathways occurring. The structure of the major product was proven by X-ray crystallography, generating the first structure of a Series 4 compound derived from a late stage functionalisation. The structure showed that functionalisation had again occurred at C8 (Scheme 17, d). The X-ray structure of the starting material was also obtained (Scheme 17, b), and a comparison between the two (Scheme 17, c) showed minor changes to the molecule conformation resulting from the substitution of the aromatic hydrogen with the CF_3 group, for example the dihedral angle between the planes occupied by the triazolopyrazine and pendant aromatic rings. Determination

of the absolute structure of both molecules is useful for more than just characterisation and may provide insight into how these compounds interact with their target. When **46** was evaluated for biological activity, it was found to have no activity (> 10 μM).

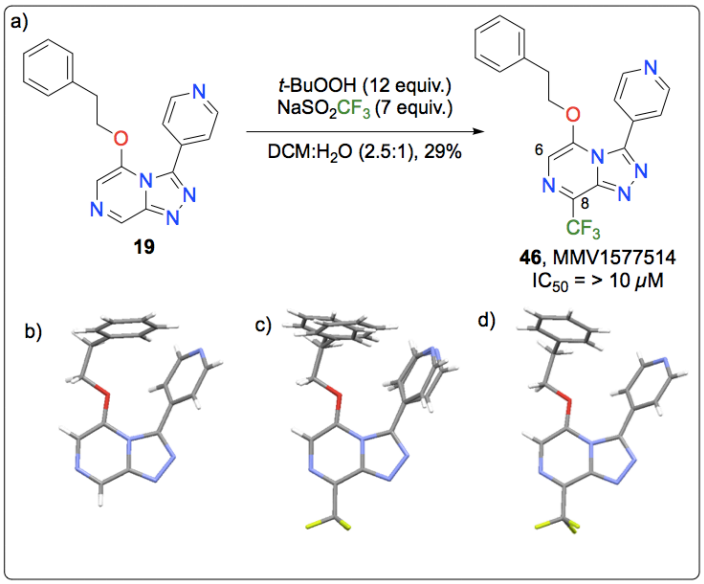

Scheme 17. a) Trifluoromethylation of **19** using sodium trifluoromethanesulfinate (**9**) under oxidative conditions to form **46** b) X-ray crystal structure of **19**. c) Overlay of X-ray crystal structure of **19** and product, **46**. d) X-ray crystal structure of product, **46**.

^{19}F NMR spectroscopy of the crude reaction mixture showed trace amounts of other fluorinated material, with a single main singlet peak at δ –66.64 ppm, while baseline spots and streaking visualised on TLC further supported the idea of competitive pathways. A possible source of side-products is from the decomposition of the *tert*-butylhydroperoxide to isobutene, leading to a fluoroalkyl radical adduct that can add itself to aromatic rings (Scheme 18),[90] though such species were not specifically identified in our procedure.

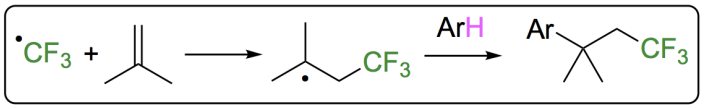

Scheme 18. Potential formation of fluoroalkyl side-products from *tert*-butylhydroperoxide decomposition.

We did not isolate any other major products, unlike the findings of the original authors for several substrates.[40] To understand why the regioisomer isolated was the major product, an appreciation of the sterics and electronics of the reaction was considered. First, the heteroaromatic core is more electron rich, as compared to the pyridine ring: the electronegativity of the pyridine nitrogen makes the adjacent C–H bonds comparatively electron poor, while the two C–H groups of the core benefit from electron donation through the

ether side-group. It may be further stabilised through delocalisation of π-electrons from the adjacent triazolo ring. For this reason, the heteroaromatic core may be more prone than the pyridine side-group to attack by an electrophilic radical such as $^{\bullet}CF_3$.

Second, the resonance structures generated from attack at the C8-position may be more stable than those derived from attack at the C6-position (Fig. 11). Attack at the C6-position generates a structure for which there are two resonance forms with partially-positively charged radicals (on the ring-nitrogen and on the ether-oxygen). The electron deficiency of these atoms in these resonance forms destabilises these structures. Attack at the C8 position is comparatively more stabilised, resulting in resonance forms with a partially-positive radical on only the oxygen: the nitrogen-centred radical occurring from attack at the *para*-position is stabilised by favourable π-system interactions from its remaining lone-pair.

Third, approach of the $^{\bullet}CF_3$ radical to the heteroaromatic ring may be affected by steric factors (principally the phenyl ethyl ether group); the high barrier to inversion of the pyramidal $^{\bullet}CF_3$ radical may slow substitutions where steric factors are involved.[92]

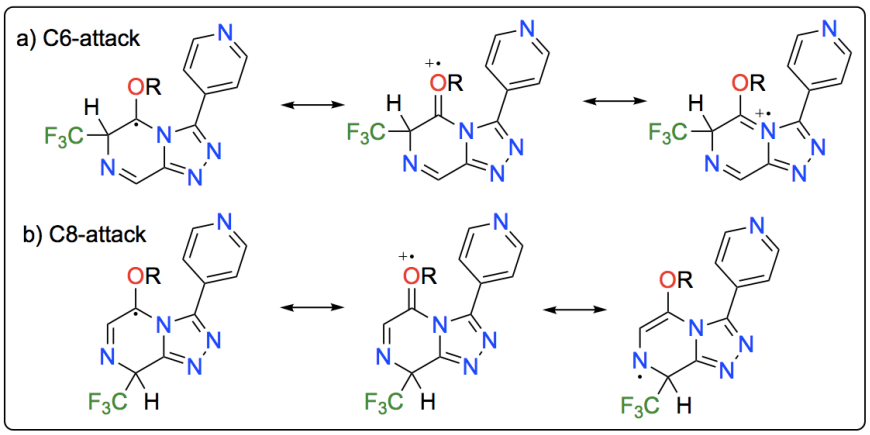

Figure 11. Resonance structures of intermediates formed *via* electrophilic trifluoromethyl radical attack at C6 and C8 positions on the triazolopyrazine core.

The ease and lower costs of this procedure, as compared to other methods, as well as the simplicity of product isolation, demonstrates this procedure to be a useful tool in the LSF toolbox for trifluoromethylation. After demonstrating trifluoromethylation at a C–H bond in the triazolopyrazine core of the model OSM Series 4 ether compound **19**, we performed the same procedure on **20** (Scheme 19). We were surprised to find that reaction did not proceed in the same dichloromethane (DCM)/water (2.5:1) mixture as described for the general procedure of the original report. A dimethyl sulfoxide (DMSO)/water (4:1) mixture was employed instead, following suggestion from the original paper.[40] Despite a more tedious work-up procedure (extensive washing of the organic layer with a water/ice mixture), this solvent mixture allowed

conversion to a trifluoromethylated derivative in a yield of 4% (Scheme 18). Disappearance of the most downfield proton observed with ^{1}H NMR spectroscopy, previously shown to be the C8 position, suggested that the isolated compound was a similar regioisomer to that of our previous trifluoromethylated derivative, while HRMS confirmed the mass of the isolated compound. Functionalisation of **20** to **47** reduced activity of the drug from 250 nM to > 10 μM. This decrease in activity was less than that caused by methyl substitution in a similar (known compound, with 3,4-difluorinated ring in place of phenyl) substrate (6920 *vs*. 281 nM) (Fig. 12), [84, 94] while chlorination at this position actually improves activity (160 nM *vs*. 281 nM).[83]

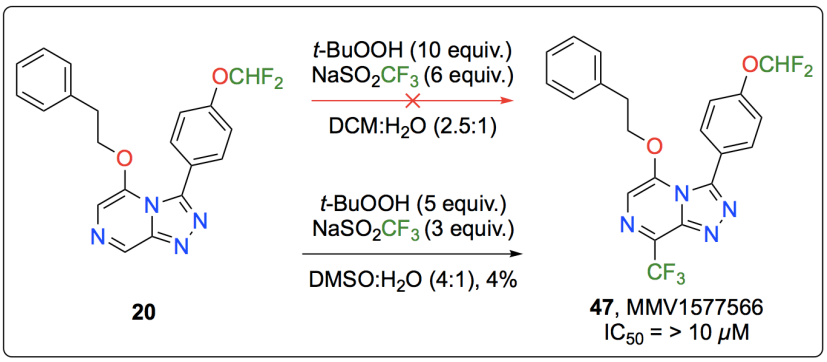

Scheme 19. Trifluoromethylation of **20** using sodium trifluoromethanesulfinate (**8**) under oxidative conditions to form **47.**

The very small isolated yield of this reaction is not indicative of conversion, which was near complete; isolation of the product was difficult due to its co-elution with two other products that were not isolated or fully characterised. LCMS analysis was performed on the crude reaction mixture to assess the presence of other compounds (Appendix A.3). Ions with *m/z* values 519 and 587 indicate di- or tri-trifluoromethylated products. The ratio of the areas under their peaks, monitored at 254 nm was 8.6:3.5:1, indicating a favourable RNS(3) of 36%. Neither the di- or tri-trifluoromethylated products could be isolated in the time available but this separation is clearly of importance for future work. Analysis showed no other ions with the same mass as the isolated mono-functionalised product, suggesting no other (separable) regioisomers were present.

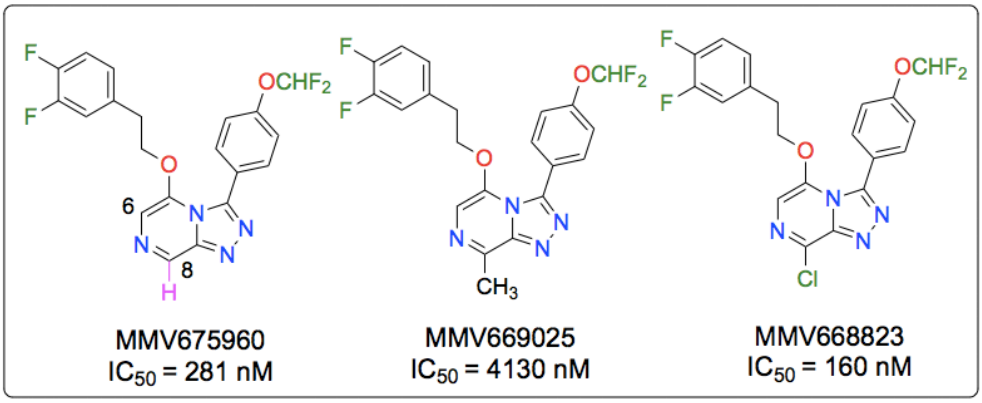

Figure 12. Pre-existing data in OSM: methylated (MMV669025) and chlorinated (MMV668823) derivatives of MMV675960. Methylation of the C8-position decreases activity, while chlorination improves it.

4 Conclusions and Future Work

This thesis describes the assessment of several potential LSF reactions giving conversion to desirable compounds. These results lead to several clear pathways for future work, centred on non-selective azidation, hydroxylation and fluorination methodologies. Non-selective conversion of starting material to products with good conversion has been quantitatively defined by the RNS protocol, in order to easily compare LSF reactions.

Routes towards non-selective reaction optimisation of an aliphatic azidation reaction using DOE are reported. We found that each variable studied, specifically, reaction time, temperature, concentration, equivalents of catalyst, oxidant and azide, and azide solution concentration, had significant effects on reaction non-selectivity. These findings will need to be explored further to finish the reaction's optimisation. However, failure to identify other regioisomers of ibuprofen methyl-ester derivatives may mean that another substrate containing different positions may be better suited as a substrate. Bexarotene methyl ester has a range of different C–H positions that may have more similar reactivities and may allow for a range of regioisomers to be isolated (Fig. 13c). We would also like to explore the effect of other variables on the reaction such as pH, different solvent effects, use of a different oxidant, or the addition of additives such as lithium chloride, caesium chloride or *N*-methylmorpholine *N*-oxide (NMO).

We report the first X-ray structures of crystals from inactive, active, and a late-stage functionalised OSM Series 4 compounds. These structures provide not only confirmation of the absolute structure of these compounds but may also be useful in determining possible conformation *in vivo*, which can aid in more rational drug design strategies to complement these

phenotypic hits. Isolation of a fluorinated derivative of an OSM Series 4 compound at the C8-position or benzylic position would strongly contribute to current SAR findings and should be a focus of future work. Multi-functionalised derivatives following trifluoromethylation of **20** were identified by LCMS. Isolation and characterisation of these compounds would aid our understanding of reaction selectivity towards this, and similar substrates. Application of DOE to the trifluoromethylation of OSM Series 4 compounds is an essential route forward for the non-selective formation of trifluoromethylated products. It is also comparatively simpler than the azidation strategy, which has more variables, and more sensitive products.

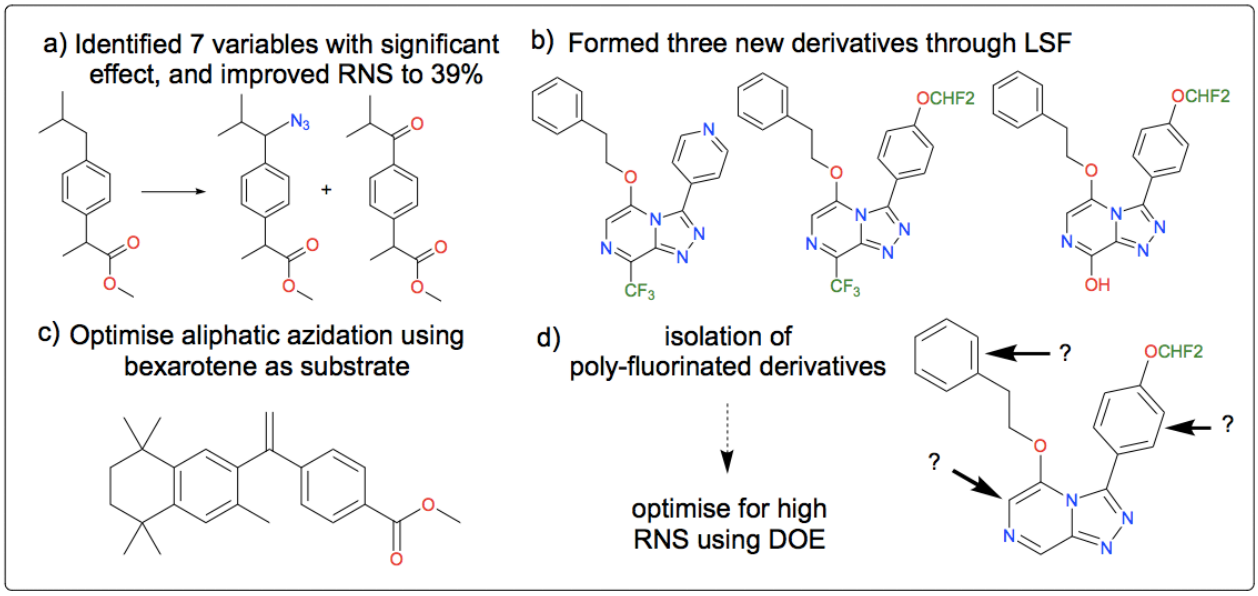

Figure 13. a) We have identified the most significant variables to reaction non-selectivity in an aliphatic azidation of ibuprofen methyl ester. b) We have synthesised three new OSM Series 4 compounds using LSF. c) Future work should use a DOE approach and bexarotene methyl ester as substrate to optimise non-selective aliphatic azidation. d) The identification of polyfluorinated derivatives will provide insight into trifluoromethylation reaction selectivity, and is also good candidate for DOE optimisation.

We have assayed a number of LSF strategies and their conditions, successfully establishing preparative and analytical methods towards the non-selective functionalisation of C–H bonds in drug-like molecules. These methods were used to generate several LSF-derived compounds, providing useful SAR data to a currently-active medicinal chemistry campaign.

5 Experimental Details

5.1 General Experimental Details

Reagents used were purchased from Sigma Aldrich, Combi-blocks, Alfa Aesar, AK Scientific, Merck, Ajax or Fisher Scientific. All reagents were used as supplied and without further purification, unless specified otherwise. Reactions at elevated temperature were conducted using either silicone oil baths, sand baths or metal heating blocks, controlled by an attached temperature probe. Thin-layer chromatography was performed using Merck Silica Gel 60 $F_{254\ nm}$ aluminium-backed plates, and visualised under 254 nm UV light, unless otherwise stated. Flash chromatography was performed using the automatic purification system, Biotage Isolera Spektra with Grace Davison 40–63 μm (230–400 mesh) silica gel.

5.2 General Analytical Details

Infrared spectroscopy was performed using a Bruker Alpha-E, with atmospheric compensation, and was processed using OPUS 6.5 software. Melting points were obtained using a Stanford Research Systems OptiMelt apparatus, with crude melting points obtained using a 20 degree per minute ramp rate, then precise melting points obtained using a 2 degree per minute ramp rate. Nuclear magnetic resonance spectroscopy was performed at 300 K using Bruker spectrometers. Either an AVANCE 200 (^{1}H at 200 MHz, ^{13}C at 50 MHz), AVANCE 300 (^{1}H at 300 MHz, ^{13}C at 75 MHz), AVANCE III 400 (^{1}H at 400 MHz, ^{13}C at 101 MHz), or AVANCE III 500 (^{1}H at 500 MHz, ^{13}C at 126 MHz) was used, with spectra processed using Topspin. Deuterated solvents ($CDCl_3$, DMSO-d_6, CD_3CN) were purchased from Cambridge Isotope Laboratories. ^{1}H and ^{13}C chemical shifts were reported in parts per million (ppm) with respect to TMS at 0.00 ppm. Chemical shifts were calibrated to residual solvent peaks: $CDCl_3$ 7.26, DMSO-d_6 2.50, CD_3CN 1.94 for ^{1}H NMR spectroscopy, $CDCl_3$ 77.16, DMSO-d_6 39.52 for ^{13}C NMR spectroscopy, or to external TMS (0.00) for ^{19}F NMR spectroscopy. Signal splitting was reported as: s = singlet, d =doublet, t = triplet, q = quartet, m = multiplet. Multiple couplings were reported as combinations of these letters, such as dd = doublet of doublets. Where the signal splitting was not fully resolved, the notation $_{app}$ for apparent was reported after the multiplicity, such as for non first-order couplings. Coupling constants, J, were reported in Hertz (Hz). Integrals are calibrated relative to a peak of interest. Low resolution mass spectrometry (m/z) was performed using Bruker's amaZon SL in methanol or acetonitrile using electrospray

ionisation (ESI) or atmospheric-pressure chemical ionisation (APCI). High resolution mass spectrometry (HRMS) was performed with a Bruker 7T FT-ICR using ESI or APCI. Positive or negative ion detection is shown by the charge on the ion, such as $[M + H]^+$ for a positive protonated ion. Liquid-chromatography mass-spectrometry (LCMS) was performed using a Shimadzu LCMS-2020 instrument, with UV detection using SPD-M20A prominence photo diode array detector. Gradients were run in 0–100% acetonitrile in water with 0.1% formic acid over one hour.

5.3 Experimental Procedures

5.3.1 LSF Substrates and their Derivatives

5.3.1.1 Methyl 2-(4-isobutylphenyl)propanoate, (11)

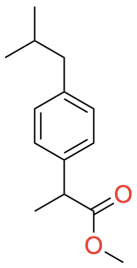

Compound was synthesised by modification of a general procedure.[95] Anhydrous methanol (250 mL) was cooled to 0 °C, then thionyl chloride (2.38 g, 1.46 mL, 20.0 mmol, 1.03 equiv.) was added slowly with stirring. (±)-Ibuprofen (8.03 g, 38.9 mmol, 1 equiv.) dissolved in anhydrous methanol (200 mL) was added in small portions over 10 min. After a further 15 min stirring at 0 °C, the reaction was removed from the ice bath and left to warm to rt over 30 min. The solvent was removed under reduced pressure. The crude material (10.0 g) was dissolved in diethyl ether (50 mL) and washing with water (3 × 20 mL). The combined aqueous layers were extracted with diethyl ether (3 × 20 mL). The combined organic layers were dried over sodium sulfate, and the solvent removed *in vacuo* to give **11** as a clear, yellowish oil (8.18 g, 95%). ^{1}H NMR (300 MHz, $CDCl_3$): δ 7.19 (d, J = 8.1 Hz, 2H, Ar*H*), 7.08 (d, J = 8.1 Hz, 2H, Ar*H*), 3.69 (q, J = 7.1 Hz, 1H, COC*H*), 3.64 (s, 3H, OCH_3), 2.44 (d, J = 7.1 Hz, 2H, CH_2), 1.91–1.76 (m, 1H, $CHCH_2$), 1.48 (d, J = 7.2 Hz, 3H, $ArCHCH_3$), 0.89 (d, J = 6.6 Hz, 6H, $C(CH_3)_2$); ^{13}C NMR (75 MHz, $CDCl_3$): δ 175.1, 140.5, 137.7, 129.3, 127.0, 51.9, 45.0, 44.9, 30.1, 22.3, 18.5; LRMS (ESI+) 262.2 ($[M + H + MeCN]^+$, 100%), 221 ($[M + H]^+$, 85%). Spectroscopic data matched those in the literature.[96]

5.3.1.2 Procedure for aliphatic azidation of ibuprofen methyl-ester.

Reaction was performed according to a modification of reported procedure.[97] To a round-bottom flask containing **11** (423 mg, 1.92 mmol, 1 equiv.) and *N*,*N*'-bis(3,5-di-tert-butylsalicylidene)-1,2-cyclohexanediaminomanganese(III) chloride (Jacobsen's (*R*,*R*) catalyst, 39.0 mg, 61.4 μmol, 3 mol%), and ethyl acetate (1.00 mL) was added iodosylbenzene (328 mg,

1.49 mmol, 0.8 equiv.) under argon with stirring. The flask was heated to 40 °C, then charged with aqueous sodium azide solution (3.00 mL, 1.5 M, 4.5 mmol, 2 equiv.) followed by ethyl acetate (3 mL) with stirring. Once the iodosylbenzene had been visibly consumed (*ca*. 30 min, colour change from cloudy brown to dark brown), aqueous sodium azide solution (1.00 mL, 1.5 M, 1.5 mmol, 0.8 equiv.), ethyl acetate (1.00 mL), and iodosylbenzene (402 mg, 1.83 mmol, 1 equiv.) were added in order. The reaction was stirred at 40 °C for 18 h. Brine (20 mL) and ethyl acetate (30 mL) was added, the layers separated, and the aqueous layer was extracted with ethyl acetate (3 × 20 mL). The combined organic layers were washed with water (30 mL) and brine (30 mL) and dried over magnesium sulfate. The solvent was removed under reduced pressure. The crude material (752 mg) was purified by automated column chromatography (0–5% ethyl acetate in hexanes) and dried *in vacuo* to yield **4** (118 mg, 24%) as a clear yellowish oil, and **37** (184 mg, 41%) as a clear reddish oil. Starting material was also reclaimed (69.8 mg, 17%).

5.3.1.3 Methyl 2-(4-(1-azido-2-methylpropyl)phenyl)propanoate, (4).

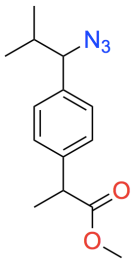

^{1}H NMR (300 MHz, $CDCl_3$): δ 7.32–7.27 (m, 2H, Ar*H*), 7.23–7.18 (m, 2H, Ar*H*), 4.12 (d, *J* = 7.9 Hz, 1H, C*H*N_3), 3.73 (q, *J* = 7.2 Hz, 1H, ArC*H*CH_3), 3.67 (s, 3H, OCH_3), 1.97 (m, 1H, C*H*$(CH_3)_2$), 1.50 (d, *J* = 7.2 Hz, 3H, ArCHC*H*$_3$), 1.00 (d, *J* = 6.6 Hz, 3H, C*H*(C*H*$_3$)(CH_3)), 0.79 (d, *J* = 6.6 Hz, 3H, C*H*(CH_3)(C*H*$_3$); ^{13}C NMR (75 MHz, $CDCl_3$): δ 175.0, 140.3, 138.0, 127.8, 73.0, 52.2, 45.2, 34.1, 29.8, 19.7, 19.3, 18.7; LRMS (ESI+) 284.1 ([M + Na]$^+$, 100%), 234.2 ([M – N_2 + H]$^+$, 100%). Spectroscopic data matched those in the literature.[31]

5.3.1.4 Methyl 2-(4-isobutyrylphenyl)propanoate, (38).

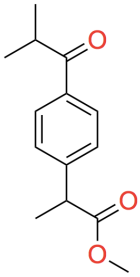

^{1}H NMR (300 MHz, $CDCl_3$): δ 7.91 (d, *J* = 8.2 Hz, 2H, Ar*H*), 7.38 (d, *J* = 8.2 Hz, 2H, Ar*H*), 3.66 (s, 3H, COOC*H*$_3$), 3.52 (septet, *J* = 6.8 Hz, 1H, ArC*H*CH_3)), 1.51 (d, *J* = 7.0 Hz, 3H, ArCHC*H*$_3$), 1.19 (d, *J* = 7.0 Hz, 6H, CO(C*H*$_3$)$_2$); ^{13}C NMR (75 MHz, $CDCl_3$): δ 203.9, 174.3, 145.4, 135.0, 128.7, 127.7, 52.2, 45.3, 35.2, 19.1, 18.3; LRMS (ESI+) 235.2 ([M + H]$^+$, 100%). Spectroscopic data matched those in the literature.[98]

5.3.1.5 Methyl 2-(4-(1-fluoro-2-methylpropyl)phenyl)propanoate, (45).

To **11** (522 mg, 2.37 mmol, 1 equiv.) in anhydrous acetonitrile (3 mL) was added N-fluorobenzenesulfonimide (NFSI, 1.29 g, 4.09 mmol, 1.7 equiv.), tetrabutylammonium decatungstate (TBADT, 308 mg, 92.8 μmol, 4 mol%) and sodium bicarbonate (199 mg, 2.37 mmol, 1 equiv). The mixture was degassed by 3 freeze-pump-thaw cycles, then irradiated with

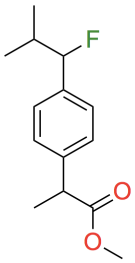

a light centred on 365 nm for 96 h. The solvent was removed under reduced pressure to give a residue, which was dissolved in ethyl acetate (5 mL). The mixture was filtered through a pad of Celite, washing with ethyl acetate (3 × 5 mL). The filtrate was collected, and the solvent was removed under reduced pressure, then dried *in vacuo* overnight to give the product as a mixture with NFSI (1.19 g). Conversion was calculated to be 60% by ^{1}H NMR spectrum of the crude mixture, integrating AUC for peaks at 5.07 ppm (product, ArC*H*F) and 2.44 ppm (starting material, ArCH_2). ^{1}HNMR (300 MHz, $CDCl_3$): δ 7.27 (d, *J* = 8.2 Hz, 2H, Ar*H*), 7.24 (d, *J* = 8.2 Hz, 2H, Ar*H*), 5.07 (dd, *J* = 47 Hz, *J* = 6.9 Hz, 1H, C*H*F), 3.73 (q, *J* = 7.0 Hz, 1H, ArC*H*), 3.60 (s, 3H, OCH_3), 2.16–1.99 (m, 1H, ArCHFC*H*), 1.47 (d, *J* = 7.2 Hz, 3H, ArCHCH_3), 0.99 (d, *J* = 6.6 Hz, 3H, ArCHFCH_3), 0.82 (d, *J* = 6.9 Hz, 3H, ArCHFCH_3); ^{13}C NMR (75 MHz, $CDCl_3$): δ 175.2, 140.4, 138.4, 127.3, 126.5, 126.4, 98.9 (d, *J* = 173 Hz), 51.9, 45.0, 34.2 (d, *J* = 23 Hz), 18.6, 18.3 (d, *J* = 6.0 Hz), 17.5 (d, *J* = 5.2 Hz); ^{19}F NMR (282 MHz, $CDCl_3$): δ –179.8; LRMS (ESI+) 239.1 ([M + H]$^+$, 100%). Spectroscopic data matched those in the literature.[99]

5.3.1.6 2-Chloro-6-hydrazineylpyrazine, (16).

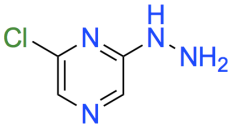

To 2,6-dichloropyrazine (32.9 g, 221 mmol) in absolute ethanol (320 mL), was added hydrazine monohydrate (11.1 g, 10.8 mL, 221 mmol, 1 equiv.) with stirring, turning the solution cloudy. The mixture was stirred at reflux for 2 h, during which the mixture changed from cloudy white to clear yellow. The reaction was monitored by TLC (hexanes/ethyl acetate, 7:3, R_f = 0.8). After completion, solvent was removed under reduced pressure to give a crude residue containing a white precipitate. Hot methanol was added (40 mL), and the mixture filtered, washing with hot methanol (2 × 75 mL). The filtrate was collected, and solvent removed under reduced pressure to give the product as an orange crystalline solid (20.7 g, 65%). Product was taken directly to the next step without further purification. ^{1}H NMR (500 MHz, $CDCl_3$): δ 8.12 (s, 1H, *pyrz-H*), 7.89 (s, 1H, *pyrz-H*), 6.30 (s, br, 1H, N*H*NH_2), 3.85 (s, br, 2H, NHNH_2); ^{13}C NMR (126 MHz, $CDCl_3$): 156.3, 146.6, 132.3, 128.9; LRMS (ESI+): *m/z* 144.0 ([M+H]$^+$, 100%). Spectroscopic data matched those in previously in the group and available online.[100]

5.3.1.7 (*E*)-2-Chloro-6-(2-(pyridin-4-ylmethylene)hydrazineyl)pyrazine, (17).

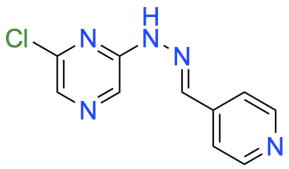

To **16** (3.88 g, 26.8 mmol, 1 equiv.) in 400 mL absolute ethanol was added isonicotinaldehyde (4.39 g, 41.0 mmol, 1.5 equiv) in absolute ethanol (20 mL) dropwise over 5 min with stirring, resulting in formation of a bright yellow precipitate. The mixture was left to stir

overnight at rt (monitoring by TLC (hexanes/ethyl acetate, 7:3, $R_f = 0.3$)), before it was filtered, and the residue washed with cold absolute ethanol (200 mL). Residue was dried *in vacuo* and collected as crude to yield a total of 4.05 g (65%) product as a tan-orange solid. Crude solid was taken directly to the next step without further purification. ^{1}H NMR (500 MHz, DMSO-d^6): 11.92 (s, 1H, N*H*), 8.78 (s, 1H, C*H*), 8.62 (d, $J = 5.0$ Hz, 2H, *pyr-H*), 8.15 (s, 1H, *pyrz-H*), 8.18 (s, 1H, *pyrz-H*), 7.79 (d, $J = 5.0$ Hz, 2H, *pyr-H*); ^{13}C NMR (126 MHz, DMSO-d_6): δ 160.4, 150.6, 150.3, 149.6, 140.7, 138.6, 122.2, 120.3; LRMS (ESI+): *m/z* 234.0 ([M+H]$^+$, 100%). Spectroscopic data matched those in previously in the group and available online.[101]

5.3.1.8 5-Chloro-3-(pyridin-4-yl)-[1,2,4]triazolo[4,3-*a*]pyrazine, (18).

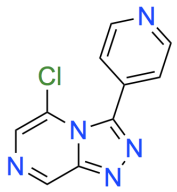

To **17** (4.05 g, 17.4 mmol, 1 equiv.) suspended in anhydrous dichloromethane (180 mL), was added (diacetoxy)iodobenzene (8.86 g, 18.2 mmol, 1.1 equiv) over 5 min, changing the colour from tan-orange to a darker orange-red, monitoring by TLC (ethyl acetate, product $R_f = 0.1$). The reaction was left to stir for 18 h at rt, before saturated sodium bicarbonate aqueous solution (250 mL) was added and the mixture was transferred to a separatory funnel. Aqueous layer was extracted with dichloromethane (3 × 150 mL), then the organic layers were combined and washed with water (150 mL), then brine (150 mL), before solvent was removed under reduced pressure. Crude residue was purified by automated column chromatography (25–100% ethyl acetate in hexanes, then, 0–10% methanol with 1% ammonium hydroxide in ethyl acetate) to give **18** as a tan orange solid (2.50 g, 62%). ^{1}H NMR (500 MHz, $CDCl_3$): δ 9.31 (s, 1H, *pyrz-H*), 8.76 (d, $J = 6.1$ Hz, 2H, *pyr-H*), 7.89 (s, 1H, *pyrz-H*), 7.53 (d, $J = 6.0$ Hz, 2H, *pyr-H*); ^{13}C NMR (126 MHz, $CDCl_3$): 160.4, 150.6, 150.3, 149.6, 140.7, 138.6, 122.2, 120.3; LRMS (APCI+): *m/z* 232.0 ([M+H]$^+$, 100%). Spectroscopic data matched those in previously in the group.[101]

5.3.1.9 5-Phenethoxy-3-(pyridin-4-yl)-[1,2,4]triazolo[4,3-*a*]pyrazine, (19).

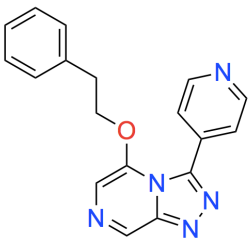

To crude **18** (2.24 g, 9.67 mmol, 1 equiv.) was added 2-phenylethan-1-ol (1.36 g, 11.1 mmol, 1.1 equiv) in toluene (70 mL), 18-crown-6 (137 mg, 517 μmol, 0.05 equiv), and potassium hydroxide (1.80 g, 32.0 mmol, 3.3 equiv). Upon addition of the potassium hydroxide, the reaction mixture exothermed and turned dark brown. Reaction was stirred at rt for 3.5 h, monitoring by TLC (methanol with 1% ammonium hydroxide/diethyl ether, 1:9, $R_f = 0.2$). The reaction mixture was diluted with water (50 mL) and transferred to a separatory funnel. The aqueous layer was extracted with ethyl acetate (3 × 100 mL), then the organic layers were combined and washed with water (200 mL), and brine (200 mL), and dried over sodium sulfate.

Solvent was removed under reduced pressure. Crude was then dissolved in a minimal volume of hot methanol and gently heated in a well-cleaned conical flask until the formation of surface precipitate. This was followed by slow addition of hot mixture of diethyl ether/methanol (1:1) until all solids had again dissolved. The flask was left to stand overnight, before yielding 559 mg (18%) of **19** as large yellow-orange crystals (Appendix A.4). A second recrystallisation yielded a further 707 mg of product as a fine dull yellow powder. Finally, the crude mother liquor was purified by automated silica gel column chromatography (methanol with 1% ammonium hydroxide/diethyl ether, 99:1 to 9:1) to give **19** as a dull tan orange solid (1.736 g, 49%). m.p. (°C) = 159–161; ^{1}H NMR (300 MHz, $CDCl_3$): δ 9.02 (s, 1H, *pyrz-H*), 8.69 (d, *J* = 4.8 Hz, 2H, *pyr-H*), 7.54 (d, *J* = 5.3 Hz, 2H, Ar*H*), 7.41 (s, 1H, *pyrz-H*), 7.26-7.21 (m, 2H, Ar*H*), 6.94-6.89 (m, 2H, Ar*H*), 4.53 (t, *J* = 6.6 Hz, 2H, CH_2), 3.00 (t, *J* = 6.6 Hz, 2H, CH_2); ^{13}C NMR (75 MHz, $CDCl_3$): δ 149.3, 147.9, 144.9, 143.6, 136.2, 135.9, 135.4, 128.8, 128.4, 127.1, 124.8, 108.8, 71.4, 34.4; HRMS (ESI+) calcd for $C_{18}H_{15}N_5ONa$ $[M + Na]^+$ = 340.1174, found 340.1171; FTIR (neat): v_{max} 1603, 1505, 1365, 1295, 973, 820, 753, 698, 589, 567, 538; Anal. Calcd for $C_{18}H_{15}N_5O$: C, 68.13; H, 4.76; N, 22.07. Found: C, 63.16; H, 4.22; N, 14.81. Sample used for CHN was submitted as whole crystal and had been sitting for ca. one month in the X-ray crystallographic analysis facility before submission and will be re-evaluated as future work. Structure assignment was supported by X-ray crystallographic data.

5.3.1.10 6-Chloro-*N*-(pyridin-4-yl)pyrazine-2-carboxamide, (12).

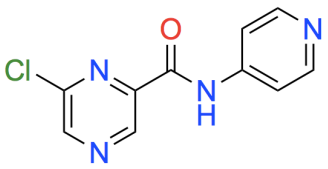

To 6-chloropyrazine-2-carboxylic acid (2.51 g, 15.8 mmol, 1 equiv.) in anhydrous ethyl acetate (100 mL) was added *N*,*N*-diisopropylethylamine (DIPEA, 4.08 g, 5.50 mL, 31.6 mmol, 2 equiv.), then pyridin-4-amine (1.49 g, 15.8 mmol, 1 equiv.), before the mixture was cooled to –10 °C. Propylphosphonic anhydride solution (T3P, 50% by weight in ethyl acetate, 15.0 mL, 25.2 mmol, 1.6 equiv.) was added dropwise over 1 h with stirring. Anhydrous dimethylformamide (80 mL) was added to aid in the dissolution of the carboxylic acid. After about 30 min, the reaction changed from a cloudy grey colour to a clear golden-yellow. After 24 h, the reaction was determined to be complete by TLC (ethyl acetate, product R_f = 0.4). The mixture was diluted with ethyl acetate (50 mL), before it was transferred to a separating funnel. The organic layer was washed with saturated sodium bicarbonate aqueous solution (3 × 80 mL). Aqueous layers were combined and extracted with ethyl acetate (3 × 80 mL). Organic layers were combined and washed with water (100 mL), then brine (150 mL), before the organic layer was dried over sodium sulfate, and the solvent was concentrated under

reduced pressure. Crude residue was purified by automated column chromatography (50–100% ethyl acetate in hexanes). Product containing fractions were combined, and solvent removed under reduced pressure to give a fluffy yellow-white solid. This solid was dissolved in a minimal amount of hot ethanol that crystallised **12** as a botryoidal crystalline solid (1.97 g, 53%). ^{1}H NMR (300 MHz, $CDCl_3$): δ 9.68 (s, 1H, N*H*), 9.39 (s, 1H, *pyrz-H*), 8.86 (s, 1H, *pyrz-H*), 8.60 (d, *J* = 5.5 Hz, 2H, *pyr-H*), 7.73 (d, *J* = 5.0 Hz, 2H, *pyr-H*); ^{13}C NMR (75 MHz, $CDCl_3$): δ 163.2, 155.7, 151.3, 148.9, 144.2, 143.9, 143.2, 109.4; LRMS (APCI+): *m/z* 235.01 ([M + H]$^+$, 100%). Spectroscopic data matched that previously reported in the group.[102]

5.3.1.11 6-Hydrazineyl-*N*-(pyridin-4-yl)pyrazine-2-carboxamide, (13).

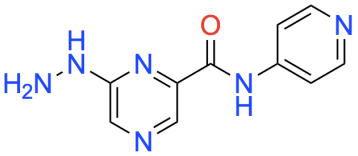

To **12** (1.50 g, 6.39 mmol, 1 equiv.) in ethanol (142 mL) was added hydrazine monohydrate (654 mg, 636 µL, 13.1 mmol, 2 equiv.). The mixture was stirred at reflux for 24 h, monitoring by TLC (5% methanol with 1% ammonium hydroxide in dichloromethane, R_f = 0.3). With time, the clear yellow solution formed a bright yellow precipitate. Solvent was removed under reduced pressure, before ethyl acetate (150 mL) was added and the mixture transferred to a separatory funnel. The organic layer was washed with water (3 × 100 mL), then brine (100 mL), then dried over sodium sulfate. Solvent was removed under reduced pressure to give **13** as a mustard-yellow solid (812 mg, 55%). ^{1}H NMR (500 MHz, DMSO-d_6): δ 10.62 (s, 1H, CON*H*), 8.57 (s, 1H, *pyrz-H*), 8.52 (d, *J* = 5.0 Hz, 2H, *pyr-H*), 8.33 (s, 1H, N*H*NH_2), 8.23 (s, 1H, *pyrz-H*), 7.85 (d, *J* = 5.7 Hz, 2H, *pyr-H*), 4.65 (s, 2H, NHNH_2); ^{13}C NMR (126 MHz, DMSO-d_6): δ 163.9, 155.5, 150.9, 145.4, 141.1, 136.4, 130.4, 114.8; LRMS (ESI+): *m/z* 231.07 ([M+H]$^+$, 100%), LRMS (ESI–): *m/z* 229.09 ([M–H]$^-$, 100%). Spectroscopic data matched that previously reported in the group.[103]

5.3.1.12 (*E*)-6-(2-Benzylidenehydrazineyl)-*N*-(pyridin-4-yl)pyrazine-2-carboxamide, (14).

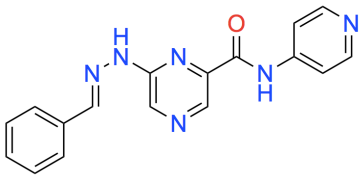

To **13** (500 mg, 2.17 mmol, 1 equiv.) in absolute ethanol (50 mL) was added benzaldehyde (388 mg, 3.66 mmol, 1.6 equiv.) dissolved in absolute ethanol (5 mL) with stirring. The reaction as monitored by TLC (ethyl acetate, R_f = 0.2) and left to stir. A bright yellow precipitate formed in the yellow solution after about 1 h. After 4 h, solvent was removed under reduced pressure to a crude residue. Crude product was filtered, and the residue washed with cold methanol (100 mL), then dried *in vacuo* to yield 270 mg (41%) of product as a mustard-yellow solid. ^{1}H NMR (500 MHz, DMSO-d_6): δ 11.51 (s, 1H, CON*H*), 10.62 (s, 1H,

pyrz-N*H*), 8.91 (s, 1H, *pyrz-H*), 8.61 (s, 1H, *pyrz-H*), 8.53 (d, *J* = 6.1 Hz, 2H, *pyr-H*), 8.18 (s, 1H, NHNC*H*Ar), 7.82 (d, *J* = 6.4 Hz, 2H, *pyrz-H*), 7.78 (d, *J* = 7.6 Hz, 2H, Ar*H*), 7.49–7.36 (m, 3H, Ar*H*); ^{13}C NMR (126 MHz, DMSO-d_6): δ 163.9, 151.7, 151.0, 145.4, 142.9, 142.5, 135.0, 134.8, 134.0, 129.9, 129.3, 127.1, 114.4. HRMS (ESI+) calcd for $C_{18}H_{15}N_5ONa$ [M + Na]$^+$ = 341.1127, found 341.1125.

5.3.1.13 3-Phenyl-*N*-(pyridin-4-yl)-[1,2,4]triazolo[4,3-*a*]pyrazine-5-carboxamide, (15).

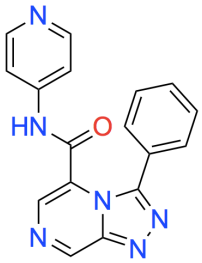

To **14** (221 mg, 694 μmol) suspended in anhydrous dichloromethane (14 mL) was added (diacetoxy)iodobenzene (226 mg, 702 μmol, 1 equiv), and the mixture left to stir for 2.5 h, monitoring by TLC (10% methanol with 1% ammonium hydroxide in dichloromethane, R_f = 0.4). To the reaction was added saturated sodium bicarbonate aqueous solution (20 mL), before transfer to a separatory funnel. Dichloromethane (20 mL) was added, then the aqueous layer was extracted with dichloromethane (3 × 25 mL). The organic layers were combined and washed with water (50 mL), then brine (50 mL), before drying the organic layer over sodium sulfate. Solvent was removed under reduced pressure to a crude residue. Crude product was purified by automated column chromatography (25–100% ethyl acetate in hexanes, then, 0–10% methanol with 1% ammonium hydroxide in ethyl acetate) to form the desired product as a tan solid (112 mg, 51%). m.p. (°C) = 217–220 °C; ^{1}H NMR (300 MHz, DMSO-d_6): δ 11.08 (s, br, 1H, CON*H*), 9.69 (s, 1H, *pyrz-H*), 8.41 (d, *J* = 5.0 Hz, 2H, *pyr-H*), 8.35 (s, 1H, *pyrz-H*), 7.63 – 7.60 (m, 2H), 7.40 – 7.33 (m, 3H, Ar*H*), 7.28 (d, *J* = 6.1 Hz, 2H, *pyr-H*); ^{13}C NMR (75 MHz, DMSO-d_6): δ 159.0, 151.0, 148.5, 147.2, 146.6, 144.9, 131.4, 130.8, 129.2, 129.1, 128.0, 125.0, 114.5; HRMS (ESI+) calcd for $C_{17}H_{13}N_6O$ [M + H] = 339.0965, found 339.0968; FTIR (neat): ν_{max} 1675, 1578, 1519, 1456, 1374, 1323, 1215, 1073, 695, 653, 598, 569, 502.

5.3.1.14 5-Phenethoxy-3-(pyridin-4-yl)-8-(trifluoromethyl)-[1,2,4]triazolo[4,3-*a*]pyrazine, (46).

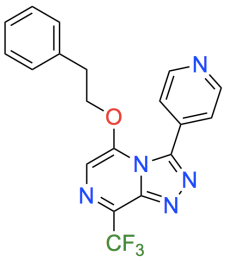

To **19** (76.0 mg, 239 μmol, 1 equiv.), sodium trifluoromethanesulfinate (130 mg, 833 μmol, 3.5 equiv.), dichloromethane (1 mL) and water (0.4 mL), was added *tert*-butylhydroperoxide (70% in water, 200 uL, 1.46 mmol, 6 equiv.) over 20 min at 0 °C with rapid stirring. Starting material was still observed by TLC (ethyl acetate, product R_f = 0.7), so this step was repeated, leaving the reaction to stir in an ice-bath and equilibrate to rt overnight. The mixture was transferred to a separatory funnel with dichloromethane (15 mL) and water (15 mL).

Aqueous layer was extracted with dichloromethane (3 × 10 mL), before organic layers were combined and dried over sodium sulfate. Solvent was removed under reduced pressure, before crude was purified by automated column chromatography (0–15% methanol in ethyl acetate) to yield **46** as a greenish-yellow powder (27.0 mg, 29%). m.p. (°C) = 142–144 °C; ^{1}H NMR (300 MHz, $CDCl_3$): δ 8.72 (s, 2H, *pyrz-H*), 7.52 (d, 2H, *pyr-H*), 7.45 (s, 1H, *pyrz-H*), 7.25 (d, 1H, *pyr-H*), 6.91-6.88 (m, 2H, Ar*H*), 4.60 (t, 2H, OCH_2CH_2Ar), 3.01 (t, 2H, OCH_2CH_2Ar); ^{13}C NMR (75 MHz, $CDCl_3$): δ 149.4, 145.7, 145.4, 144.3, 135.3, 134.9, 129.0, 128.3, 127.4, 124.9, 121.8, 118.1, 107.2, 72.3, 34.3; ^{19}F NMR (282 MHz, $CDCl_3$): δ –66.6; HRMS (ESI+): calcd for $C_{19}H_{14}F_3N_5ONa$ $[M + Na]^+$ = 408.10481, found 408.10467; FTIR (neat): v_{max} 1607, 1522, 1500, 1455, 1419, 1367, 1287, 1260, 1216, 1114, 1069, 981, 954, 829, 801, 771, 736, 701, 639, 612, 586, 533, 493; Anal. Calcd for $C_{19}H_{14}F_3N_5O$: C, 59.22; H, 3.66; N, 18.17. Found: C, 58.69; H, 3.48; N, 17.96. Sample used for CHN was submitted as whole crystal and had been sitting for ca. one month in the X-ray crystallographic analysis facility before submission and will be re-evaluated as future work. Crystals were grown using the same procedure as for **19**.

5.3.1.15 3-(4-(Difluoromethoxy)phenyl)-5-phenethoxy-[1,2,4]triazolo[4,3-*a*]pyrazine, (20).

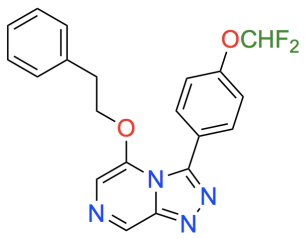

To 2-phenylethan-1-ol (691 mg, 5.66 mmol, 1.3 equiv.) in toluene (40 mL) was added 5-chloro-3-(4-(difluoromethoxy)phenyl)-[1,2,4]triazolo[4,3-*a*]pyrazine (1.30 g, 4.38 mmol, 1 equiv.), 18-crown-6 (62.2 mg, 235 μmol, 0.05 equiv.).With stirring, potassium hydroxide (381 mg, 14.8 mmol, 3.4 equiv.) was added in small portions over 10 min, with an immediate colour change from orange-yellow to an orange-brown colour, then dark brown. The reaction was left to stir for 45 min, and monitored by TLC (ethyl acetate, product R_f = 0.2). The mixture was diluted with water (100 mL) before transfer to a separatory funnel. The aqueous layer was extracted with ethyl acetate (3 × 150 mL), before the organic layers were combined and washed with water (200 mL), then brine (200 mL). Solvent was dried over sodium sulfate, then removed under reduced pressure to a crude residue. Crude was purified by automated column chromatography (0–10% methanol in ethyl acetate) to yield **20** as a yellowish powder (1.25 g, 75%). m.p. (°C) = 115–116 °C; ^{1}H NMR (300 MHz, $CDCl_3$): δ 9.00 (s, 1H, *pyrz-H*), 7.64 (d, *J* = 8.6 Hz, 2H, *pyr-H*), 7.22–7.18 (m, 4H, Ar*H*), 7.16 (s, 1H, *pyrz-H*), 6.89–6.86 (m, 2H, Ar*H*), 6.56 (t, *J* = 73 Hz, 1H, $OCHF_2$), 4.44 (t, *J* = 6.5 Hz, 2H, OCH_2CH_2Ar), 2.95 (t, *J* = 6.5 Hz, 2H, OCH_2CH_2Ar); ^{13}C NMR (75 MHz, $CDCl_3$): δ 152.5, 147.9, 146.4, 144.0, 136.5, 136.3, 132.5, 128.8, 128.5, 127.2, 125.0, 118.7, 115.7 (t, *J* = 261.3

Hz, O*C*HF$_2$), 108.4, 71.3, 34.6; ^{19}F NMR (282 MHz, CDCl$_3$): δ –81.3 (d, *J* = 73.1 Hz, OCHF$_2$); HRMS (ESI+): calcd for $C_{20}H_{17}F_2N_4O_2$ [M + H]$^+$ = 383.1314, found 383.1311; FTIR (neat): v_{max} 1611, 1508, 1463, 1363, 1298, 1227, 1190, 1106, 1048, 977, 886, 818, 753, 698, 588, 559, 534, 490, 446; Anal. Calcd for $C_{20}H_{16}F_2N_4O_2$: C, 62.82; H, 4.22; N, 14.65. Found: C, 67.54; H, 4.66; N, 22.00. Sample used for CHN was submitted as whole crystal and had been sitting for ca. one month in the X-ray crystallographic analysis facility before submission and will be re-evaluated as future work. Spectroscopic data matched that reported previously.[104] Crystals were grown using the same procedure as for **19**.

5.3.1.16 3-(4-(Difluoromethoxy)phenyl)-5-phenethoxy-8-(trifluoromethyl)-[1,2,4]triazolo[4,3-*a*]pyrazine, (47).

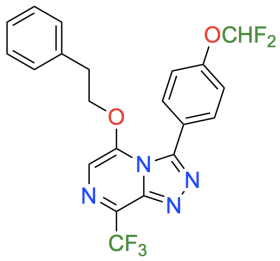

To **20** (214 mg, 560 µmol, 1 equiv.), sodium trifluoromethanesulfinate (262 mg, 1.68 mmol, 3 equiv.), dimethylsulfoxide (4 mL) and water (1 mL), was added *tert*-butylhydroperoxide (70% in water, 360 mg, 3.05 mmol, 3 equiv.) over 20 min at 0 °C with rapid stirring, then the reaction was left to stir overnight. A second addition was repeated the next day, before again leaving to stir overnight. The mixture was transferred to a separatory funnel with dichloromethane (50 mL) and water (20 mL) in ice (*ca*. 30 g). Aqueous layer was extracted with dichloromethane (3 × 40 mL), before organic layers were combined and washed with cold water (3 × 40 mL), then brine (40 mL) and dried over sodium sulfate. Solvent was removed under reduced pressure, before crude was purified by automated column chromatography (0–100% ethyl acetate in hexanes) to yield **47** as a yellowish powder (10.3 mg, 4%). m.p. (°C) = 101–103 °C; ^{1}H NMR (300 MHz, CDCl$_3$): δ 7.62 (d, *J* = 8.6 Hz, 2H, *pyr-H*), 7.37 (s, 1H, *pyrz-H*), 7.24–7.21 (m, 4H, Ar*H*), 7.18 (s, 1H, Ar*H*), 6.88–6.85 (m, 2H, Ar*H*), 4.55 (t, *J* = 6.4 Hz, 2H, OC*H*$_2$CH$_2$Ar), 2.97 (t, *J* = 6.4 Hz, 2H, OCH$_2$C*H*$_2$Ar); ^{13}C NMR (75 MHz, CDCl$_3$): δ 152.8, 147.2, 145.8, 144.2, 135.8, 132.6, 128.9, 128.5, 127.4, 124.2, 118.9, 115.6 (t, *J* = 261 Hz, O*C*HF$_2$), 106.9, 72.2, 34.4; ^{19}F NMR (282 MHz, CDCl$_3$): δ –66.71 (s, ArC*F*$_3$), –81.50 (d, *J* = 73 Hz, OCH*F*$_2$); HRMS (ESI+): calcd for $C_{21}H_{16}F_5N_4O_2$ [M + H]$^+$ = 451.1188, found 451.1187; FTIR (neat): v_{max} 1611, 1508, 1463, 1363, 1298, 1227, 1190, 1106, 1048, 977, 886, 818, 753, 698, 588, 559, 534, 490, 446;

5.3.1.17 3-(4-(Difluoromethoxy)phenyl)-5-phenethoxy-[1,2,4]triazolo[4,3-*a*]pyrazin-8(7*H*)-one, (44).

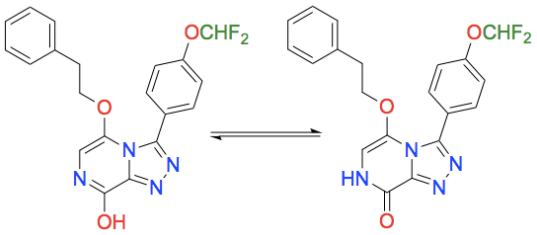

To **20** (37.3 mg, 97.6 μmol, 1 equiv.) was added dimethyldioxirane solution in acetone (0.16 M, 2.4 mL, 390 μmol, 4 equiv.) at –78 °C with stirring. The mixture was left to stir for 1 hour, then warmed to rt while stirring over an hour, before solvent was removed *in vacuo*. The residue was purified by automated column chromatography (0–100% ethyl acetate in hexanes) to yield **44** as an off-white powder (9.06 mg, 23%). ^{1}H NMR (400 MHz, $CDCl_3$): δ 7.60 (d, *J* = 8.8 Hz, 2H, *pyr-H*), 7.31–7.29 (m, 3H, Ar*H*), 7.25–7.23 (m, 5H, Ar*H*), 7.20 (t, *J* = 9.6 Hz, 1H, OC*H*F_2), 7.60 (d, *J* = 8.6 Hz, 2H, Ar*H*), 7.24–7.22 (m, 3H, Ar*H*), 7.20 (s, 2H, Ar*H*), 7.17 (s, 1H, *pyrz-H*), 6.85–6.82 (m, 2H, Ar*H*), 6.57 (t, *J* = 73 Hz, 1H, OC*H*F_2), 4.35 (t, *J* = 6.4 Hz, 2H, OC$H_2$$CH_2$Ar), 2.94 (t, *J* = 6.4 Hz, 2H, OCH_2CH_2Ar); ^{13}C NMR (126 MHz, $CDCl_3$): δ 148.4, 147.0, 145.7, 144.1, 135.6, 132.4, 129.1, 129.0, 128.5, 128.9, 128.9, 127.5, 127.4, 123.8 (t, *J* = 137 Hz, O*C*HF_2), 119.1, 115.5, 108.4, 72.6, 34.3; ^{19}F NMR (282 MHz, $CDCl_3$): δ –81.6 (d, *J* = 73 Hz, $OCHF_2$); FTIR (neat): v_{max} 3408, 3352, 3068, 2928, 1639, 1510, 1486, 1463, 1380, 1222, 1119, 1033, 971, 837, 731, 699, 549; HRMS (ESI+): calcd for $C_{20}H_{16}F_2N_4O_3$ $[M + H]^+$ = 399.1263, found 399.1265.

5.3.1.18 1,1,4,4,6-Pentamethyl-1,2,3,4-tetrahydronaphthalene, (25).

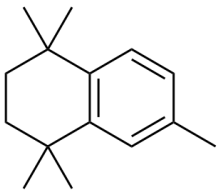

Compound was synthesised and characterised according to a previously reported procedure.[61] To 2,5-dimethyl-2,5-hexanediol (14.14 g, 96.70 mmol, 1 equiv.) was added concentrated hydrochloric acid (400 mL) while stirring. The mixture was left to stir at rt for 3 h before it was transferred with dichloromethane (100 mL) to a separatory funnel. The aqueous layer was extracted with dichloromethane (3 × 100 mL), then the organic layer was dried over magnesium sulfate, and solvent removed under reduced pressure until crystals of the intermediate 2,5-dichloro-2,5-dimethylhexane started to form. Crystals were dissolved in toluene (100 mL) and the reaction cooled to 0 °C stirring under nitrogen. Slowly, aluminium trichloride (645 mg, 4.84 mmol, 5 mol%) was added in small portions over 1 h. With addition, reaction changed from clear to an orange-yellow colour. The reaction was left to stir overnight, warming to rt. Ice (*ca*. 200 g) was added with stirring, changing the mixture to a cloudy white colour. The mixture was left to stir for 20 min, before stirring was stopped and the mixture was transferred to a separatory funnel. Aqueous layer was extracted with dichloromethane (3 × 100 mL), before organic layers were

combined and dried over magnesium sulfate. Solvent was removed under reduced pressure, concentrating the mixture to a crude yellow oil. This oil was cooled with liquid nitrogen while stirring, and the upper oil layer was decanted off. The remaining off-white crystalline solid was filtered and washed with cold pentane (2 × 50 mL) until all yellow colour was removed to yield 6.44 g (43%) of the product as white needle-like crystals. m.p. (°C) = 32–33 (*lit*. 34–36);[57] ^{1}H NMR (300 MHz, $CDCl_3$): δ 7.20 (d, *J* = 8 Hz, 1H, Ar*H*), 7.10 (s, 1H, Ar*H*), 6.95 (d, *J* = 8 Hz, 1H, Ar*H*), 2.30 (s, 3H, ArCH_3), 1.67 (s, 4H, 2 × CH_2), 1.27 (s, 6H, 2 × CH_3), 1.26 (s, 6H, 2 × CH_3); ^{13}C NMR (126 MHz, $CDCl_3$): δ 144.7, 141.8, 134.7, 127.0, 126.5, 126.4, 35.2, 34.1, 33.9, 31.9, 31.8, 21.1; LRMS (ESI+): *m/z* 203.2 ([M + H]$^+$, 100%).

5.3.1.19 Dimethyl terephthalate, (27).

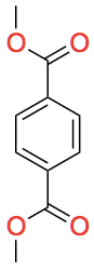

Compound was synthesised and characterised according to a previously reported procedure.[57] To terephthalic acid (8.08 g, 48.6 mmol, 1 equiv.) in methanol (500 mL), was added thionyl chloride (20 mL, excess) was added dropwise over 30 min with stirring at 0 °C. The mixture was allowed to warm to rt, then heated at reflux overnight. The reaction was monitored by TLC (ethyl acetate, product R_f = 0.8). Solvent was removed under reduced pressure. The crude reaction mixture was transferred to a separatory funnel, and ethyl acetate (400 mL) and concentrated sodium bicarbonate aqueous solution (200 mL) was added. The aqueous layer was extracted with ethyl acetate (3 × 150 mL), before the organic layers were combined and washed with water (200 mL), sodium carbonate aqueous solution (100 mL), then brine (200 mL). Solvent was removed under reduced pressure, and product was dried *in vacuo* to yield the product white crystalline solid (8.25 g, 87%). m.p. (°C) = 140–142 (*lit*. 141.5–142);[105] ^{1}H NMR (300 MHz, $CDCl_3$): δ 8.10 (s, 4H, Ar*H*), 3.94 (s, 6H, ArCOOCH_3); ^{13}C NMR (75 MHz, $CDCl_3$): δ 166.4, 134.1, 129.7, 52.6; LRMS (ESI+): *m/z* 195.1 ([M + H]$^+$, 100%).

5.3.1.20 4-(Methoxycarbonyl)benzoic acid, (28).

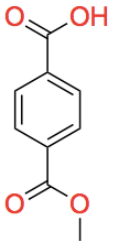

Compound was synthesised and characterised according to a previously reported procedure.[106] **27** (5.45 g, 28.1 mmol, 1 equiv.) in methanol (250 mL) was heated to reflux with stirring, then cooled to rt, before potassium hydroxide (1.65 g, 29.4 mmol, 1.05 equiv.) was added in small portions. The mixture stirred at reflux overnight, monitoring by TLC (ethyl acetate, product R_f = 0.5). The cloudy white mixture was cooled to 0 °C before stirring was stopped to allow the white precipitate to settle. The mixture was filtered, and the residue washed with cold methanol (2 × 100 mL) and dried under vacuum to yield 3.91 g (77%) of product as a white crystalline solid. m.p. (°C) = 222–

223 (*lit*. 221–223);[107] ^{1}H NMR (300 MHz, $CDCl_3$): δ 8.01 (d, *J* = 5.0 Hz, 6H, Ar*H*), 7.94 (d, *J* = 5.0 Hz, 4H, Ar*H*), 3.91 (s, 3H, ArCOOCH_3); ^{13}C NMR (75 MHz, $CDCl_3$): δ 171.2, 167.9, 135.4, 134.2, 130.7, 129.8, 49.9; LRMS (ESI+): *m/z* 185.1 ([M + H]$^+$, 100%).

5.3.1.21 Methyl 4-(chlorocarbonyl)benzoate, (29).

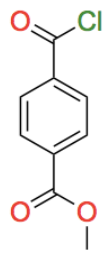

Compound was synthesised according to a previously reported procedure.[57] To **28** (3.04 g, 16.9 mmol, 1 equiv.) was added thionyl chloride (90 mL) at 0 °C with stirring. The mixture was left to stir for 15 min, before it was heated to reflux for 3 h. The mixture changed from cloudy white to a yellow-green colour. The reaction was left to cool, before solvent was removed under reduced pressure with dichloromethane (5 x 100 mL) as a cosolvent to azeotropically remove unreacted thionyl chloride. Crude product was dried under high vacuum overnight to give the product as a crude yellow solid (3.52 g, 105%). The crude reaction mixture was taken directly to the next step with no further purification.

5.3.1.22 Methyl 4-(3,5,5,8,8-pentamethyl-5,6,7,8-tetrahydronaphthalene-2-carbonyl)benzoate, (30).

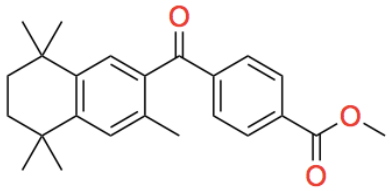

Compound was synthesised and characterised according to a previously reported procedure.[57] To crude methyl 4-(chlorocarbonyl)benzoate (1.18 g, 5.94 mmol, 1 equiv.) in anhydrous dichloromethane (10 mL) was added 1,1,4,4,6-pentamethyl-1,2,3,4-tetrahydronaphthalene (1.26 g, 6.23 mmol, 1.05 equiv.) with stirring at 0 °C. To this mixture was added aluminium trichloride (1.78 g, 13.4 mmol, 2.3 equiv.) in small portions over 10 min, with each addition turning the yellow solution a deeper red colour. After 30 min, the reaction was heated to reflux for 15 min, the cooled to rt. The reaction was determined to be complete by TLC (ethyl acetate, product R_f = 0.5). Ice (*ca*. 10 g) was added with a 20% hydrochloric acid solution (20 mL), before the mixture was transferred to a separatory funnel. Ethyl acetate (50 mL) was added and the aqueous layer was extracted with ethyl acetate (3 × 50 mL). Organic layers were combined and washed with water (50 mL), brine (50 mL), then dried over sodium sulfate. Solvent was removed under reduced pressure. Crude product was purified by automated column chromatography (0–30% ethyl acetate in hexanes) to give the product as an off-white solid (497 mg, 22%). m.p. (°C) = 142–143 (*lit*. 143–144);[57] ^{1}H NMR (300 MHz, $CDCl_3$): δ 8.15 (d, *J* = 6.7 Hz, 2H, Ar*H*), 7.89 (d, *J* = 6.7 Hz, 2H, Ar*H*), 7.30 (s, 1H, Ar*H*) 7.25 (s, 1H, Ar*H*), 4.00 (s, 3H, ArCOOCH_3), 2.39 (s, 3H, ArCH_3), 1.74 (s, 4H, 2 × CH_2), 1.35 (s, 6H, 2 × CH_3), 1.24 (s, 6H, 2 × CH_3); ^{13}C NMR (75 MHz, $CDCl_3$): δ

197.7, 166.4, 148.4, 141.9, 141.8, 134.7, 134.5, 133.4, 129.9, 129.5, 129.4, 128.4, 52.4, 34.9, 34.8, 34.3, 33.8, 31.7, 31.6, 20.0; LRMS (ESI+): *m/z* 387.2 ([M + Na]$^+$, 100%).

5.3.1.23 Methyl 4-(1-(3,5,5,8,8-pentamethyl-5,6,7,8-tetrahydronaphthalen-2-yl)vinyl)benzoate, (23).

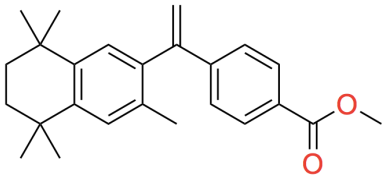

Compound was synthesised and characterised according to a previously reported procedure.[57] To methyltriphenylphosphonium bromide (341 mg, 955 µmol, 1. 5 equiv.) in anhydrous THF (1 mL) was added sodium amide (52 mg, 1.34 mmol, 2.1 equiv.) under argon. The mixture was slowly added to a solution of methyl 4-(3,5,5,8,8-pentamethyl-5,6,7,8-tetrahydronaphthalene-2-carbonyl)benzoate (232 mg, 634 µmol, 1 equiv.) in anhydrous THF (2 mL) over 15 min at 0 °C under nitrogen while stirring. The reaction mixture was allowed to warm to rt, and stirred for 45 min, before ice (*ca.* ~10 g) was added, and reaction mixture extracted with ethyl acetate (3 × 20 mL). Organic layers were combined, and washed with water (30 mL), then brine (30 mL), then solvent was removed under reduced pressure to afford a crude white residue (251 mg), which was purified using automated column chromatography (1–7% ethyl acetate in hexanes) to afford the product as an off-white solid (30.7 mg, 13%). m.p. (°C) = 159–161 (*lit.* 160–161);[57] ^{1}H NMR (300 MHz, $CDCl_3$): δ 7.96 (d, *J* =8.3 Hz, 2H, Ar*H*), 7.34 (d, *J* = 8.7, 2H, Ar*H*), 7.13 (s, 1H, Ar*H*), 7.08 (s, 1H, Ar*H*), 5.81 (d, *J* = 1.2 Hz, 1H, ArCH_2), 5.33 (d, *J* = 1.2 Hz, 1H, ArCH_2), 3.91 (s, 3H, COOCH_3), 1.94 (s, 3H, ArCH_3), 1.71 (s, 4H, $(CH_2)_2$), 1.31 (s, 6H, ArC$(CH_3)_2$), 1.27 (s, 6H, ArC$(CH_3)_2$); ^{13}C NMR (75 MHz, $CDCl_3$): δ 166.9, 149.1, 145.5, 144.3, 142.3, 137.9, 132.7, 129.6, 128.9, 128.1, 128.0, 126.5, 116.8, 52.0, 35.1, 33.9, 33.8, 31.9, 31.8, 19.9; LRMS (ESI+): *m/z* 384.2 ([M+Na]$^+$, 100%).

5.3.2 Preparation of Reagents

5.3.2.1 Iodosylbenzene, (33).

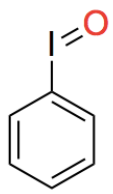

Reaction was performed according to reported procedure.[108] To finely ground iodosylbenzene diacetate (18.0 g, 55.9 mmol) was added aqueous sodium hydroxide dropwise (3 M, 90 mL) with vigorous stirring over 15 min. Large clumps that formed were broken up with a stirring rod. Addition of base turned the mixture a soft yellow/green colour. Following the addition, the mixture was stirred for 45 min, before water (75 mL) was added. The precipitate was collected by filtration, then added to water (150 mL). This mixture was then stirred for 3 h, before it was filtered, washing with

water (150 mL), then dried by vacuum filtration under air. *Caution must be taken to not expose the product to high vacuum due to risk of explosion*. The solid was added to chloroform (75 mL), stirred for 2 h, filtered, and dried by vacuum filtration under air, to give iodosylbenzene as an off-white solid (10.8 g, 88%). Product was iodometrically titrated and determined to be > 95% pure.

5.3.2.2 3,3-Dimethyldioxirane (DMDO), (44).

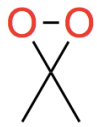

Reaction was performed according to modification of a reported procedure.[109] A three-necked round-bottomed flask was charged with sodium bicarbonate (29.4 g, 350 mmol, 1 equiv.) and water (27 mL), and left to stir, forming a slurry. The reaction was cooled to 0 °C, before oxone (55 g, 361 mmol, 1.05 equiv.) was added in small portions over 2 min, resulting in the evolution of gas. The collecting flask and cold finger were cooled to -78 °C, before acetone (25 mL, 20 g, 344 mmol, 1 equiv.) was quickly added to the stirring mixture. The reaction was sealed, while the collection flask's second opening was left open to prevent overpressure. About ten seconds after acetone addition, a white vapour was seen to pass through the cold finger, collecting on the glass walls. The reaction was left stirring for one hour, after which the rate of collection dropped, and the distillate was collected (12 mL). Solution molarity was calculated to be 0.25 M by iodometric titration, which gives a yield of was 0.87%.

5.3.2.3 3-Methyl-3-(trifluoromethyl)dioxirane (TFDO), (45).

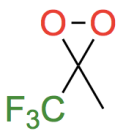

Reaction was performed according to the procedure for DMDO (**44**), using 1,1,1-trifluoropropan-2-one in place of acetone. Molarity of the collected distillate (8.2 mL) was calculated by iodometric titration to be 0.16 M, which gives a yield of 0.47%. Due to the increased volatility of 1,1,1-trifluoropropan-2-one, it is recommended that it be cooled to –20 °C prior to addition and used as soon as possible.

5.3.3 Synthesis of Catalysts

5.3.3.1 *N,N'*-Bis(salicylidene)ethylenediaminomanganese(III), (34).

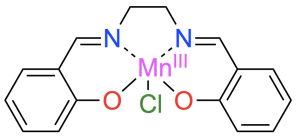

Reaction was performed according to reported procedure. Manganese(II) diacetate tetrahydrate (912 mg, 3.72 mmol, 2 equiv.) was added to a solution of 1,2-bis(salicylidenamino)ethane (500 mg, 1.86 mmol) dissolved in hot absolute ethanol (19 mL), turning the bright yellow solution orange-brown. The formed precipitate became a lighter orange colour over 30 min. The mixture was stirred at reflux for 1 h. Lithium chloride (237 mg, 5.58 mmol, 3 equiv.) was added, and the reaction mixture was stirred at reflux for another 30 min. The solvent was removed under

vacuum to give a dark residue, which was dissolved in dichloromethane (5 mL). This mixture was filtered, and the filtrate was collected. The filtrate was concentrated to 5 mL under reduced pressure to give a residue. After cooling to 0 °C, a black crystalline solid formed that was isolated by filtration, washed with cold absolute ethanol (3 × 5 mL), and dried *in vacuo* to give the product as a dark brown powder (47 mg, 7%). m.p. (°C) = >293 (decomp.) (*lit*. >300 decomp.);[110] LRMS (ESI+): *m/z* 391.0 ([M + Na]$^+$, 100%).

5.3.3.2 *N,N'*-Bis(salicylidene)ethylenediaminocobalt(III), (35).

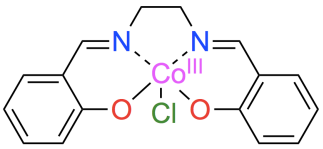

Co(III)(salen)Cl was prepared according to the procedure for Mn(III)(salen)Cl using 268 mg ligand (1 mmol) and 274 mg cobalt(II) acetate (1.1 mmol) to the product as a dark green solid (106.6 mg, 30%). Product was purified by recrystallisation in ethanol, then dried *in vacuo* prior to use. m.p. (°C) = >310 (decomp.) (*lit*. >300 decomp.);[110] LRMS (ESI+): *m/z* 383.0 ([M + Na]$^+$, 100%).

5.3.3.3 *N,N'*-Bis(salicylidene)ethylenediaminoiron(III), (36).

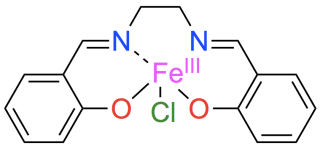

Reaction was performed according to reported procedure.[70] Iron(III) diacetate tetrahydrate (178 mg, 3.72 mmol, 2 equiv.) dissolved in absolute ethanol (20 mL) was added to a solution of 1,2-bis(salicylidenamino)ethane (268 mg, 1.86 mmol) dissolved in hot absolute ethanol (200 mL). Addition of the yellow iron(III) solution to the yellow salen solution resulted in a colour change to dark red. The mixture was refluxed with stirring for 1 h, after which triethylamine (202 mg, 280 uL, 2.0 mmol) in ethanol (20 mL) was added dropwise. The mixture was allowed to cool to rt overnight, then solvent was removed under reduced pressure to a dark residue. The mixture was dissolved in dichloromethane (20 mL) and filtered washing with dichloromethane (2 × 20 mL). Filtrate was collected, and the solvent was removed under reduced pressure to a residue, before cooling to 0 °C. The mixture was filtered, and the residue washed with cold methanol (2 × 20 mL), then dried under vacuum to give a dark purple-black free-flowing black solid, which was recrystallisation in ethanol, then dried *in vacuo* to give **36** (253 mg, 71%). m.p. (°C) = >300 (decomp.) (*lit*. >230);[111] LRMS (ESI+): *m/z* 380.0 ([M + Na]$^+$, 100%).

5.3.3.4 *N,N'*-Bis(salicylidene)ethylenediaminochromium(III), (37).

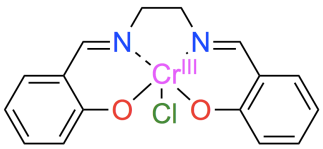

Cr(III)(salen)Cl was prepared according to the procedure for Fe(III)(salen)Cl using 268 mg ligand (1 mmol) and 174 mg chromium(III) chloride (1.1 mmol) to give the product as a dark green solid (106.6 mg, 30%). Product was purified by recrystallisation in ethanol, then dried *in*

vacuo. m.p. (°C) = >245 (decomp.) (*lit*. 245–250).[112] LRMS (ESI+): *m/z* 376.0 ([M + Na]$^+$, 100%).

5.3.3.5 Tetrabutylammonium decatungstate (TBADT)

Compound was synthesised and characterised according to a previously reported procedure.[113] To separate Erlenmeyer flasks, tetrabutylammonium bromide (2.20 g, 6.8 mmol) and sodium tungstate dihydrate (4.60 g, 14 mmol), were dissolved in deionised water (150 mL each). The pH of each solution was adjusted to 2 with conc. hydrochloric acid with stirring. The mixtures were heated to 90 °C, combined to form a white suspension, and left to cool to rt. The precipitate was filtered, washed with water and dried in an oven at 120 °C for 3 h. After the precipitate was allowed to cool to rt it was suspended in dichloromethane (50 mL), stirred at rt for 2 h, filtered, washed with dichloromethane (50 mL), and dried *in vacuo* overnight to give the product as a white powder (2.85 g, 68%). Purity was determined by UV analysis (*lit*. $\varepsilon_{323\ nm}$ = 1.35 x 10^4 $dm^3.mol^{-1}.cm^{-1}$ in acetonitrile)[113] and determined to be > 95%.

5.3.3.6 (–)-2-(((*R*)-2-((*R*)-1-(Pyridin-2-ylmethyl)pyrrolidin-2-yl)pyrrolidin-1-yl)methyl)pyridine (PDP), (38)

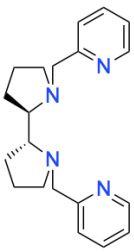

Compound was synthesised and characterised according to a previously reported procedure.[72] To (2*R*,2'*R*)-2,2'-bipyrrolidine tartrate trihydrate (528 mg, 1.53 mmol) in water (5 mL) and dichloromethane (5 mL) was added sodium hydroxide (453 mg, 11.3 mmol, 7.4 equiv.) and 2-picolyl chloride hydrochloride (552 mg, 3.37 mmol, 2.2 eq.). The reaction was stirred overnight at rt, monitoring by TLC (dichloromethane/methanol/ammonium hydroxide, 93:5:2, product R_f = 0.4). The mixture was diluted with aqueous sodium hydroxide solution (1 M, 15 mL) and transferred to a separatory funnel. The aqueous layer was extracted with dichloromethane (3 × 15 mL), and the combined organic extracts were dried over magnesium sulfate and concentrated *in vacuo*. The dark brown crude product (751 mg) was purified by flash column chromatography (1–10% methanol with 1% ammonium hydroxide/dichloromethane). Product containing fractions were combined, washed with aqueous sodium hydroxide solution (1 M, 100 mL), dried over sodium sulfate and concentrated *in vacuo* to give **38** as a dark brown solid (322 mg, 65%). ^{1}H NMR (300 MHz, $CDCl_3$): δ 8.49 (appd, *J* = 4.7 Hz, 2H), 7.60 (dt, *J* = 1.7, 7.7 Hz, 2H), 7.39 (d, *J* = 7.9 Hz, 2H), 7.11 (appt, *J* = 6.0 Hz, 2H), 4.19 (d, *J* = 14 Hz, 2H), 3.49 (d, *J* = 14 Hz, 2H), 2.99 (pentet, *J* = 4.7 Hz, 2H), 2.70 (m, 2H), 2.22 (appq, *J* = 8.4 Hz, 2H), 1.77–1.64 (m, 8H); ^{13}C NMR (75 MHz, CDCl3): δ

160.4, 148.8, 136.3, 122.7, 121.6, 65.3, 61.1, 55.3, 25.9, 23.5; LRMS (ESI+): *m/z* 323.2 ([M + H]$^+$, 100%).

5.3.3.7 [Fe(II)(*R,R*-PDP)(CH_3CN)$_2$]Cl_2, (39)

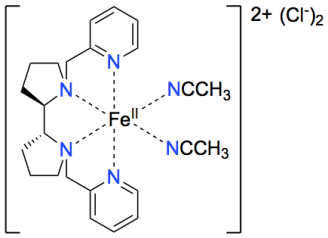

Compound was synthesised and characterised according to a previously reported procedure.[72] To **38** (318 mg, 987 μmol, 1 equiv.) in anhydrous acetonitrile (10 mL) was added iron(II) chloride tetrahydrate (198 mg, 1.00 mmol, 1.01 equiv.) at once with stirring under nitrogen, forming a dark orange-brown precipitate. The reaction mixture was sealed and left stirring overnight. Cold diethyl ether (20 mL) was added and stirring was stopped. Once the reaction mixture settled, the upper diethyl ether layer was gently removed by pipette, repeating (3 × 20 mL) until the upper diethyl ether layer was colourless. The orange precipitate was filtered and washed with diethyl ether (2 × 30 mL), then dried under a stream of nitrogen for 4 h to give **39** as an orange powder (351 mg, 67%). LRMS (ESI+): *m/z* 413.1 ([M - Cl]$^+$, 100%).

5.3.3.8 [Fe(*R,R*-PDP)(CH_3CN)$_2$](SbF_6)$_2$, Chen-White catalyst, (5)

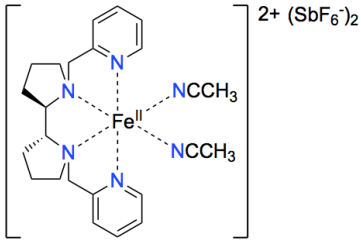

Compound was synthesised and characterised according to a previously reported procedure.[72] **39** (350.9 mg, 661 μmol, 1 equiv.) was suspended in anhydrous acetonitrile (9 mL) under nitrogen in an oven dried round-bottom flask covered in aluminium foil. Silver hexafluoroantimonte (722 mg, 2.10 mmol, 1.6 equiv.) was added to the flask at once with vigorous stirring. The reaction was sealed, and left stirring overnight. Anhydrous acetonitrile (10 mL) was added, and the mixture was filtered through a Celite pad (*ca.* 10 g, ~ 5 cm), and washed with anhydrous acetonitrile (50 mL). The crude cloudy purple mixture was purified by passing it through a 0.22 μM syringe filter five times to remove any remaining silver salts. Product was dried under a stream of nitrogen for 2 h, then dried *in vacuo* to **5** as a dark purple crystalline solid (598 mg, 96%).

5.3.3.9 Tris(pyridin-2-ylmethyl)amine (TPA), (40)

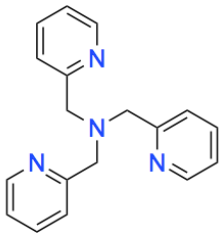

Compound was synthesised and characterised according to a previously reported procedure.[76] To 2-(aminomethyl)pyridine (2.28 g, 21.1 mmol, 1 equiv.) in dichloromethane (100 mL) was added sodium triacetoxyborohydride (13.9 g, 65.6 mmol, 3.1 eq.) under nitrogen while stirring, before pyridine-2-carboxaldehyde (9.03 g, 84.3 mmol, 4 equiv.) was added in small portions over 2 min. The reaction was sealed and left to stir overnight at rt

under nitrogen. Saturated sodium bicarbonate aqueous solution was added (50 mL), and the aqueous layer was extracted with ethyl acetate (3 × 20 mL). The combined organic layers were dried over magnesium sulfate, and solvent removed *in vacuo* to give the crude product (8.03 g) as a dark orange oil. Product was isolated by addition of cold pentane to the crude mixture, then stirring for 30 min at 0 °C. The cold pentane was decanted and this was repeated twice more. The pentane layers were combined, and solvent removed *in vacuo* to give **40** as a pale yellow solid (3.73 g, 61%). ^{1}H NMR δ (300 MHz, $CDCl_3$): δ 8.53 (3H, m, *pyr*-C*H*), 7.57-7.69 (6H, m, *pyr*-C*H*), 7.14 (3H, m, *pyr*-C*H*), 3.89 (6H, s, CH_2); ^{13}C NMR (75 MHz, $CDCl_3$): δ 159.3, 149.1, 136.4, 123.0, 122.0, 60.1; LRMS (ESI+): *m/z* 313.14 ([M + H]$^+$, 100%).

5.3.3.10 [Fe(II)(TPA)(CH_3CN)$_2$](OTf)$_2$, (6)

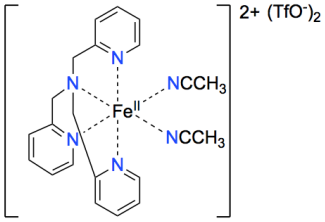

Compound was synthesised and characterised according to a previously reported procedure.[76] To **40** (631 mg, 2.17 mmol) in acetonitrile (15 mL) was added iron(II) triflate (769 mg, 2.17, 1 equiv.), turning the mixture from a deep red to dark green. Over the next 30 min, the colour progressed from dark green, through to dark brown, then dark red. The mixture was left to stir under nitrogen for another 30 min, before -30 °C diethyl ether was added, precipitating out a dark red-brown solid. This crude mixture was filtered, leaving a dark brown residue. This residue was dissolved in hot acetonitrile (3 mL), and the product was left to crystallise *via* ether diffusion to give **6** as an orange-red crystalline solid (625 mg, 40%). m.p. (°C) = 58–60 (*lit*. 58–59);[76] ^{1}H NMR (300 MHz, CD_3CN): δ 12.12 (s, br, 3H), 9.02 (s, 3H), 8.92 (s, 3H), 7.33 (t, *J* = 7.2 Hz, 3H), 7.09 (s, 6H); LRMS (ESI+): *m/z* 495.0 ([M – OTf]$^+$, 100%).

References

[1] Adams, C.; Brantner, V. Estimating The Cost Of New Drug Development: Is It Really $802 Million? http://www.healthaffairs.org/doi/pdf/10.1377/hlthaff.25.2.420 (accessed Nov 23, 2017).

[2] Pathan, H.; Williams, J. *Br. J. of Pain* 2012, *6*, 11–16.

[3] Knoelker, H. *Alkaloid Synthesis*; Springer Berlin: Berlin, 2014; pp. 34–39.

[4] Manglik, A.; Lin, H.; Aryal, D.; McCorvy, J.; Dengler, D.; Corder, G.; Levit, A.; Kling, R.; Bernat, V.; Hübner, H.; Huang, X.; Sassano, M.; Giguère, P.; Löber, S.; Da Duan; Scherrer, G.; Kobilka, B.; Gmeiner, P.; Roth, B.; Shoichet, B. *Nature* 2016, *537*, 185–190.

[5] Houston, J.; Banks, M. *Curr. Opin. in Biotechnol.* 1997, *8*, 734-740.

[6] Corey, E.; Cheng, X. *The logic of chemical synthesis*; 1st ed.; John Wiley: New York, 1995.

[7] Drug Approval Package: EMEND (Aprepitant) NDA #21-549 https://www.accessdata.fda.gov/drugsatfda_docs/nda/2003/21-549_Emend.cfm (accessed Nov 7, 2017).

[8] Snider, R.; Constantine, J.; Lowe, J.; Longo, K.; Lebel, W.; Woody, H.; Drozda, S.; Desai, M.; Vinick, F.; Spencer, R.; et, a. *Science* 1991, *251*, 435-437.

[9] Hale, J.; Mills, S.; MacCoss, M.; Finke, P.; Cascieri, M.; Sadowski, S.; Ber, E.; Chicchi, G.; Kurtz, M.; Metzger, J.; Eiermann, G.; Tsou, N.; Tattersall, F.; Rupniak, N.; Williams, A.; Rycroft, W.; Hargreaves, R.; MacIntyre, D. *J. of Med. Chem.* 1998, *41*, 4607-4614.

[10] Meanwell, N. *J. of Med. Chem.* 2011, *54*, 2529-2591.

[11] Hagmann, W. *J. of Med. Chem.* 2008, *51*, 4359-4369.

[12] Shah, P.; Westwell, A. *J. Enzym. Inhib. and Med. Chem.* 2007, *22*, 527-540.

[13] Yale, H. *J. Med. and Pharm. Chem.* 1959, *1*, 121–133.

[14] Wong, D.; Bymaster, F.; Engleman, E. *Life Sci.* 1995, *57*, 411-441.

[15] Roman, D.; Walline, C.; Rodriguez, G.; Barker, E. *Eur. J. Pharmacol.* 2003, *479*, 53-63.

[16] Cernak, T.; Dykstra, K.; Tyagarajan, S.; Vachal, P.; Krska, S. *Chem. Soc. Rev.* 2016, *45*, 546-576.

[17] Tron, G.; Pirali, T.; Billington, R.; Canonico, P.; Sorba, G.; Genazzani, A. *Med. Res. Rev.* 2008, *28*, 278-308.

[18] Hashiguchi, B.; Bischof, S.; Konnick, M.; Periana, R. *Acc. Chem. Res.* 2012, *45*, 885-898.
[19] Wencel-Delord, J.; Glorius, F. *Nat. Chem.* 2013, *5*, 369-375.
[20] Brückl, T.; Baxter, R.; Ishihara, Y.; Baran, P. *Acc. Chem. Res.* 2011, *45*, 826-839.
[21] Dai, H.; Stepan, A.; Plummer, M.; Zhang, Y.; Yu, J. *J. Amer. Chem. Soc.* 2011, *133*, 7222-7228.
[22] Blanksby, S.; Ellison, G. *Acc. Chem. Res.* 2003, *36*, 255–263.
[23] (Fu, G.; Yuan, R.; Wan, H.; Xu, X. *J. .Energy Chem.* 2016, *25*, 1045–1050.
[24] Lai, W.; Li, C.; Chen, H.; Shaik, S. *Angew. Chem. Int. Ed.* 2012, *51*, 5556-5578.
[25] Meunier, B. *Biomimetic oxidations catalyzed by transition metal complexes*; 1st ed.; Imperial College Press: London, 2000; p. 18.
[26] O'Hara, F.; Blackmond, D.; Baran, P. *J. Amer. Chem. Soc.* 2013, *135*, 12122–12134.
[27] Godula, K.; Sames, D. *Science* 2006, *312*, 67–72.
[28] Hill, C.; Smegal, J.; Henly, T. *J. Org. Chem.* 1983, *48*, 3277-3281.
[29] Sharma, A.; Hartwig, J. *Nature* 2015, *517*, 600-604.
[30] Liu, W.; Groves, J. *Acc. Chem. Res.* 2015, *48*, 1727–1735.
[31] Huang, X.; Bergsten, T.; Groves, J. *J. Amer. Chem. Soc.* 2015, *137*, 5300-5303.
[32] Chen, M.; White, M. *Science* 2007, *318*, 783-787.
[33] Mitra, M.; Lloret-Fillol, J.; Haukka, M.; Costas, M.; Nordlander, E. *Chem. Commun.* 2014, *50*, 1408–1410.
[34] Chen, K.; Que, L. *J. Amer. Chem. Soc.* 2001, *123*, 6327-6337.
[35] Kamata, K.; Yonehara, K.; Nakagawa, Y.; Uehara, K.; Mizuno, N. *Nat. Chem.* 2010, *2*, 478-483.
[36] Lai, W.; Li, C.; Chen, H.; Shaik, S. *Angew. Chem. Int. Ed.* 2012, *51*, 5556-5578.
[37] Fier, P.; Hartwig, J. *J. Amer. Chem. Soc.* 2014, *136*, 10139–10147.
[38] Differding, E.; Ofner, H. *Synlett* 1991, *1991*, 187–189.
[39] Halperin, S.; Fan, H.; Chang, S.; Martin, R.; Britton, R. *Angew. Chem.* 2014, *126*, 4778-4781.
[40] Ji, Y.; Brueckl, T.; Baxter, R.; Fujiwara, Y.; Seiple, I.; Su, S.; Blackmond, D.; Baran, P. *Proc. Nat. Acad. Sci.* 2011, *108*, 14411–14415.
[41] Wender, P.; Hilinski, M.; Mayweg, A. *Org. Lett.* 2005, *7*, 79-82.
[42] 4-Isobutyl-alpha-methylphenylacetic acid, 99% - Ibuprofen https://www.alfa.com/en/catalog/B20989/ (accessed Sep 31, 2017).

[43] Williamson, A.; Ylioja, P.; Robertson, M.; Antonova-Koch, Y.; Avery, V.; Baell, J.; Batchu, H.; Batra, S.; Burrows, J.; Bhattacharyya, S.; Calderon, F.; Charman, S.; Clark, J.; Crespo, B.; Dean, M.; Debbert, S.; Delves, M.; Dennis, A.; Deroose, F.; Duffy, S.; Fletcher, S.; Giaever, G.; Hallyburton, I.; Gamo, F.; Gebbia, M.; Guy, R.; Hungerford, Z.; Kirk, K.; Lafuente-Monasterio, M.; Lee, A.; Meister, S.; Nislow, C.; Overington, J.; Papadatos, G.; Patiny, L.; Pham, J.; Ralph, S.; Ruecker, A.; Ryan, E.; Southan, C.; Srivastava, K.; Swain, C.; Tarnowski, M.; Thomson, P.; Turner, P.; Wallace, I.; Wells, T.; White, K.; White, L.; Willis, P.; Winzeler, E.; Wittlin, S.; Todd, M. *ACS Cent. Sci.* 2016, *2*, 687-701.

[44] Midega, J. "Supermalaria" Is on the Way https://blogs.scientificamerican.com/observations/supermalaria-is-on-the-way/ (accessed Dec 9, 2017).

[45] Rich, S.; Leendertz, F.; Xu, G.; LeBreton, M.; Djoko, C.; Aminake, M.; Takang, E.; Diffo, J.; Pike, B.; Rosenthal, B.; Formenty, P.; Boesch, C.; Ayala, F.; Wolfe, N. *Proc. Nat. Acad. Sci.* 2009, *106*, 14902–14907.

[46] Desjardins, R.; Canfield, C.; Haynes, J.; Chulay, J. *Antimicrob. Agents Chemother.* 1979, *16*, 710-718.

[47] Littler, C. OpenSourceMalaria/Series4 https://github.com/OpenSourceMalaria/Series4/wiki/hERG-Activity (accessed Nov 13, 2018).

[48] Bridgland-Taylor, M.; Hargreaves, A.; Easter, A.; Orme, A.; Henthorn, D.; Ding, M.; Davis, A.; Small, B.; Heapy, C.; Abi-Gerges, N.; Persson, F.; Jacobson, I.; Sullivan, M.; Albertson, N.; Hammond, T.; Sullivan, E.; Valentin, J.; Pollard, C. *J. Pharmacol. Toxicol. Methods* 2006, *54*, 189–199.

[49] Ng, H. Poll to decide which compounds to synthesise next as 'Pfizer phenol' analogues · Issue #555 · OpenSourceMalaria/OSM_To_Do_List, https://github.com/OpenSourceMalaria/OSM_To_Do_List/issues/555 (accessed Dec 24, 2017).

[50] Zhang, C.; Richon, V.; Ni, X.; Talpur, R.; Duvic, M. *J. Invest. Derma.* 2005, *125*, 1045–1052.

[51] Talpur, R.; Ward, S.; Apisarnthanarax, N.; Breuer-McHam, J.; Duvic, M. *J. Amer. Acad. Derma.* 2002, *47*, 672-684.

[52] Farol, L.; Hymes, K. *Exp. Rev. Anticancer Ther.* 2004, *4*, 180–188.

[53] Altucci, L.; Leibowitz, M.; Ogilvie, K.; de Lera, A.; Gronemeyer, H. *Nat. Rev. Drug Disc.* 2007, *6*, 793–810.
[54] Cramer, P.; Cirrito, J.; Wesson, D.; Lee, C.; Karlo, J.; Zinn, A.; Casali, B.; Restivo, J.; Goebel, W.; James, M.; Brunden, K.; Wilson, D.; Landreth, G. *Science* 2012, *335*, 1503–1506.
[55] McFarland, K.; Spalding, T.; Hubbard, D.; Ma, J.; Olsson, R.; Burstein, E. *ACS Chem. Neurosci.* 2013, *4*, 1430–1438.
[56] Schäfer, A.; Burstein, E.; Olsson, R. *Bioorganic Med. Chem. Lett.* 2014, *24*, 1944–1947.
[57] Wagner, C.; Jurutka, P.; Marshall, P.; Groy, T.; van der Vaart, A.; Ziller, J.; Furmick, J.; Graeber, M.; Matro, E.; Miguel, B.; Tran, I.; Kwon, J.; Tedeschi, J.; Moosavi, S.; Danishyar, A.; Philp, J.; Khamees, R.; Jackson, J.; Grupe, D.; Badshah, S.; Hart, J. *J. of Med. Chem.* 2009, *52*, 5950–5966.
[58] 2,5-Dimethyl-2,5-hexanediol, 143618 https://www.sigmaaldrich.com/catalog/product/aldrich/143618?lang=en&region=AU (accessed Dec 14, 2017).
[59] Toluene 179965 https://www.sigmaaldrich.com/catalog/product/sigald/179965?lang=en&region=AU (accessed Dec 17, 2017).
[60] Terephthalic acid 185361 https://www.sigmaaldrich.com/catalog/product/aldrich/185361?lang=en&region=AU (accessed Dec 17, 2017).
[61] Faul, M.; Ratz, A.; Sullivan, K.; Trankle, W.; Winneroski, L. *J. Org. Chem.* 2001, *66*, 5772-5782.
[62] Leardi, R. *Anal. Chim. Acta.* 2009, *652*, 161–172.
[63] Montgomery, D. *Design and analysis of experiments*; 8th ed.; John Wiley & Sons: Massachusetts.
[64] Mansuy, D.; Bartoli, J.; Momenteau, M. *Tetrahedron Lett.* 1982, *23*, 2781–2784.
[65] Srinivasan, K.; Michaud, P.; Kochi, J. *J. Amer. Chem. Soc.* 1986, *108*, 2309–2320.
[66] Groves, J.; Kruper, W. *Isr. J. Chem.* 1985, *25*, 148–154.
[67] Groves, J.; Kruper, W.; Nemo, T.; Myers, R. *J. Mol. Catal.* 1980, *7*, 169–177.
[68] Groves, J.; Nemo, T.; Myers, R. *J. Amer. Chem. Soc.* 1979, *101*, 1032–1033.
[69] Chang, C.; Kuo, M. *J. Amer. Chem. Soc.* 1979, *101*, 3413–3415.

[70] Zhang, W.; Jacobsen, E. *J. Org. Chem.* 1991, *56*, 2296–2298.
[71] Böttcher, A.; Grinstaff, M.; Labinger, J.; Gray, H. *J. Mol. Catal. A: Chem.* 1996, *113*, 191–200.
[72] Chen, M.; White, M. *Science* 2007, *318*, 783–787.
[73] Hinman, A.; Du Bois, J. *J. Amer. Chem. Soc.* 2003, *125*, 11510–11511.
[74] Breslow, R.; Baldwin, S.; Flechtner, T.; Kalicky, P.; Liu, S.; Washburn, W. *J. Amer. Chem. Soc.* 1973, *95*, 3251–3262.
[75] Das, S.; Incarvito, C.; Crabtree, R.; Brudvig, G. *Science* 2006, *312*, 1941–1943.
[76] Diebold, A.; Hagen, K. *Inorg. Chem.* 1998, *37*, 215–223.
[77] Curci, R.; Dinoi, A.; Rubino, M. *Pure Appl. Chem.* 1995, *67*, 811–822.
[78] Asensio, G.; Gonzalez-Nunez, M.; Bernardini, C.; Mello, R.; Adam, W. *J. Amer. Chem. Soc.* 1993, *115*, 7250–7253.
[79] Bernini, R.; Mincione, E.; Sanetti, A.; Mezzetti, M.; Bovicelli, P. *Tetrahedron Lett.* 2000, *41*, 1087–1090.
[80] Adam, W.; Zhao, C.-G.; Jakka, K. Dioxirane Oxidations of Compounds other than Alkenes. *Organic React.* 2008, 69, 1–10.
[81] MacDonald, T. Development of Routes to Access and Functionalise [1,2,4]Triazolo[4,3-a]pyrazine Amides as New Antimalarial Compounds. Undergraduate honours thesis, The University of Sydney, 2014.
[82] Compounds sent for testing in Dundee, December 2017 · Issue #10 · OpenSourceMalaria/Series4 https://github.com/OpenSourceMalaria/Series4/issues/10 (accessed Dec 25, 2017).
[83] Todd, M. OpenSourceMalaria:Triazolopyrazine (TP) Series https://ses.library.usyd.edu.au/bitstream/2123/15389/3/OSM%20Series%204%20Wiki%20Snapshot%20Jul%202016.pdf (accessed Dec 25, 2017).
[84] Todd, M. Biological Evaluation of Compounds http://malaria.ourexperiment.org/biological_data/11216 (accessed Jan 10, 2018).
[85] Murray, R. *Chem. Rev.* 1989, *89*, 1187–1201.
[86] (7) Nodwell, M.; Bagai, A.; Halperin, S.; Martin, R.; Knust, H.; Britton, R. *Chem. Commun.* 2015, *51*, 11783–11786.
[87] Nodwell, M.; Bagai, A.; Halperin, S.; Martin, R.; Knust, H.; Britton, R. *Chem. Commun.* 2015, *51*, 11783–11786.

[88] Tanielian, C.; Seghrouchni, R.; Schweitzer, C. *J. Phys. Chem. A* 2003, *107*, 1102–1111.
[89] Huyser, E.; Bedard, E. *J. Org. Chem.* 1964, *29*, 1588–1590.
[90] Ji, Y.; Brueckl, T.; Baxter, R.; Fujiwara, Y.; Seiple, I.; Su, S.; Blackmond, D.; Baran, P. *Proc. Nat. Acad. Sci.* 2011, *108*, 14411–14415.
[91] Langlois, B.; Laurent, E.; Roidot, N. *Tetrahedron Lett.* 1991, *32*, 7525–7528.
[92] Studer, A. *Angew. Chem. Int. Ed.* 2012, *51*, 8950–8958.
[93] Fujiwara, Y.; Dixon, J.; O'Hara, F.; Funder, E.; Dixon, D.; Rodriguez, R.; Baxter, R.; Herlé, B.; Sach, N.; Collins, M.; Ishihara, Y.; Baran, P. *Nature* 2012, *492*, 95–99.
[94] OpenSourceMalaria:Triazolopyrazine (TP) Series https://openwetware.org/wiki/OpenSourceMalaria:Triazolopyrazine_%28TP%29_Series#Modification_of_Pyrazine_Substitution_Pattern (accessed Dec 25, 2017).
[95] Gee, M. *Anal. Chem.* 1965, *37*, 926–928.
[96] Fujisawa, H.; Fujiwara, T.; Takeuchi, Y.; Omata, K. *Chem. Pharm. Bull.* 2005, *53*, 524–528.
[97] Lee, W.; Kim, K.; Kim, M.; Lee, S. *J. Ferment. Bioeng.* 1995, *80*, 613–615.
[98] Inoue, M.; Kamijo, S.; Amaoka, Y. *Synthesis* 2010, *2010*, 2475–2489.
[99] Nodwell, M.; Bagai, A.; Halperin, S.; Martin, R.; Knust, H.; Britton, R. *Chem. Commun.* 2015, *51*, 11783–11786.
[100] Hollock, N. Synthesis of 5-(3-flurophenethoxy)-3-(4-(pyrrolidin-1-yl)phenyl)-[1,2,4]triazole[4,3-a]pyrazine. http://malaria.ourexperiment.org/_ru17nh/16019/The_formation_of_2chloro6pyrazine_hydrazine.html (accessed May 12, 2017).
[101] Chami, J.; Hockings, E.; Kalas, J.; Manton-Hall, J.; Orsmond, A.; Shaw, M. Synthesis of Antimalarial Compounds from the Triazolopyrazine Ether Series. Highschool Extracurricular Chemistry Project, Sydney Grammar School.
[102] MacDonald, T. Synthesis of 6-chloro-N-(pyridin-4-yl)pyrazine-2-carboxamide (TM 39-1) http://malaria.ourexperiment.org/triazolopyrazine_se/10709/Synthesis_of_6chloroNpyridin4ylpyrazine2carboxamide_TM_391.html (accessed Jun 28, 2017).
[103] MacDonald, T. Synthesis of 6-hydrazinyl-N-(pyridin-4-yl)pyrazine-2-carboxamide (TM 48-1) http://malaria.ourexperiment.org/triazolopyrazine_se/10789/Synthesis_of__6hydrazinylNpyridin4ylpyrazine2carboxamide_TM_481.html (accessed Jun 17, 2017).

[104] Tse, E. Edwin Tse's LabNotebook https://au-mynotebook.labarchives.com/share/Edwin%20Tse/MzE0LjZ8MTUwOS8yNDIvVHJlZU5vZGUvMTAwOTA2NjQxfDc5OC42 (accessed Dec 25, 2017).
[105] Pines, H.; Ipatieff, V. *J Org. Chem.* 1941, *06*, 242-251.
[106] Khan, A.; Kamena, F.; Timmer, M.; Stocker, B. *Org. Biomol. Chem.* 2013, *11*, 881–885.
[107] Ebert, G.; Juda, W.; Kosakowski, R.; Ma, B.; Dong, L.; Cummings, K.; Phelps, M.; Mostafa, A.; Luo, J. *J. Org. Chem.* 2005, *36*.
[108] Saltzman, H.; Sharefkin, J. *Org. Synth.* 1963, *43*.
[109] TFDO Synthesis Procedure http://openflask.blogspot.com.au/2014/01/tfdo-synthesis-procedure.html (accessed Sep 17, 2017).
[110] Emara, A.; Ali, A.; El-Asmy, A.; Ragab, E. *J. Saudi Chem. Soc.* 2014, *18*, 762-773.
[111] Routier, S.; Vezin, H.; Lamour, E.; Bernier, J.; Catteau, J.; Bailly, C. *Nucleic Acids Res.* 1999, *27*, 4160–4166.
[112] Aranha, P.; dos Santos, M.; Romera, S.; Dockal, E. *Polyhedron* 2007, *26*, 1373–1382.
[113] Protti, S.; Ravelli, D.; Fagnoni, M.; Albini, A. *Chem. Commun.* 2009, 7351.

Appendix

A.1 Example ^{1}H and ^{13}C NMR spectrum of a Series 4 compound, 5-Phenethoxy-3-(pyridin-4-yl)-[1,2,4]triazolo[4,3-*a*]pyrazine, **19**.

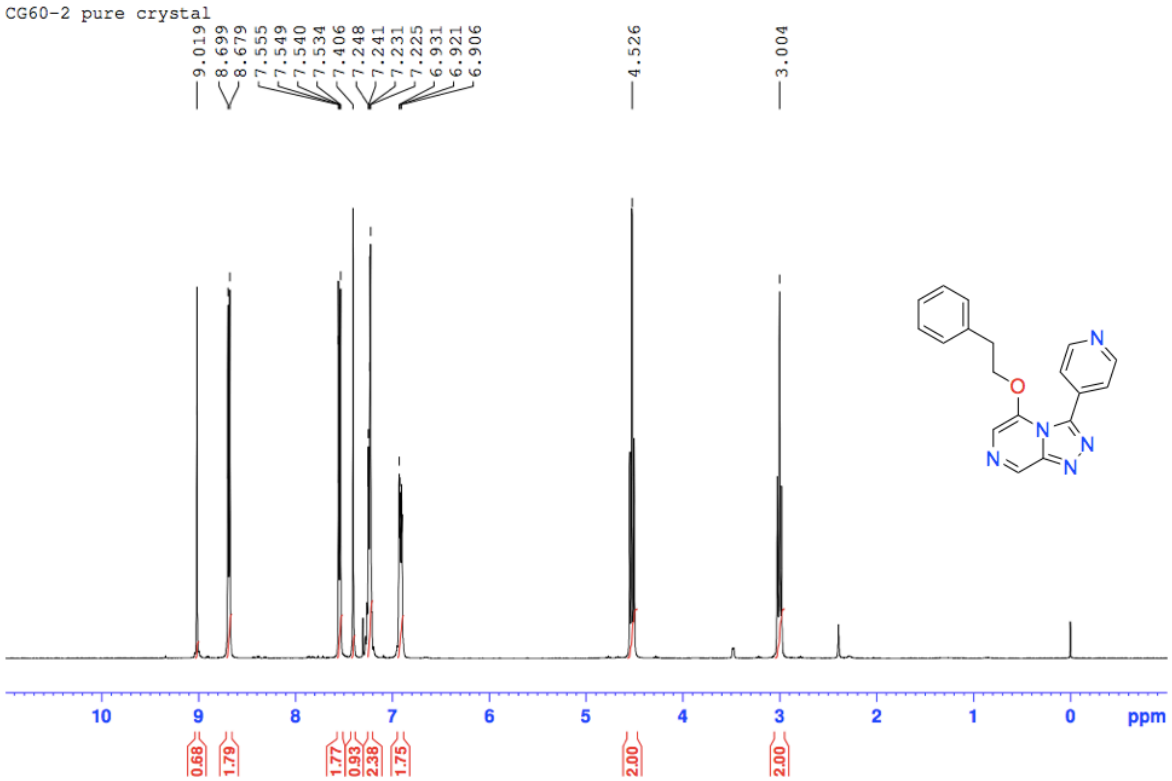

CG60-2 pure crystal CNMR

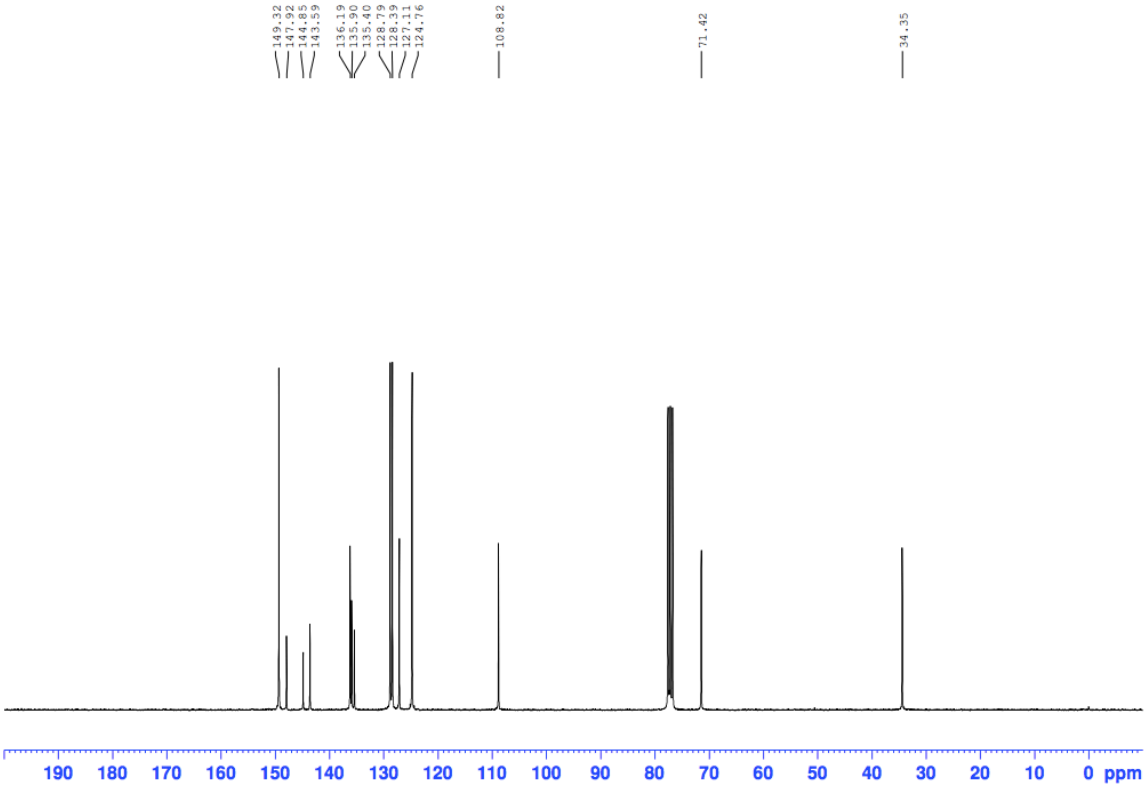

A.2 Example LCMS chromatogram from aliphatic azidation using Fe(salen)Cl

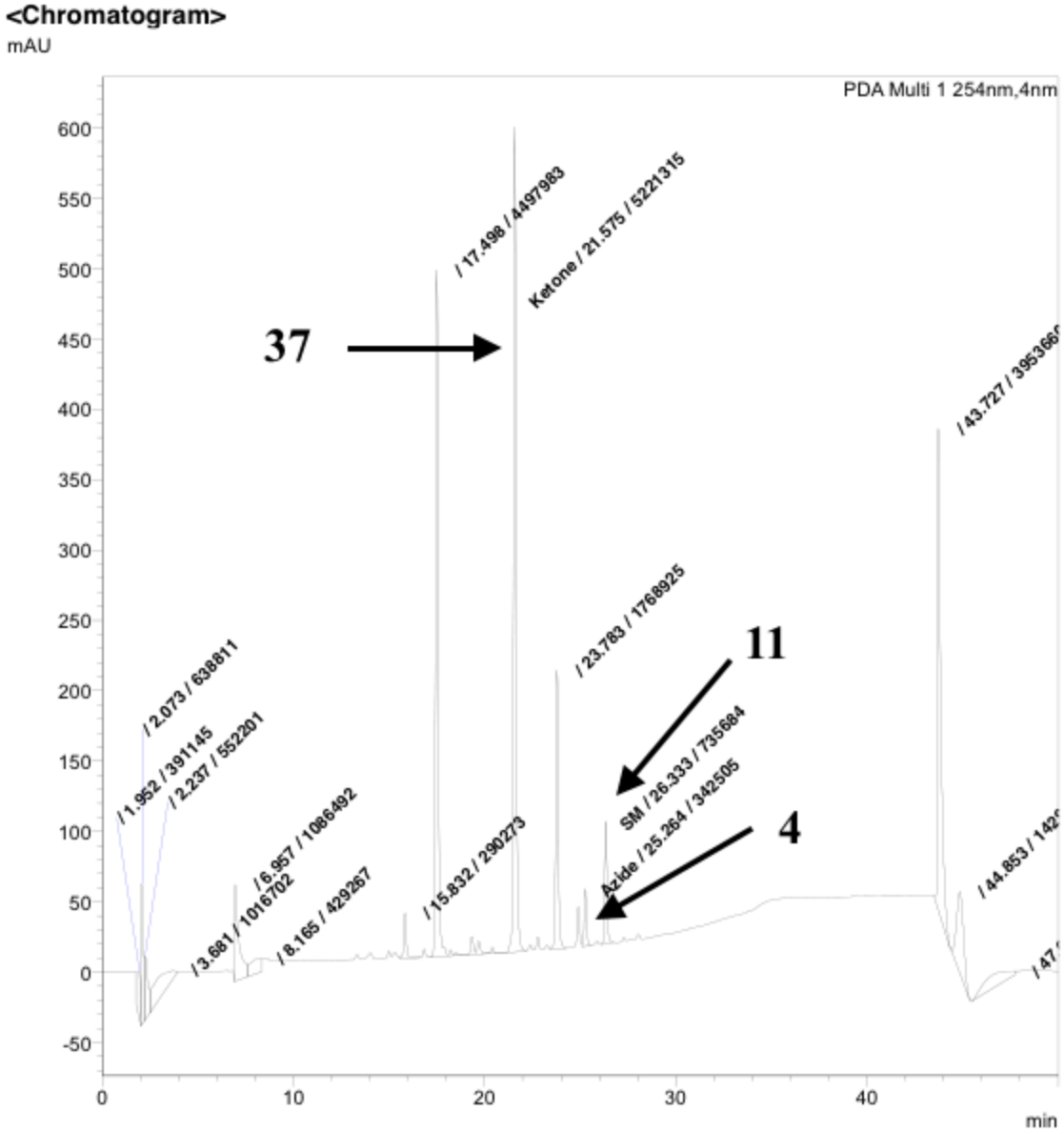

A.3 LCMS data of trifluoromethylation reaction on **20**.

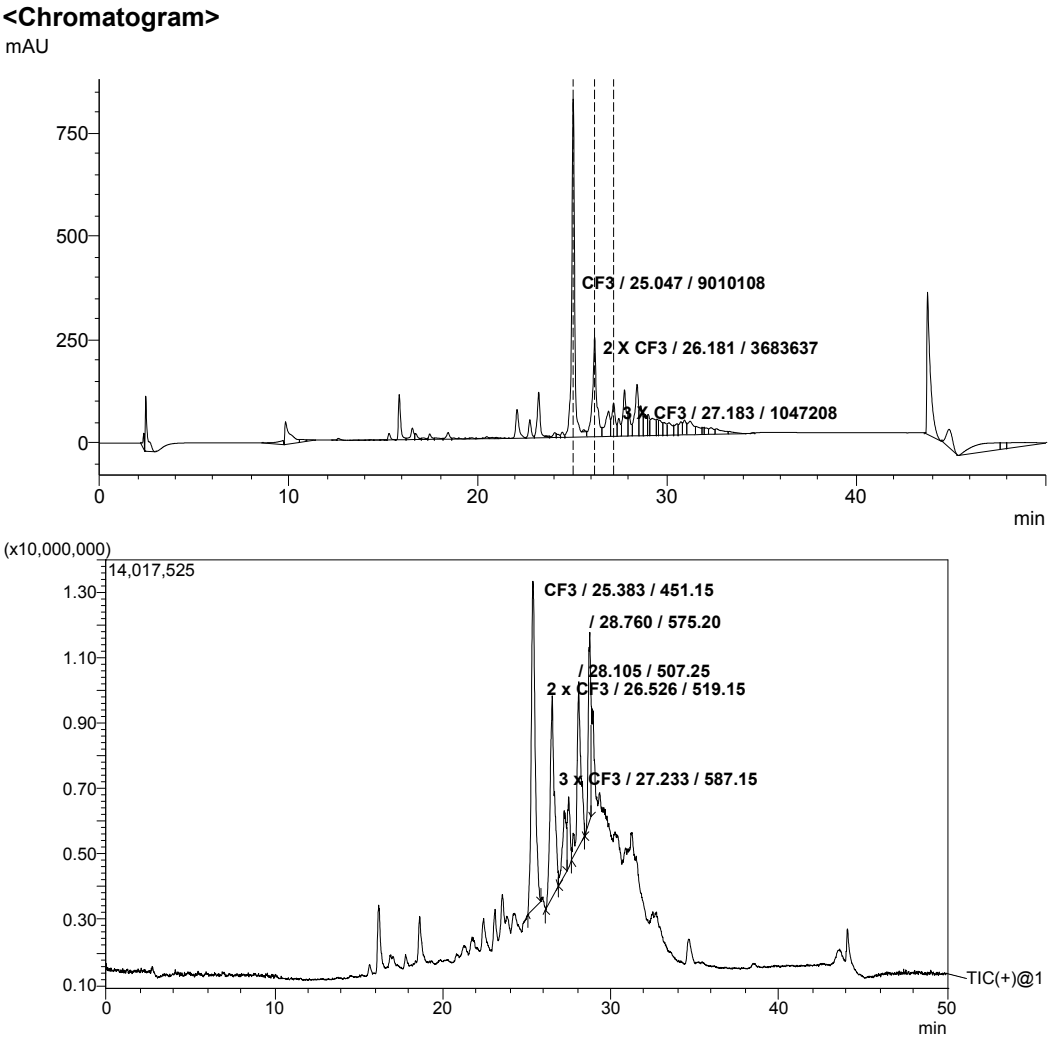

A.4 Crystals of **19** grown in diethyl ether and methanol.

A.5 Multiple linear regression statistics for DOE example.

Coefficients, standard errors, computed *t*-values and *P*-values for linear, quadratic and interaction terms, found by performing regression statistics to the data from Figure 10 (grey circles). High R^2 value (1.00) suggests a good fit of our model to the experimental data.

Terms	Coefficients	Standard Errors	Computed *t*-value	*P*-value
Linear				
ß0	-20.83	1.65	-12.61	0.001
ß1	1.83	0.05	34.29	0.000
ß2	2.54	0.09	29.11	0.000
Quadratic				
ß11	-0.02	0.00	-20.00	0.000
ß22	-0.02	0.00	-21.18	0.000
Interaction				
ß12	-0.02	0.00	-29.12	0.000
R^2	1.00			

When we apply the above data with the following equation, where T is temperature, and *t* is time:[62]

$$Y = ß_0 + ß_1\mathrm{T} + ß_2 t + ß_{12} Tt + ß_{11} T^2 + ß_{22} t^2$$

We find

$$Y = -20.83 + 1.83\mathrm{T} + 2.54t - 0.02\mathrm{T}t - 0.02\mathrm{T}^2 - 0.02t^2$$

Using the *Microsoft Excel* add-in, *Solver*, we can predict the highest yield of 56.9% can be obtained when T = 19.2 °C and *t* = 46.7 minutes.

A.6 Correction to levels chosen for aliphatic azidation experiment on **11**.

Corrected α improves rotatability of the design, increasing precision of the data. It is not expected to have a significant effect on our results.

Conditions	Levels				
	Lower limit (–α, –1.68)	–1	0 (Control)	+1	Upper limit (+α, 1.68)
Solution molarity (M)	0.10	0.22	0.30	0.48	0.60
Catalyst (mol%)	2.5	4.0	5.0	8.0	10
Equivalents of azide	1.1	2.2	3.0	4.8	6.0
Sodium azide solution molarity (M)	1.0	2.2	3.0	4.2	5.0
Equivalents of iodosylbenzene	1.1	2.2	3.0	4.8	6.0
Temperature (°C)	0	14	24	45	60
Time (h)	1.0	3.4	5.0	7.4	9.0

Incorrect

Conditions	Levels				
	Lower limit (–α, –1.41)	–1	0 (Control)	+1	Upper limit (+α, 1.41)
Solution molarity (M)	0.10	0.20	0.30	0.51	0.60
Catalyst (mol%)	2.5	4.3	5.0	8.5	10
Equivalents of azide	1.1	2.4	3.0	5.1	6.0
Sodium azide solution molarity (M)	1.0	2.4	3.0	4.4	5.0
Equivalents of iodosylbenzene	1.1	2.4	3.0	5.1	6.0
Temperature (°C)	0	17	24	49	60
Time (h)	1.0	3.8	5.0	7.8	9.0

A.7 Cooling apparatus used for DOE

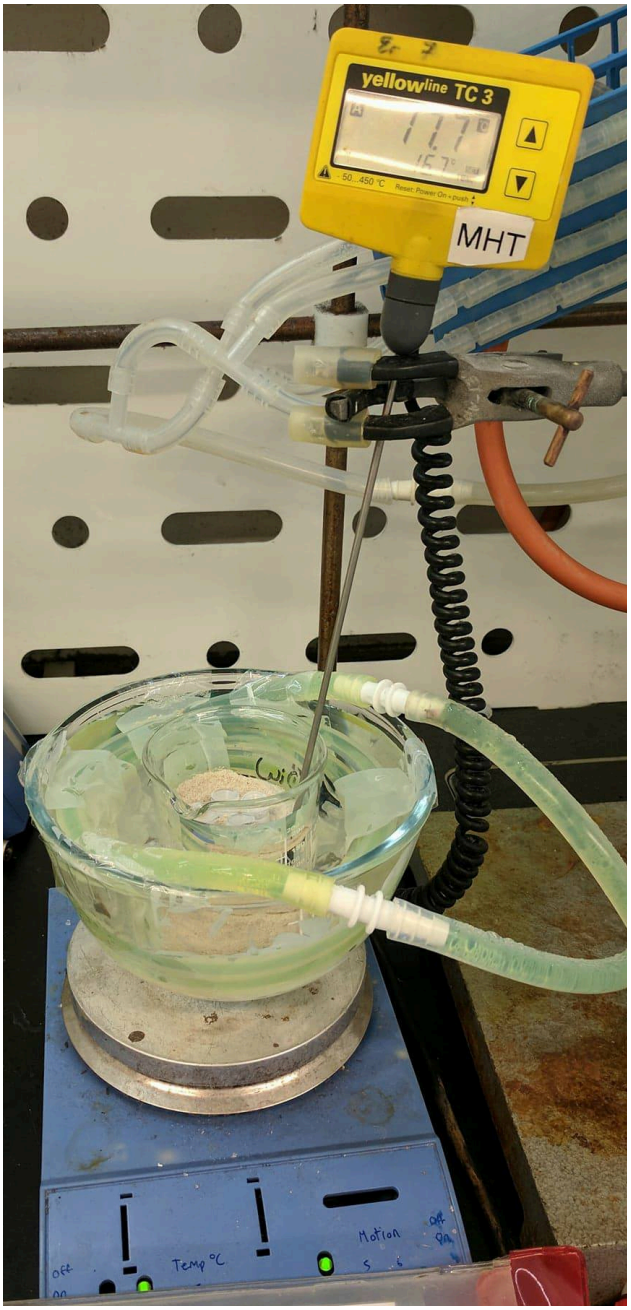

A condenser hose containing water cooled to 10 °C is piped through sand, while a heating element linked to a thermometer maintains the temperature of the sand to around 17 – 18 °C. Reaction vials are placed in a beaker full of sand positioned in the middle.

A.8 Further experiments needed to optimise non-selective yield of aliphatic azidation.

Run #	Conditions						
	Solution molarity	Equivalents of catalyst	Equivalents of azide	Azide molarity	Amount of oxidant	Temperature	Time
1	–	0	0	0	0	0	0
2	+	0	0	0	0	0	0
3	0	–	0	0	0	0	0
4	0	+	0	0	0	0	0
5	0	0	–	0	0	0	0
6	0	0	+	0	0	0	0
7	0	0	0	–	0	0	0
8	0	0	0	+	0	0	0
9	0	0	0	0	–	0	0
10	0	0	0	0	+	0	0
11	0	0	0	0	0	–	0
12	0	0	0	0	0	+	0
13	0	0	0	0	0	0	–
14	0	0	0	0	0	0	+

A.8 Experimental setup for the synthesis of DMDO and TFDO.

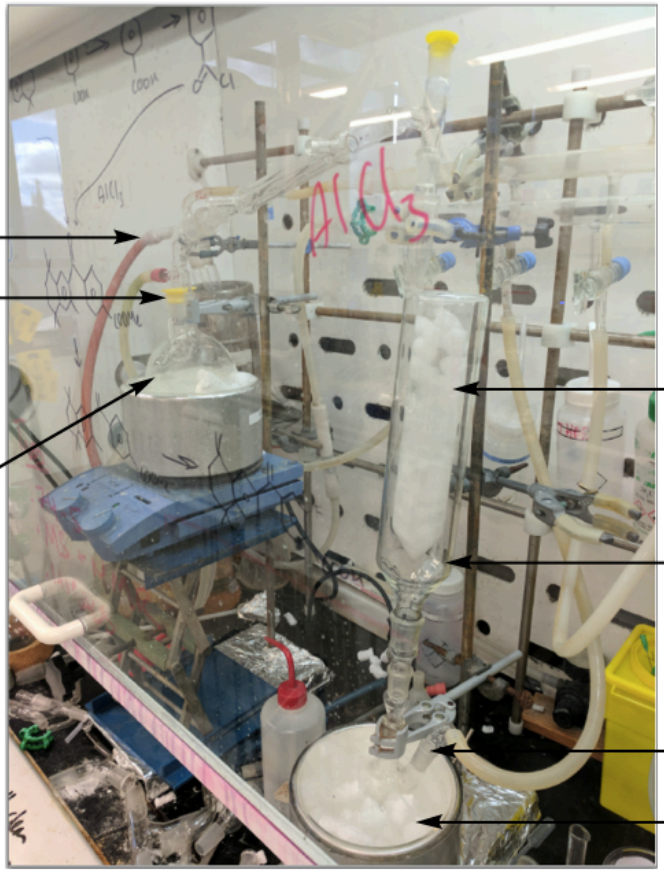

A.9 Colour change when using TBADT catalyst in acetonitrile

TBADT changes to a dark blue colour under UV irradiation.
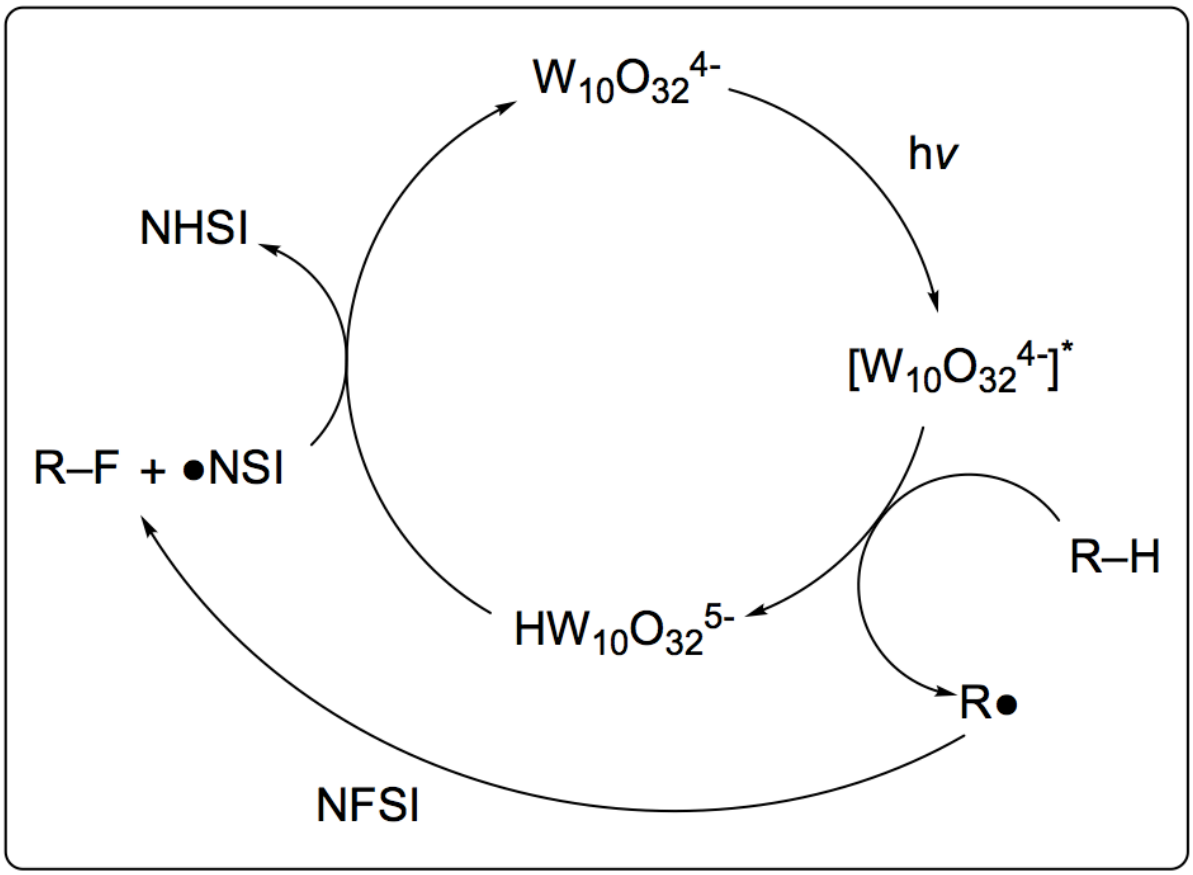
A.10 Reaction mechanism for TBADT-catalysed fluorination of aliphatic bonds using NFSI as fluorine source.